SPECIFIC HEAT INVESTIGATIONS OF MAGNETIC AND MOLECULAR ORDERING

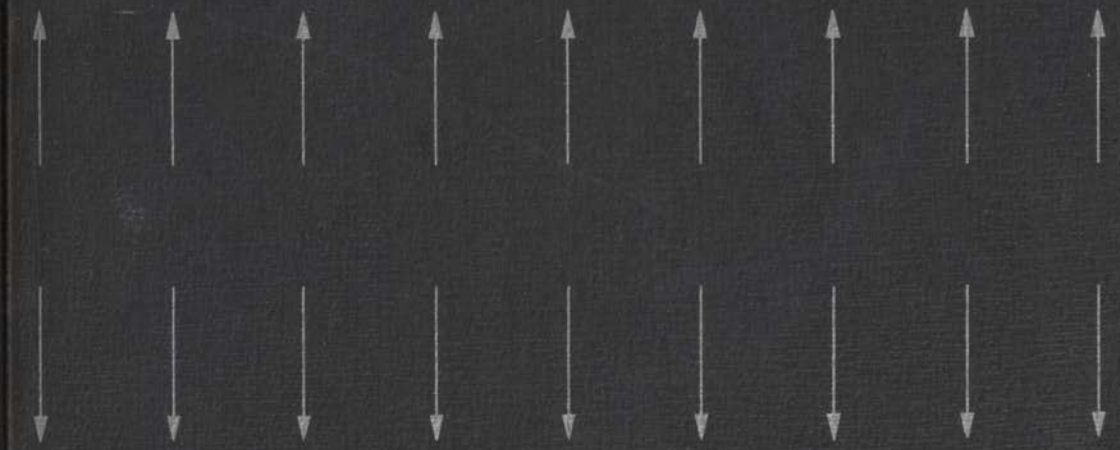

F. W. KLAAIJSEN

SPECIFIC HEAT INVESTIGATIONS OF MAGNETIC AND MOLECULAR ORDERING

PROEFSCHRIFT

TER VERKRIJGING VAN DE GRAAD VAN DOCTOR IN DE WISKUNDE EN NATUURWETENSCHAPPEN AAN DE RIJKSUNIVERSITEIT TE LEIDEN, OP GEZAG VAN DE RECTOR MAGNIFICUS DR. A.E. COHEN, HOOGLERAAR IN DE FACULTEIT DER LETTEREN, VOLGENS BESLUIT VAN HET COLLEGE VAN DEKANEN TE VERDEDIGEN OP WOENSDAG 16 OKTOBER 1974 TE KLOKKE 16.15 UUR

door

François Willem Klaaijsen
geboren te Breskens in 1942

Krips Repro - Meppel

PROMOTOR: *PROF. DR. W.J. HUISKAMP*

DIT PROEFSCHRIFT IS TOT STAND GEKOMEN
ONDER LEIDING VAN *DR. Z. DOKOUPIL*

STELLINGEN

I

Bij lage temperatuur calorimetrie aan polykristallijne verbindingen kan samenpersen van het preparaat in de calorimeter belangrijke voordelen opleveren.
Dit proefschrift, hoofdstuk II.

II

De door Herpin en Keffer gebruikte antiferromagnetische-paramagnetische fase-diagrammen voor karakterisering van metamagnetische stoffen zijn niet volledig en bevatten enkele onjuistheden.
Herpin, A., "Théorie du magnétisme" Presses Universitaires de France (1968).
Keffer, F., "Handbuch der Physik" Vol. XVIII/2, Springer-Verlag (1966).

III

Bij de analyse van de electrische quadrupool hyperfijn interactie in $YbCl_3.6H_2O$ geven Dunlap et al. een foutieve berekening van de electrische veldgradient veroorzaakt door ladingen die het Yb-ion omringen.
Dunlap, B.D., Shenoy, G.K. and Kalvius, G.M., Phys. Rev., B 10 (1974) 26.

IV

De door Brandt voorgestelde formule voor de magnetisatie van een type II supergeleider leidt tot een susceptibiliteit bij $H_{c2}(T=0)$, die gelijk is aan nul. Dit resultaat wijkt af van de naar T=0 K geëxtrapoleerde experimentele bepalingen van deze grootheid.
Brandt, H., Phys.Lett., 29 A (1969) 568.

V

Dat soortelijke warmte metingen aan type II supergeleiders, bij voorafgaande koeling in de aan- én afwezigheid van een magneetveld, gelijke resultaten opleveren, zou volgens Ehrat en Rinderer geen voldoende aanwijzing zijn dat deze resultaten omkeerbare eigenschappen van de preparaten beschrijven. Het door hen gegeven bewijs hiervoor is echter niet volledig.

Ehrat, R. and Rinderer, L., J.Low Temp. Phys. , 7(1972) 533.

VI

In een mengsel van een meeratomig gas en een edelgas wordt de transversale thermodiffusie coëfficiënt D_T^{tr} (H) gegeven door

$$D_T^{tr} = \sqrt{x(1 - x)\, D^{tr}\, \frac{\lambda^{tr}}{nk}}$$

x = concentratie
n = deeltjes dichtheid
k = Boltzmann constante
D^{tr} = transversale diffusie coëfficiënt
λ^{tr} = transversale warmtegeleidings coëfficiënt.

VII

De door Hurley en Gerstein gegeven interpretatie van hun soortelijke warmte metingen aan $(CH_3)_4NNiCl_3$ is aanvechtbaar.

Hurley, M. and Gerstein, B.C., J.Chem.Phys., 59 (1973) 6667.

VIII

Dat het hexagonale poly-type van de spinelstructuur niet voorkomt, kan met behulp van het ionogene bindingsmodel aannemelijk gemaakt worden.

IX

In $CoCl_2.6H_2O$ bestaat er een verschil tussen de waarde voor de wisselwerkingsconstante J/k, bepaald uit soortelijke warmte en susceptibiliteitsmetingen bij hoge temperaturen en die bepaald uit de totale magnetische energie. Deze discrepantie kan voor een groot gedeelte aan nulpuntseffecten worden toegeschreven.

Robinson, W.K. and Friedberg, S.A., Phys.Rev., 117 (1960) 402.

X

Voor een beter begrip van de vrijwel vrije rotatie van CH_3-groepen in bijvoorbeeld γ-picoline zijn soortelijke warmtemetingen bij lage temperaturen van belang, omdat ze directe informatie geven over de energie niveaux en de symmetrie eigenschappen van de gehinderde rotator.

XI

Aan de universiteiten zou meer zorg en mankracht besteed moeten worden aan documentatie van meetgegevens en meetapparatuur, die in laboratoria achterblijven na het afsluiten van een onderzoek.

XII

Het gebruik van doping door sportlieden is uitsluitend levensgevaarlijk indien langdurig grote krachtsinspanningen geleverd worden.

F.W.Klaaijsen

Leiden, 16 oktober 1974

Aan mijn ouders

Aan Mieke,

Murielle en Severine.

CONTENTS

CHAPTER I

GENERAL INTRODUCTION

Many physical experiments are carried out at low temperatures, by which we usually mean temperatures where liquid helium is the refrigerant. In most cases this is done just to obtain as wide a temperature profile as possible for a particular measurement, with no particular attention being paid *per se* to any special low-temperature phenomena. On the other hand a variety of phenomena of wide interest are either observable only at low temperatures or else, may be observed more easily at low temperatures without being obscured by unsought-after effects. The specific heat of solids is one quantity which may fit into any of the above categories, depending on the interest of the experiments. A practical point concerning the low-temperature heat capacity is the discovery of materials that may be used either in connection with refrigeration of the apparatus or which may be used for other physical experiments. But, despite the above discussion the principal interest to-day in the measurement of specific heats at low temperatures lies in quantum phenomena, which are readily observed in this fashion. The study of these phenomena is the main subject of this thesis.

Magnetic interactions are one of the most interesting areas of physics which are suitably studied by heat capacity measurements at low temperatures, as they are then observable in a region where the lattice contribution has usually become relatively small, although the high-temperature results are often useful in a subsidiary fashion in order to help characterize the lattice specific heat. The magnetic and thermal behaviour of a substance containing permanent magnetic moments, e.g. from 3d transition metal ions, depends strongly on the lattice dimensionality. Much of the recent experimental and theoretical interest in magnetism is focussed on interactions between spins coupled in a one dimensional array. This is because this many particle problem is most amenable to theoretical investigations and because the large body of theoretical work can be used to interpret the experimental data.

For a one dimensional lattice the interaction hamiltonian is usually written as

$$H = -2J \sum_{i=1}^{N} \{a(S_{i,x} S_{i+1,x} + S_{i,y} S_{i+1,y}) + b S_{i,z} S_{i+1,z}\},$$

where the summation is taken over neighbouring spins and J is the exchange constant while S_x, S_y and S_z are the spatial spin components. Several different types of exchange interactions between the magnetic moments exist which can have a positive (ferromagnetic) or negative (antiferromagnetic) sign of J. The form of the interactions depends strongly on the number of spatial components of the spins, which is generally called the spin dimensionality D, that participate in the interaction. If the interaction is isotropic (a = 1, b = 1) D equals three and the Heisenberg model is obtained. In a number of cases crystalline field effects and spin-orbit coupling give rise to a reduction of the spin dimensionality. Thus reducing D to two (b = 0, a = 1), which is called the XY model or the planar Heisenberg model, or if the spins are constrained to a crystal axis to D = 1, which is the extreme anisotropic case with b = 1 and a = 0 and denotes the Ising model. Also intermediate models have been studied in which a and b can take any value between 0 and 1.

Apart from the spin dimensionality the spin value may be varied, i.e. the quantity S_i in the hamiltonian which denotes the spin operator of the quantum mechanical system with $S=\frac{1}{2}$, 1, ... or in the classical limit $S=\infty$, where J is replaced by J/S^2 and S is allowed to tend to infinity.

As a general result of the theoretical investigations it turned out that the one dimensional lattice models are not just a simplified generalization of the higher dimensional models, but certain features of the thermodynamic properties are characteristic for the one-dimensional system. In particular, one-dimensional systems with nearest neighbour interactions only cannot support long-range order at any non-zero temperature, independent of the spin value and dimensionality. Consequently the magnetic entropy of such a system has to be removed in short-range order processes as the temperature decreases, and the specific heat as a function of temperature should display a broad maximum only. Naturally such a behaviour will not be observed experimentally because of the always present weak coupling between the chains, which gives rise to a long-range ordered state below a critical temperature T_c. In favourable cases, however,

the chains should be almost independent over wide temperature intervals and the theoretical values based on a one-dimensional model may be used to interpret the experimental measurements. Thus far, however, theoretical discussions have often been focussed on one-dimensional models with spin $\frac{1}{2}$. The purpose of the experimental investigations described in this thesis is to contribute to a better understanding of the thermal properties of linear chain systems having spin values $S > \frac{1}{2}$. Information about the type of exchange interactions and their magnitude, as well as the single-ion properties of the magnetic ions have been obtained for a number of closely related compounds.

Apart from the vibrational modes of the lattice parts (which may have a collective character) and exchange interactions between the magnetic moments fixed at certain lattice points, groups of atoms or molecules can contribute to the heat capacity by rotational motions which may be free to a certain extent, even at low temperatures. In contrast to the vibrational frequencies of the lattice which are usually high, rotational frequencies can be quite low thus giving rise to a large contribution to the low-temperature specific heat and entropy of the system. Generally speaking molecular rotations are observed in polyatomic molecules such as gaseous ethane $CH_3.CH_3$, where instead of eighteen internal vibrational frequencies there are only seventeen, the remaining vibration being replaced by rotations of the two CH_3 groups relative to one another. Also in the solid state, for instance in solid hydrogen and methane, rotations of the molecules were observed down to low temperatures. Although not frequently, co-ordination compounds exhibit features characteristic for hindered rotations of groups of atoms in the crystal.

A particular example being the extended series of metal(II)hexammine halides of formula $M(II)(NH_3)_6X_2$, of which we shall explore in more detail the thermal behaviour of several metal hexammine iodide compounds. On the basis of earlier experiments of Aiello *et al.* and Van Kempen *et al.* (for references we refer to the chapter in question), we realized that the series of hexammine compounds would present suitable candidates for the study of the thermal properties of a hindered rotator in a crystalline solid, over a large temperature interval. Previous measurements indicate that the barrier against rotation of the ammonia .

molecules is of the order of several hundred Kelvin only. The contribution to the heat capacity was expected to be relatively large, because six rotators are present in one molecule; nevertheless quite a large number of other anomalies in the heat capacity could be expected, which form a challenge to detect and localize the several contributions in the respective temperature regions. Concerning the theoretical approach to the problems connected with the hexammine compounds we need to mention the study of Bates and Stevens who worked out a model based on the electrostatic interactions of the proton triangles of the ammonia molecules. The presence of these interactions should be responsible for the local and collective behaviour of the ammonia molecules in these substances.

CHAPTER II

EXPERIMENTAL METHODS

1. Introduction. The need for low-temperature thermal measurements was felt at the beginning of this century with the theoretical development of quantum mechanics and its application to lattice vibrations, and was closely related to the formulation of the third law of thermodynamics. With the systematic research by Eucken, Nernst and other workers in this field, the principle of the vacuum calorimeter was introduced. Except for some minor modifications this method is still widely used.

At present, the experimental arrangement is often made in such a way that the lengthy and tedious calculations can be performed by means of a computer. In this chapter a description of the data logging system is given. Furthermore, special emphasis is given to the measuring temperature range, which covers temperatures between 1.3 and 80 K, and to methods for speeding up internal thermal equilibrium of the powdered samples avoiding the use of exchange gas.

The principle of the measurements follows from the definition of the heat capacity,

$$C_{x,y} = \lim_{\Delta T \to 0} (\Delta Q/\Delta T)_{x,y,..}$$

where x,y,.. are quantities which are kept constant during the measurement. Therefore, the heat capacity of a specimen can be obtained by observing the temperature rise ΔT, which occurs when a known amount of heat ΔQ, is supplied to the specimen. The experimental heat capacity is defined as C_{exp}. Standard techniques for measuring the heat capacity for crystalline phases at low temperatures, however, make the difference between C_{exp} and C_p negligible. On the other hand the difference between C_p and C_V, which is given by the thermodynamic relation

$$C_p - C_V = \alpha^2 VT/\beta$$

in which α is the coefficient of the thermal expansion, β the compressibility and V the molar volume, is also quite small for

crystalline phases, in particular at low temperatures. For example, for copper the ratio C_p/C_V which decreases to unity with decreasing temperature, is approximately 1.03 at 300 K but only 1.005 at 100 K. Since throughout this work heat capacity results on solids in the temperature range between 1.3 and 80 K are given, we will not discriminate between C_p, C_V and C_{exp}.

When an arbitrary amount of material is involved in the measurements we will use the term heat capacity (unit J/K) and the term specific heat is preserved for the heat capacity of one mole of the substance (unit J/mol K). For convenience the experimentally obtained specific heat of a compound will be denoted as C_p.

2. Apparatus. The heat capacity measurements were performed in the temperature range between 1.3 and 80 K. As refrigerants liquid helium, hydrogen and oxygen were used, in which the lower part of the apparatus, the vacuum chamber, is immersed. In fig. 1 a schematic drawing of this part of the apparatus is shown. It includes a mechanical heat switch and the sample container. The use of a sample container was necessary because the specimens used throughout this work were usually powdered polycrystalline samples. The heat capacity of the sample holder, including the resistance thermometer and the heater, was measured separately and was then subtracted from the raw data which include both sample and sample holder. In order to keep the heat capacity of the latter small in comparison with that of the sample, mainly copper was used in the construction. A number of such sample holders have been constructed and used, all of the same design, namely thin walled copper cylinders (wall thickness 0.15 mm) with an outer diameter of 19.7 mm and a length of 28 mm. Four copper vanes were hard soldered to the inner wall of the cylinder to enlarge the contact area with the powders. A cross of an additional set of four copper vanes, hard soldered to a copper rod, was placed in the center of the cylinder. The stainless steel capillary in the german silver bottom lid served as a feedthrough for the copper rod to which the thermometer is soldered outside the calorimeter can and as a support for the cross. The upper lid of the sample holder was made of copper and provided with a (copper) capillary tube. All copper parts were gold plated (layer thickness 5μ) to avoid

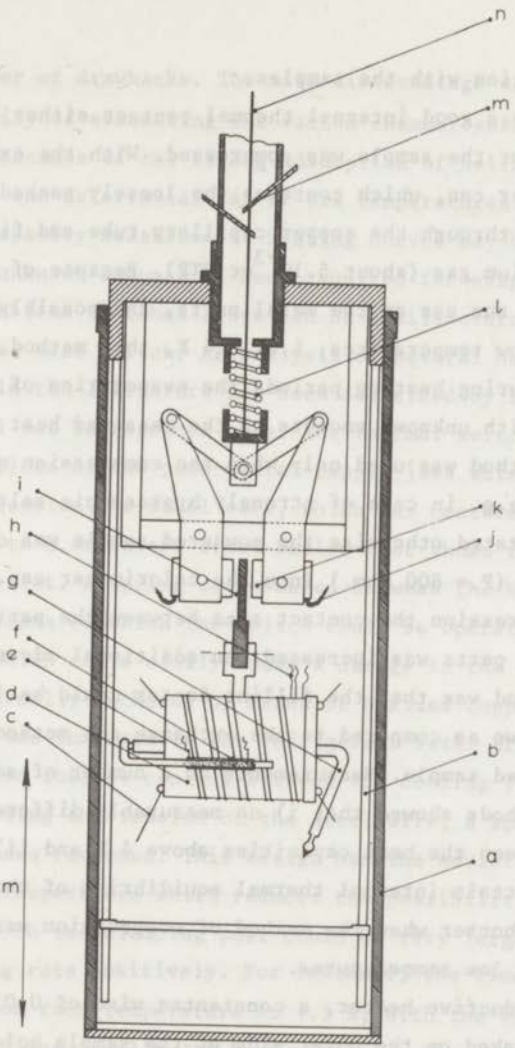

Fig. 1. *Apparatus for measuring the specific heat of powdered samples; the mechanical heat switch and the sample holder.*

a	*vacuum can*	*h*	*heater leads*
b	*inner frame*	*i*	*clamp post*
c	*nylon suspension threads*	*j*	*braided copper for thermal anchoring of the jaws*
d	*sample holder*	*k*	*jaws of the mechanical heat switch*
e	*thermometer leads*	*l*	*spring to reopen the switch*
f	*thermometer*	*m*	*radiation shields*
g	*copper capillary tube*	*n*	*pulling thread*

chemical reaction with the samples.

To ensure a good internal thermal contact either helium exchange gas was used or the sample was compressed. With the exchange gas method the calorimeter can, which contains the loosely packed powdered sample, was evacuated through the copper capillary tube and filled with a small amount of helium gas (about 5.10^{-3}cc NTP). Because of the strong adsorption of the gas on the metal parts, and possibly on the sample as well, at low temperatures, i.e. $T<4$ K, this method has serious disadvantages. During heating periods the evaporation of the adsorbate contributes with unknown amounts to the measured heat capacity. Therefore, this method was used only when the compression method could not be employed; e.g. in case of strongly hygroscopic salts.

If not stated otherwise the powdered sample was compressed hydraulically (P = 800 atm.) into the calorimeter can. Because of the powerful compression the contact area between the particles and the sample holder parts was increased. An additional advantage of our compression method was that the filling factor could be increased roughly by a factor two as compared to the exchange gas method with the loosely packed powdered sample. Measurements on a number of salts using the two different methods showed that i) no measurable differences could be detected between the heat capacities above 4 K and ii) that the time required to attain internal thermal equilibrium of the sample was effectively shorter when the method of compression was used, in particular at low temperatures.

A non-inductive heater, a constantan wire of 0.030 mm diameter, of 100 ohm was baked on the outer side of the sample holder with varnish. The thermometer, a film-type carbon resistance, was soldered on the copper rod which was thermally connected with the inner cross of copper vanes and relatively well thermally isolated from the heater, to avoid overshooting. The sample holder was suspended with nylon thread in a frame inside the vacuum chamber.

Precooling of the sample in the specific heat measurements at temperatures down to about 4 K can be effectuated by the use of helium as exchange gas. However, for a proper measurement of the heat capacity based on eq. (1) the sample has to be thermally isolated from its surroundings. Therefore, at temperatures lower than 4 K the exchange gas

method has a number of drawbacks. The main disadvantage of the method is the impossibility of evacuating the vacuum chamber sufficiently, even with fast pumps, because of the strong adsorption of helium gas on the metal surfaces of the calorimeter can at low temperatures. Consequently during the heat capacity measurements heating curves may be quite irregular due to unknown amounts of heat required for evaporation of the adsorbate. The problems sketched above can be easily overcome by the use of a mechanical heat switch. An analysis of several heat switch devices reported in the literature has been described by Boerstoel *et al.* [1] and will not be repeated here. The thermal switch used throughout this work consists of two gold-plated copper jaws which are operated by putting under tension the steel wire, which was centered in the vacuum line and attached to a stainless steel bellow (not shown in the figure) on top of the cryostat. A spring was mounted between the bellow and the screw device, by means of which the switch could be operated, to avoid too large forces which could easily cause a damage to the switch. The steel wire was thermally anchored by means of braided copper to the vacuum line which was immersed in the refrigerant bath. Braided copper was also used to aid thermal contact between the cooling liquids and the jaws. On releasing the tension on the steel wire, a spring (fig. 1) ensured that the jaws reopened. This design has the advantage that the bellow is at room temperature which reduces the possibility of leaks. Further the forces on the clamping post could be very large, which affects the cooling rate positively. For instance, the time required to cool the sample from room temperature to 1.3 K, with the bath at the lowest temperature, was usually two hours or less. Opening of the heat switch was accompanied by an unavoidable rise in temperature of the sample, which was usually found to be less than 0.01 K.

The whole of the inner assembly was surrounded by a brass vacuum can which was immersed in the refrigerant bath. All electrical leads emerged directly in the liquid through the upper lid of the vacuum can via small feedthroughs (not shown in the figure).

3. Description of the measuring procedure. The temperature of the sample was measured with a carbon resistance thermometer in a Wheatstone bridge. The electrical heater circuit was essentially that described in ref. 2,

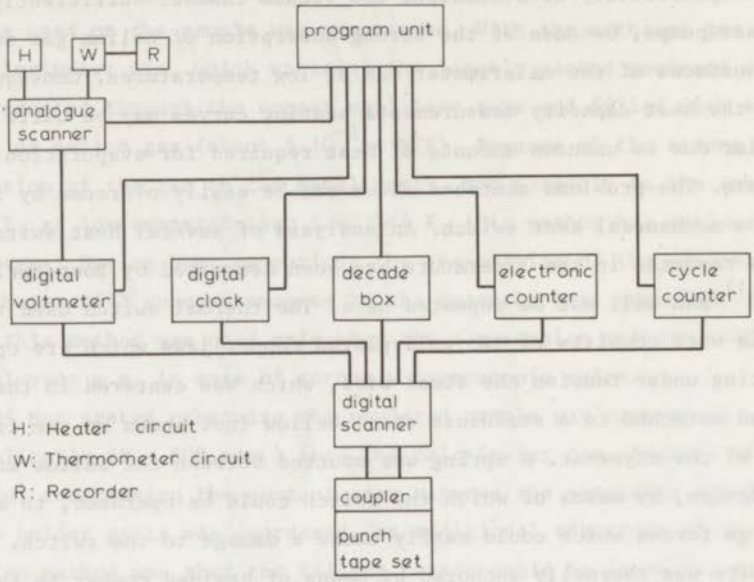

Fig. 2. *Block diagram of the automatic heat capacity measuring set up.*

modified for the automatic data logging system. The complete block diagram of the data logging system is shown in fig. 2. It comprises two features, viz. the subsequent phases of the measuring cycle, which were initiated manually by a single button of the remote control, could be followed visually on an x-t chart recorder, and the data were punched automatically onto papertape.

During the fore period, when the sample drifts to bath temperature, both co-ordinates, the out of balance signal of the Wheatstone bridge and the time of the digital clock were registrated in one-second intervals. Usually fore periods of about thirty seconds were sufficient before the heating period was started. The values of the voltage and current of the heater were then recorded automatically. Finishing of the heating and starting of the after period scanning were independent, thus making it possible to take into account irregularities due to over- and under-shooting at an early stage. During the after period the two co-ordinates, similar as in the fore period were punched. To complete the cycle of a

measuring point the heating time, the sequence number of the measured point and the resistance of the decade box were punched. The proper sequence of transmission of the data on paper tape was controlled by the program unit. The punched data were analysed by means of a computer. The equivalent of the temperature increase due to the applied heat was determined from extrapolations of the fore- and after periods, according to the Keesom and Kok method [3]. The computer program comprises a least squares analysis of the drift curves, in order to eliminate overlooked effects of under- and overshooting before the stationary thermal equilibrium state was realized. By means of an (adjustable) rejection criterion subsequently pairs of co-ordinate points at the beginning of the after period could be excluded from the minimization procedure until the preset accuracy limit of the temperature increase was attained. The applied heat was evaluated from the recorded values of voltage, current and heating time.

4. Thermometry. The thermometers for all the specific heat measurements of this work were the film-type carbon resistance thermometers which have been developed at the Kamerlingh Onnes Laboratory. The manifacture as well as a detailed analysis of their characteristics were reported by Star *et al.* [4]. The resistors were calibrated against ^4He, H_2 and O_2 vapor pressure measurements each time after recycling to room temperature. The vapor pressure of the bath was kept constant at the desired pressure by means of a manostat [5] and was read on a mercury manometer by means of a cathetometer. Below 2.17 K an oil manometer was used in addition. Fluctuations of the vapor pressure were depressed to the equivalent of less than a millidegree at liquid helium and hydrogen temperatures. The temperatures of the bath were obtained from the 1958 ^4He scale [6], the L-60 H_2 scale [7] and the international practical temperature scale of 1968 [8]. Standard temperature and hydrostatic pressure corrections were applied, if necessary. In order to take into account the ortho-para conversion of normal-H_2 a small correction was applied.

To obtain an accurate representation of the R-T relation of the resistor for the whole range of temperatures between 1.3 and 80 K, using a restricted number of calibration points, the empirical formula [4]

$$\ln T = \Sigma_{i=0}^{m} A_i (\ln R)^i \qquad (2)$$

was used. It is well-known that in the 1.3 to 80 K temperature range this formula proves to be a good representation [4]. Between 30 and 80 K the applicability of the followed calibration procedure was verified by means of measurements of the specific heat of benzoic acid (section 6), which is accurately known in this temperature range.

A six degree polynomial (m = 5 in eq.(2)) proved to be necessary and sufficient to represent the calibration data. Usually fourteen calibration points were taken in the liquid helium temperature region and nine and three points in the liquid hydrogen and oxygen region, respectively. Using the least squares method the calibration points were fitted to eq.(2) with the aid of a computer. By means of a rejection criterion (variable) in the least squares computer program, calibration points having relative temperature deviations of more than 1.10^{-3} were excluded from the minimization procedure. Differences between measured and calculated temperatures were generally found to be smaller than 1 mK, 5 mK and 50 mK in the helium, hydrogen and oxygen temperature regions, respectively.

5. Heat capacity of high-purity copper. Copper is a well-known and widely used standard material for low-temperature heat capacity measurements. A compilation of all data reported to 1967, in the temperature range below 300 K, is given by Furukawa *et al.* [9]. Later results are collected by Boerstoel *et al.* [1], together with their data in temperature range between 1.3 and 30 K.

In fig. 3 the results of specific heat measurements on a copper sample of 256.728 g, prepared in this laboratory, are compared with the reference equation due to Osborne *et al.* [10].

$$C_{r.e.} = \Sigma_{i=1}^{6} A_i T^{2i-1}, \qquad (3)$$

using coefficients A_i as reported in ref. 10. From the figure where $(C-C_{r.e.})/C_{r.e.}$ is plotted as a function of temperature, it may be seen that the accuracy of the present measurement may be estimated as better

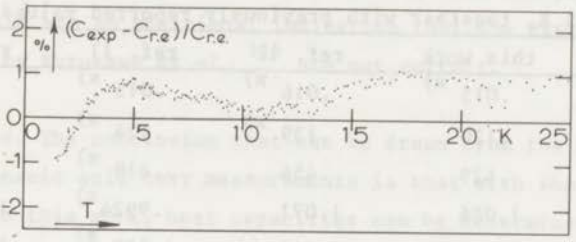

Fig. 3. *The measured specific heat of copper C_{exp} plotted as $(C_{exp}-C_{r.e.})/C_{r.e.}$ versus temperature, where $C_{r.e.}$ denotes the specific heat according to the equation given by Osborne et al.* [10].

than one per cent in the temperature range between 1.3 and 25 K. For such a determination of the accuracy in the high-temperature region we used benzoic acid, a powdered solid, where the use of a sample container was required. These results will be discussed in the next section.

6. Heat capacity of benzoic acid. Benzoic acid, C_6H_5COOH, which can be obtained with high-purity, is a generally accepted test substance for the intercomparison of precision heat capacity calorimeters in the temperature range between 10 and 350 K [11]. Heat capacity measurements on benzoic acid were performed throughout this research to check the apparatus and to determine whether the two different filling procedures of the sample container yield measurable differences in the heat capacities.

In table I we present smoothed values of an arbitrarily chosen series of the measurements on benzoic acid, which are compared with previously reported results. At N.B.S. Furukawa *et al.* [11] made measurements down to 16 K and tabulated the results together with extrapolated values down to 5 K. Clay and Staveley [12] pointed out that their own results and those of other workers [13-15] indicate that the extrapolated N.B.S. values are too low. Our low-temperature results are in fact also lower than those reported in ref. 11, whereas they compare

TABLE I

Smoothed values of the specific heat of benzoic acid in J/mol K, together with previously reported values.

T(K)	this work	ref. 12	ref. 11	ref. 13
2	.015 x)	.016 x)	.015 x)	.015 x)
4	.120	.139 x)	.124 x)	.125 x)
6	.429	.456	.419 x)	.443
8	1.086	1.071	.9924 x)	1.092
10	2.110	2.092	1.923 x)	2.096
12	3.492	3.452	3.242 x)	3.452
14	5.158	5.087	4.932 x)	5.062
16	7.003	6.883	6.824 x)	6.883
18	8.986	8.870	8.853	8.853
20	11.09	11.05	11.00	10.96
22	13.30	13.33	13.17	13.14
24	15.52	15.65	15.46	15.36
26	17.70	17.82	17.61	17.61
28	19.83	19.96	19.78	19.83
30	21.96	22.09	21.92	21.97
32	24.02	24.10	24.03	24.06
34	26.00	26.11	26.08	26.08
36	27.88	28.07	28.05	28.05
38	29.68	29.96	29.91	29.86
40	31.43	31.76	31.68	31.68
42	33.12	33.47	33.36	33.40
44	34.75	35.10	34.98	35.02
46	36.22	36.65	36.55	36.59
48	37.87	38.20	38.06	38.10
50	39.55	39.66	39.50	39.55
55	42.86	43.01	42.81	42.85
60	46.06	46.02	45.88	45.84
65	48.95	48.62	48.65	48.58
70	51.47	50.96	51.24	51.09
75	53.58	53.01	53.52	53.44
80	55.28	54.85	55.85	55.70

x) extrapolated values.

favourably with those of refs. 12-15. Because of the good agreement of our copper data with literature values we feel that the present results on benzoic acid are an additional indication that the extrapolated values given by Furukawa *et al.* [11] are not correct.

7. Conclusions. The conclusion that can be drawn from the high-purity copper and benzoic acid test measurements is that with the experimental set-up used in this work, heat capacities can be determined accurately in the extended temperature range between 1.3 and 80 K. Naturally with crystals the accuracy attained will depend on the thermal behaviour of the particular sample, which may be quite different in the respective temperature regions. The systematic error in the absolute values of the specific heat, which are due to inaccuracies in the thermometer calibration, etc. may, however, be estimated to be less than two per cent.

The obtained accuracy in the final result will of course also depend on the ratio of the heat capacities of the empty and filled sample container. Typical values for this ratio cannot be given, as these are strongly dependent on the particular salt. Since the specific heat of benzoic acid is featureless down to the lowest temperatures achieved in this research, the comparison made in this case can be seen as a very unfavourable one with respect to the ratio. With a sample of 9.13 g of benzoic acid, and a sample holder, as described in section 2, which includes the thermometer and the heater, we found for the ratio C(sample holder)/C(sample holder + sample), 0.11, 0.11, 0.11, 0.20, 0.26 and 0.30 at T = 5, 10, 20, 40, 60 and 80 K, respectively. Thus, although throughout this work only relatively small amounts of salt were used (about 10 g), errors in the empty container heat capacity do not contribute significantly to the final results.

References

1 Boerstoel, B.M., Van Dissel, W.J.J. and Jacobs, M.B.M., Physica 38 (1968) 287, Commun. Kam. Onnes Lab., Leiden, No. 363a.

2 Ferreira da Silva, J., Thesis, Leiden (1967).

3 Keesom, W.H. and Kok, J.A., Proc. Kon. Nederl. Akad. Wet., Amsterdam 35 (1932) 294; Suppl. No. 219c, Commun. Kam. Onnes Lab., Leiden; Kok, J.A., Thesis, Leiden (1935).

4 Star, W.M., Van Dam, J.E. and Van Baarle, C., J. Phys. E2 (1969) 257.

5 Van Scherpenzeel, W.J., T.H. Delft (1964).

6 Brickwedde, F.G., Van Dijk, H., Durieux, M., Clement, J.R. and Logan, J.K., J. Res. Natl. Bur. Std., 64A (1960) 1.

7 Durieux, M., Van Dijk, H., Ter Harmsel, H. and Van Rijn, C., Temperature, its measurement and control in science and industry, (Rheinhold, New York, 1963), Vol. 3, p. 383.

8 The International Practical Temperature Scale of 1968, Metrologia 5 (1969) 35.

9 Furukawa, G.T., Saba, W.G. and Reilly, M.L., National Standards Reference Data Series - Natl. Bur. Std., 18 (1968).

10 Osborne, D.W., Flotow, H.E. and Schreiner, F., Rev. Sci. Instr., 38 (1967) 159.

11 Furukawa, G.T., McCoskey, R.E. and King, G.J., J. Res. Natl. Bur. Std., 47 (1951) 256.

12 Clay, R.M. and Staveley, L.A.K., Trans Faraday Soc. (G.B.), 62 (1966) 3065.

13 Sklyankin and Strelkov, Zhur. Priklad. Mech. Tech. Fiz., 2 (1960) 100.

14 Cole, A.G., Hutchens, J.O., Robie, R.A. and Stout, J.W., J. Am. Chem. Soc., 82 (1960) 4807.

15 Osborne, D.W., Westrum jr., E.F. and Lohr, H.R., J. Am. Chem. Soc., 77 (1955) 2737.

CHAPTER III

SPECIFIC HEAT OF HYDRAZINIUM-TRANSITION METAL-SULFATE LINEAR CHAIN COMPOUNDS

Abstract. Specific heat data in the temperature range of 1.3 K to 80 K are presented on polymeric $M(II)(N_2H_5)_2(SO_4)_2$ compounds where M(II) = Cu, Ni, Co, Fe and Mn. Broad maxima in the magnetic specific heat, pointing to magnetic linear chain exchange interactions, are observed. For the Co, Fe and Mn compounds, λ-like anomalies have also been observed which are indicative of the onset of three dimensional long-range spin ordering. From the specific heat measurements information is obtained about the anisotropy of the intrachain exchange interaction, single-ion anisotropy and the magnitudes of the intrachain and interchain interaction parameters of these compounds. The results on the Cu and Mn compounds were fitted to the antiferromagnetic Heisenberg linear chain model with spin $\frac{1}{2}$ and $\frac{5}{2}$, respectively. Although this model yields reasonable fits, deviations were observed near the maxima of the curves. For the Cu compound this is ascribed to anisotropy in the exchange interactions and for the Mn compound to interchain coupling effects. In order to fit the data on the Ni and Fe compounds it was found necessary to introduce single-ion anisotropy. The results for the Ni compound were fitted to the Ising spin $\frac{1}{2}$ linear chain model with in addition a Schottky curve, and to recent calculations for the spin 1 antiferromagnetic Heisenberg linear chain model with in addition uniaxial single-ion anisotropy. The exchange parameter J/k is found to be much smaller than the zero-field splitting parameter D/k, thus giving rise to Ising properties of the spins at low temperatures. The Co compound was found to exhibit anisotropic exchange interactions which are, in contrast to what is generally found for Co^{2+}, of the planar type. The results were fitted to the spin $\frac{1}{2}$ antiferromagnetic XY linear chain model, as calculated by Katsura, with an exchange parameter J/k = -7.05 K.

1. Introduction. As part of a research program on compounds that exhibit predominantly linear chain exchange interactions between magnetic moments of ions with various spin values, we have considered it to be a

matter of interest to investigate the thermal properties of a series of polymeric compounds with general formula $M(II)(N_2H_5)_2(SO_4)_2$ where M(II) = Cu, Ni, Co, Fe and Mn. An important property of this series of compounds which provides an additional incentive is that they exhibit X-ray powder isomorphism. Further, the spin values of the 3d metal ions for this series range from $S=\frac{1}{2}$ up to $S=\frac{5}{2}$. This research program was carried out in collaboration with Reedijk [1] and Witteveen [2] who investigated closely related properties of this series by means of spectroscopic and magnetic measurements. The thermal and magnetic properties of systems with magnetic ions coupled in (infinite) linear chains by nearest neighbour exchange interactions have been the subject of several experimental studies especially during the last decade. An extensive review including this subject was published by De Jongh *et al.* [3]

Theoretically the many-particle problem of the magnetic linear chain has been treated for various spin values. Exact and accurate numerical results for the thermal and magnetic properties have been obtained particularly for $S=\frac{1}{2}$. When the exchange interactions are restricted to nearest neighbours only, the linear chain hamiltonian is usually written as

$$H = -2J\sum_{i=1}^{N}\{a(S_{i,x}S_{i+1,x} + S_{i,y}S_{i+1,y}) + b(S_{i,z}S_{i+1,z})\}. \qquad (1.1)$$

Here J is the exchange parameter which is negative for antiferromagnetic and positive for ferromagnetic interaction; N is the number of atoms contained in the chain and a and b are the anisotropy parameters. The cartesian components of the spin angular momentum of the i-th atom are denoted as $S_{i,j}$ (j = x,y,z). The majority of the one dimensional models for which theoretical results have been obtained are included in eq. (1.1). Thus when a = b = 1, the hamiltonian denotes the isotropic Heisenberg model, while the interaction is anisotropic when $a \neq b$. As special cases we mention the Ising model (a = 0 and b = 1), and the so called XY model or transverse coupled model (a = 1 and b = 0). The thermodynamic quantities of systems described by eq. (1.1) are continuous functions of the temperature T. This is reflected in the specific heat by a broad maximum, due to a gradual development of short-range order with decreasing temperature. It may be noted that linear chain short-

range exchange interactions cannot support long-range order at any temperature $T > 0$ K [4]. In real, three-dimensional crystals interactions between magnetic ions in adjacent chains are not negligible. This usually gives rise to the onset of 3-d long-range spin ordering at a temperature, $T_c \neq 0$, resulting in a λ-like anomaly in the specific heat. It has, however, been shown [3] that even if interactions between magnetic chains, the interchain interactions, are of importance, the thermodynamic properties for temperatures well above T_c can be described satisfactorily with one-dimensional models, provided $|J'/k| \ll |J/k|$ where J'/k is the interchain and J/k the intrachain exchange constant (cf eq. (1.1)).

The crystal structure of the hydrazinium metal sulfates has been established by X-ray diffraction and spectroscopic methods. Hand and Prout [5] reported that the X-ray powder diffraction patterns of $Co(N_2H_5)_2(SO_4)_2$ and $Ni(N_2H_5)_2(SO_4)_2$ are similar to that of $Zn(N_2H_5)_2(SO_4)_2$. Nieuwpoort and Reedijk [1] found that the X-ray powder diffraction patterns of $Mn(N_2H_5)_2(SO_4)_2$ and $Fe(N_2H_5)_2(SO_4)_2$ were also similar to that of the Zn compound, in accordance with their spectroscopic results on the series of $M(N_2H_5)_2(SO_4)_2$ compounds with M = Ni, Co, Fe, Mn and Zn. Slight differences in the X-ray powder diffraction patterns were observed for $Cu(N_2H_5)_2(SO_4)_2$ (refs. 1,5).

A study of the crystal structure of $Zn(N_2H_5)_2(SO_4)_2$ has been carried out by Prout and Powell [6]. The compound crystallizes in the triclinic system, space group $P\bar{1}$, $Z = 1$ (see fig. 1). The Zn ions are surrounded by four oxygens of the SO_4 groups and two monodentate N_2H_5 groups, which complete the irregular octahedral co-ordination. The distances around the Zn-ions are: Zn-N: 2.08 Å and Zn-O: 2.10 Å and 2.38 Å. The SO_4 groups bridge two different Zn ions, yielding infinite chains of $-Zn\ (O - SO_2 - O)_2\ Zn$ units along the crystal b-axis. Within the chains the Zn-Zn distance amounts to 5.3 Å. The chains are mutually linked via the N_2H_5 ligands through hydrogen bonds formed between the N_2H_5 groups of one chain and oxygens of the SO_4 groups in adjacent chains. The distances between the magnetic ions are rather large, thus direct exchange interactions should be of minor importance. Along the chains, however, superexchange can take place via the bridging SO_4 groups and although the separation between the chains is only slightly

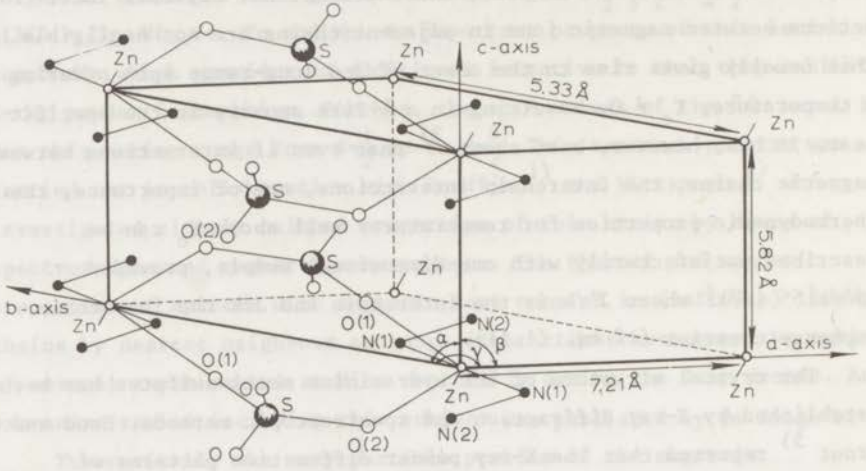

Fig. 1. *Structure of* $Zn(N_2H_5)_2(SO_4)_2$ *according to Prout and Powell* [6]. $\alpha = 99^{\circ}42'$, $\beta = 87^{\circ}27'$, $\gamma = 105^{\circ}42'$. *The chemical linear chain axis (b-axis) is approximately 10 per cent shorter than the a-axis. The compounds* $M(N_2H_5)_2(SO_4)_2$ *with M = Ni, Co, Fe and Mn are powder X-ray isomorphous with* $Zn(N_2H_5)_2(SO_4)_2$ *(refs. 1,5).*

larger than the intrachain distances between the metal ions, the more complicated superexchange pathways between the chains are expected to allow rather well-isolated magnetic linear chains in these materials. Susceptibility results on powdered samples of these series of compounds, reported by Witteveen [2], support the idea of predominantly linear chain exchange interactions in these materials.

2. Experimental. 2.1 Sample preparation. The compounds $M(N_2H_5)_2(SO_4)_2$ with M = Cu, Ni, Co, Fe and Mn were each prepared by adding a hot aqueous solution of the metal sulfate to a hot aqueous solution of $N_2H_6SO_4$ (ratio MSO_4: $N_2H_6SO_4$ = 1 : 2) (see refs. 1,5, 6). The compounds $M(N_2H_5)_2(SO_4)_2$ immediately separated as powders with the exception of the Mn compound, where cooling down to about 10° C was necessary to obtain the solid compound. The powders were collected on a glass filter, washed with water, ethanol and ether and finally dried in vacuo (0.1 torr at

about 40° C). The purity of the samples was checked by metal analysis. The results are listed in table I.

TABLE I

Metal analysis of the compounds $M(N_2H_5)_2(SO_4)_2$

	% metal (meas.)	% metal (calculated)
$Cu(N_2H_5)_2(SO_4)_2$	19.68	19.75
$Ni(N_2H_5)_2(SO_4)_2$	19.0	18.5
$Co(N_2H_5)_2(SO_4)_2$	17.9	18.5
$Fe(N_2H_5)_2(SO_4)_2$	18.2	17.8
$Mn(N_2H_5)_2(SO_4)_2$	17.9	17.5

2.2 Apparatus. The specific heat measurements were performed on powdered samples in an adiabatic calorimeter using the standard heat pulse method. The sample holders consisted mainly of copper and were gold-plated to avoid chemical reactions of the samples with the calorimeter can. A mechanical heat switch provided thermal contact between the calorimeter and the cooling liquids. Our procedure avoided the use of any helium exchange gas. To improve the internal thermal contact the powdered samples were pressed hydraulically into the calorimeter, which was provided with gold-plated copper vanes, hard soldered on the inner side of the calorimeter can. Because of the powerful compression of the samples, each sample holder could be used only once. The heat capacity of the empty calorimeter cans was determined in separate measuring runs. A typical value of the amount of specimen used in this series of measurements is 0.035 mole. This corresponds to approximately 1.5 times the weight of the empty calorimeter can. We shall discuss elsewhere [8] the punch tape procedure for recording the data on the sample thermal equilibrium periods, both before and after the heat is supplied to the calorimeter, along with the heater current and voltage, the heating time and the carbon thermometer resistance [7].

3. Experimental specific heat results. 3.1 General. The heat capacities of the compounds $Cu(N_2H_5)_2(SO_4)_2$, $Ni(N_2H_5)_2(SO_4)_2$, $Co(N_2H_5)_2(SO_4)_2$, $Fe(N_2H_5)_2(SO_4)_2$ and $Mn(N_2H_5)_2(SO_4)_2$ have been measured in the temperature range between 1.3 K and 80 K. The results are shown in figs. 2-6.

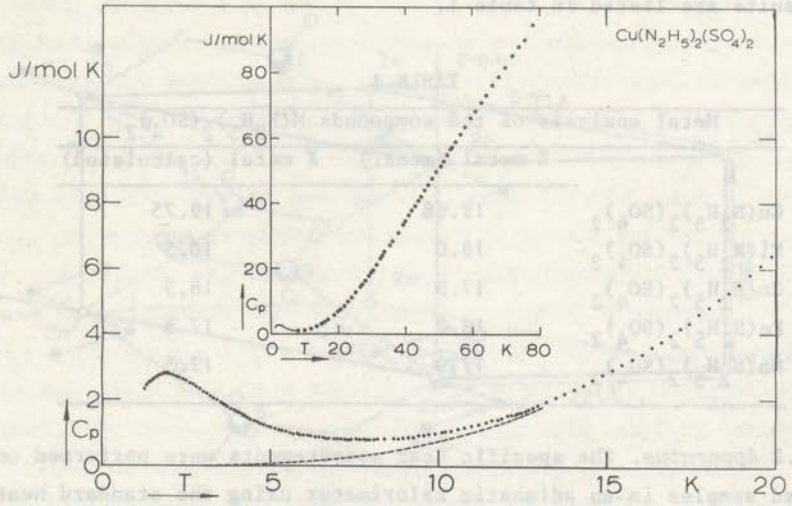

Fig. 2. *The experimental specific heat of $Cu(N_2H_5)_2(SO_4)_2$ as a function of temperature. The dashed line represents the estimated lattice specific heat, C_l. The high-temperature data (up to 80 K) are indicated in the inset.*

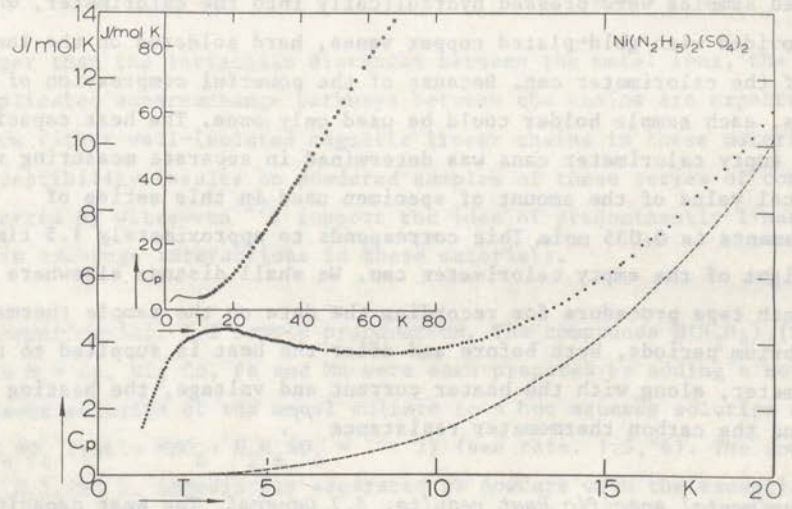

Fig. 3. *The experimental specific heat of $Ni(N_2H_5)_2(SO_4)_2$ as a function of temperature. The dashed line represents the estimated lattice specific heat, C_l. The high-temperature data are indicated in the inset.*

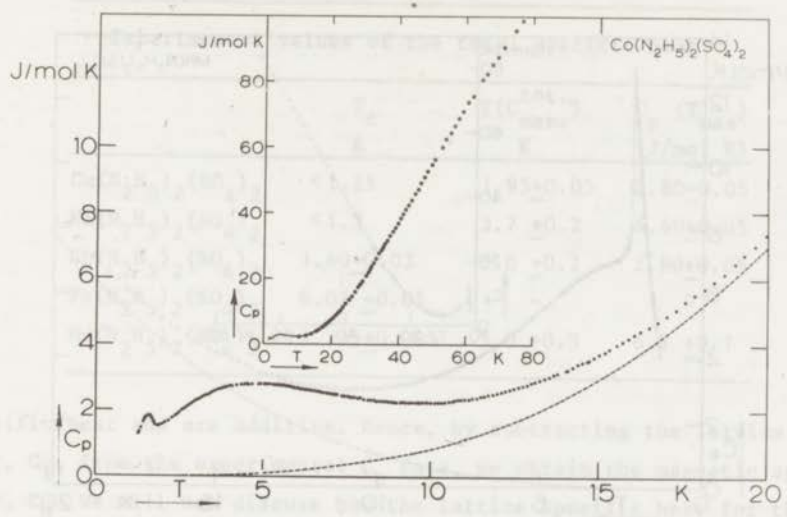

Fig. 4. *The experimental specific heat of* $Co(N_2H_5)_2(SO_4)_2$ *as a function of temperature. The dashed line represents the estimated lattice specific heat,* C_l. *The high-temperature data are indicated in the inset.*

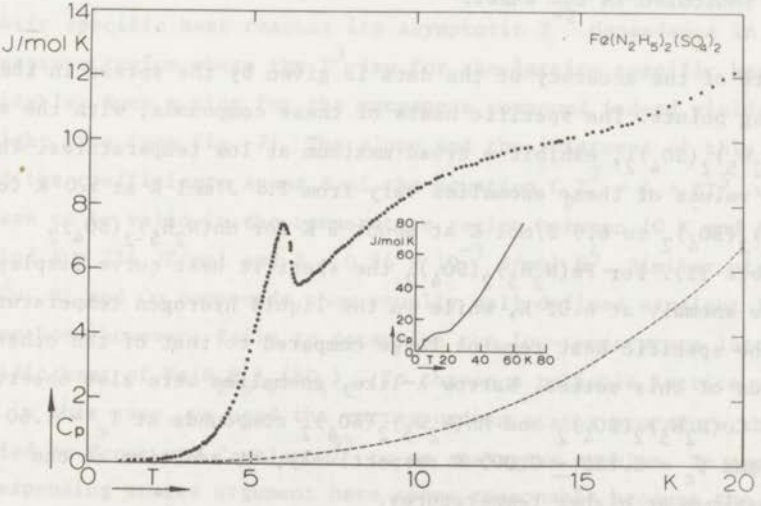

Fig. 5. *The experimental specific heat of* $Fe(N_2H_5)_2(SO_4)_2$ *as a function of temperature. The dashed line represents the lattice specific heat,* C_l. *The high-temperature results are represented by the full line in the inset.*

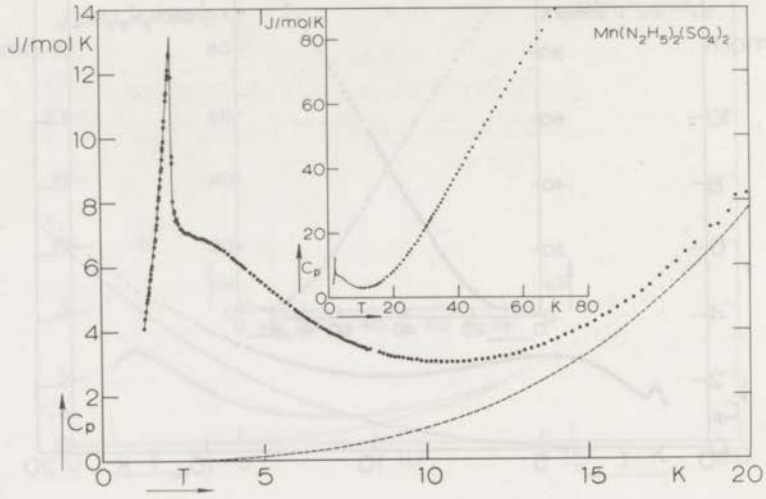

Fig. 6. *The experimental specific heat of* $Mn(N_2H_5)_2(SO_4)_2$ *as a function of temperature. The dashed line represents the estimated lattice specific heat,* C_l*. The high-temperature data (up to 80 K) are indicated in the inset.*

A measure of the accuracy of the data is given by the spread in the measuring points. The specific heats of these compounds, with the exception of $Fe(N_2H_5)_2(SO_4)_2$, exhibit a broad maximum at low temperatures. The maximum values of these anomalies vary from 2.8 J/mol K at 5.0 K for $Co(N_2H_5)_2(SO_4)_2$ to 6.9 J/mol K at about 3 K for $Mn(N_2H_5)_2(SO_4)_2$ (see table II). For $Fe(N_2H_5)_2(SO_4)_2$ the specific heat curve displays a narrow anomaly at 6.02 K, while in the liquid hydrogen temperature range the specific heat remains large compared to that of the other compounds of this series. Narrow λ-like, anomalies were also observed for the $Co(N_2H_5)_2(SO_4)_2$ and $Mn(N_2H_5)_2(SO_4)_2$ compounds at $T_c = 1.60 \pm 0.03$ K and $T_c = 2.155 \pm 0.005$ K respectively, in addition to the broad maximum at higher temperatures.

3.2 Lattice specific heats of the $M(N_2H_5)_2(SO_4)_2$ *compounds.* In order that we may subtract a lattice specific heat, we assume, as is generally done, that the lattice and the spin system contribute separately to the

TABLE II

Experimental values of the total specific heat

	T_c K	$T(C^{tot.}_{max.})$ K	C_p (T_{max}) (J/mol K)
$Cu(N_2H_5)_2(SO_4)_2$	<1.25	1.95±0.05	2.80±0.05
$Ni(N_2H_5)_2(SO_4)_2$	<1.3	3.7 ±0.2	4.40±0.05
$Co(N_2H_5)_2(SO_4)_2$	1.60±0.03	5.0 ±0.2	2.80±0.05
$Fe(N_2H_5)_2(SO_4)_2$	6.02 ±0.05	-	-
$Mn(N_2H_5)_2(SO_4)_2$	2.155±0.005	3.0 ±0.5	6.9 ±0.1

specific heat and are additive. Hence, by subtracting the lattice specific heat, C_l, from the experimental C_p data, we obtain the magnetic specific heat, C_M. We will now discuss how the lattice specific heat for the various compounds has been determined. The lattice specific heat of many compounds at low temperatures generally obeys the Debye T^3-law to good approximation. On the other hand, magnetic insulators exhibit an asymptotic high-temperature contribution $C_M \alpha\ T^{-2}$ behaviour. A plot of C_pT^2 versus T^5 should give rise to a straight line if the high-temperature tail of the magnetic specific heat reaches its asymptotic T^{-2} dependence in a temperature region where the T^3-law for the lattice specific heat is applicable. Such a plot for the manganese compound indeed yields a straight line (see fig. 7). The slope and the intercept of this line yield the coefficients A and B of the equation $C_pT^2 = A + BT^5$, which is seen to be valid in the temperature region between 10 K and 15 K. We find A = 214 JK/mol and B = 0.96×10^{-3} J/mol K^4. Similar plots for the Cu, Ni and Co compounds show equally well defined straight lines. The method, however, fails to determine the low-temperature lattice specific heat of $Fe(N_2H_5)_2(SO_4)_2$. To obtain a reliable lattice specific heat in this case, we used the corresponding states procedure that was applied by Stout and Catalano [9] to an analogous problem. To apply the corresponding states argument here seems reasonable because the investigated hydrazinium sulfates are isomorphous (or at least isostructural) and the only ions that are different all belong to the 3d-group and have very similar chemical and physical properties. The

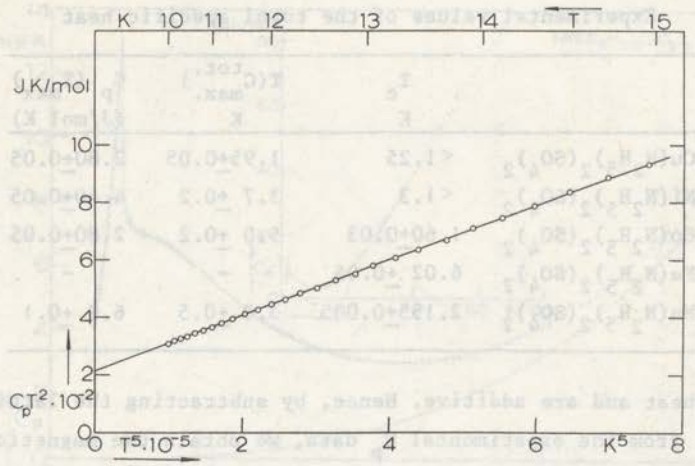

Fig. 7. *The specific heat of* $Mn(N_2H_5)_2(SO_4)_2$ *plotted as* C_pT^2 *versus* T^5. *The straight line corresponds to* $C_pT^2 = A + BT^5$ *with* $A = 214$ *JK/mol and* $B = 0.96 \times 10^{-3}$ *J/mol* K^4.

lattice specific heat C_l, for the compounds may then be written as:

$$C_l = f(T/b)$$

where f is a function that is the same for all compounds and b is a constant characteristic of a given compound. It has been verified experimentally that for the Cu, Ni and Mn compounds the law of corresponding states is, within experimental error, obeyed over a wide temperature region, ranging up to the highest temperature experimentally obtained here. Comparing the high-temperature specific heat data for $Fe(N_2H_5)_2(SO_4)_2$ with those of $Cu(N_2H_5)_2(SO_4)_2$ the ratio b(Fe)/b(Cu) = 1.020 is found. Using this value the lattice specific heat for $Fe(N_2H_5)_2(SO_4)_2$, as shown in fig. 5, is obtained. The coefficients of the T^3-law for the lattice specific heats are collected in table III.

TABLE III

Experimental results for the magnetic specific heat and related quantities

	Lattice T^3-coeff. (mJ/mol K^4)	$T(C_{max})$ K	C_{max} J/mol K	ΔS J/mol K	$\Delta S(T_c)$ J/mol K	$\Delta E(T_c)$ J/mol	$T(\chi_{max})$ K	$T(\chi_{max})/T(C_{max})$
$Cu(N_2H_5)_2(SO_4)_2$	0.785	1.95±0.05	2.80±0.05	5.6±0.1	<1.8	<1.4	2.1±0.2 [a]	1.15±0.05
$Ni(N_2H_5)_2(SO_4)_2$	1.25	3.5 ±0.1	4.30±0.05	9.1±0.1	<0.4	<0.5	8.7±0.2 [a]	2.5 ±0.1
$Co(N_2H_5)_2(SO_4)_2$	0.834	4.8 ±0.1	2.70±0.05	5.7±0.1	0.9	1.0	5.7±0.2 [a]	1.2 ±0.1
$Fe(N_2H_5)_2(SO_4)_2$	0.836	11.7 ±0.2	8.0 ±0.1	13.2±0.2	1.7	8.7	15.3±0.2 [a]	1.3 ±0.1
$Mn(N_2H_5)_2(SO_4)_2$	0.960	~2.5	~6.8	14.5±0.3	5.3	8.8	4.8±0.2 [a]	~1.6

[a] ref. 2

4. Magnetic specific heat and discussion. 4.1 $Cu(N_2H_5)_2(SO_4)_2$. The magnetic specific heat C_M obtained after subtraction of the lattice contribution from the experimental C_p data, is shown as a function of temperature in fig. 8. The curve displays a broad peak with a maximum value for C_M of 2.80 ± 0.05 J/mol K at $T(C_{max})$ = 1.95 ± 0.10 K. In the temperature region below 2 K the scatter in the measured points increases due to poor heat conductivity in the powdered sample, but we believe that a smooth line through the data represents the magnetic specific heat of the material fairly well.

In order to determine the total magnetic entropy $\Delta S = \int_0^\infty \frac{C_M}{T} dT$ and energy $\Delta E = \int_0^\infty C_M \, dT$, the curve has to be extrapolated to both T = ∞ and T = 0 K. For the high-temperature extrapolation the result of the $C_p T^2$ versus T^5 plot, giving $C_M T^2$ = 24 ± 1 JK/mol was used. Numerical integration of the C_M/T data in the temperature region 1.25 < T < 10 K with respect to temperature amounts to 3.52 J/mol K for the entropy gain. As no experimental data were obtained below 1.2 K, approximately $\frac{3}{5}$ of the value of $T(C_{max})$, large errors, especially in ΔS, may result from the extrapolation to T = 0 K. Therefore, we have used below 1.2 K the theoretical results for an isotropic Heisenberg S=½ antiferromagnetic linear chain system with exchange constant J/k = −1.99 K (vide infra). In this way a total magnetic entropy content ΔS = 5.6 ± 0.1 J/mol K is obtained, of which 33 per cent is estimated below 1.2 K. The value

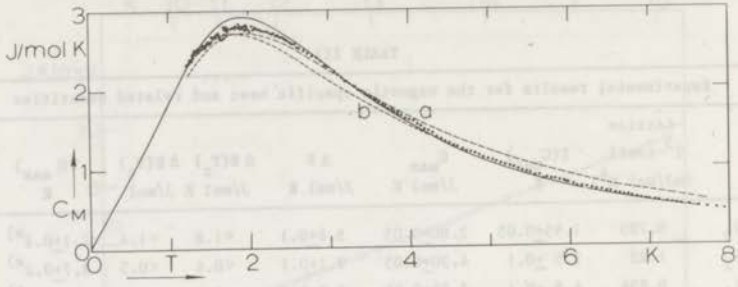

Fig. 8. *The magnetic specific heat* C_M *of* $Cu(N_2H_5)_2(SO_4)_2$ *versus T.*
..... *experimental results.*
——— *Heisenberg linear chain model for S=½, as calculated by Bonner and Fisher* [10]; *J/k = -1.99 K.*
- - - *Transverse coupled linear chain model* ($J_{//} = 0$; $J_{\perp} = J$) *for S=½, as calculated by Katsura* [24]; *a:* $|J/k| = 3.08$ *K, b:* $|J/k| = 2.88$ *K.*

of ΔS is close to the theoretical value for a spin $S=\frac{1}{2}$ system: $R\ln(2S + 1) = R\ln 2 = 5.69$ J/mol K. The total estimated magnetic energy, following a similar procedure, is $\Delta E = 14.4 \pm 0.4$ J/mol K. The broad maximum in the C_M versus T curve is characteristic of a system in which the entropy is removed by short-range order processes as the temperature decreases. This points to the existence of important linear chain exchange interactions in this compound, consistent with the crystal structure. Since the single-ion groundstate of the Cu^{2+} ions is, due to the low symmetry of the crystalline field, an orbital singlet, $^2B_{1g}$, with a two fold Kramers spin degeneracy, one would expect linear chain exchange interactions in $Cu(N_2H_5)_2(SO_4)_2$ to be fairly isotropic. Bonner and Fisher [10] have calculated the specific heat for this model with spin $S=\frac{1}{2}$. The best fit of the experimental data is obtained for $J/k = -1.99 \pm 0.02$ K (see eq. (1.1)). As can be seen from fig. 8 the agreement is good for both the high and low temperature portions of the curve. Near the maximum, however, the experimental data are lower than the calculated curve by as much as 4 per cent. The value of $J/k = -1.99$ K

is compatible with $|J/k| = 1.96 \pm 0.05$ K derived from a comparison of the total magnetic energy $\Delta E = 14.4 \pm 0.04$ J/mol and the theoretical zero-point energy $\frac{E}{N|J|} = -0.8863$ (ref. 11) as obtained for an isotropic Heisenberg antiferromagnetic linear chain.

Information on the intrachain exchange constant is also obtained from the susceptibility measurements [2)4)]. Above T = 4 K the results could be well-described with the isotropic Heisenberg linear chain model with $J/k = -2.0 \pm 0.1$ K and $g_{av} = 2.11$. Below 4 K, where a maximum in the susceptibility occurs, the agreement was poor. Therefore, to explain the discrepancies between theory and experiment as found in both the specific heat and the susceptibility results, one would like to introduce some anisotropy to the exchange interaction.

As there are no theoretical calculations available for the intermediate case a = 1, b < 1 (eq. (1.1)), we will compare our results with the XY model (a = 1, b = 0) for two values of the intrachain exchange constant, viz. $|J/k| = 3.08$ K and $|J/k| = 2.88$ K. From fig. 8 it may be seen that the experimental curve has a maximum in C_M which is below the Heisenberg model and above the XY model results. The discrepancies between the experimental curve and the two calculations are of the same order of magnitude but for the XY model they extend over a larger temperature region. It is interesting to notice that the experimental ratio $T(\chi_{max})/T(C_{max})$ amounts to 1.15 ± 0.05 while the theoretical values for this ratio are 1.33 [3)] and 1.0 [3)] for the $S=\frac{1}{2}$ antiferromagnetic Heisenberg and XY models, respectively. Anisotropic exchange interaction, probably of the Dzyaloshinski-Moriya type (refs. 13, 14) may also play a role in $Cu(N_2H_5)_2(SO_4)_2$. From the fact that $Cu(N_2H_5)_2(SO_4)_2$ is not strictly isomorphous with the Zn compound, and no crystal structure data are thus far reported for $Cu(N_2H_5)_2(SO_4)_2$ one cannot exclude the possible occurrence of a D.M. term in the exchange hamiltonian.

4.2 $Ni(N_2H_5)_2(SO_4)_2$. The magnetic specific heat of the compound $Ni(N_2H_5)_2(SO_4)_2$ is shown as a function of temperature in figs. 9 and 10. The curve displays a broad peak with a maximum value of $C_M = 4.30 \pm 0.05$ J/mol K at $T(C_{max}) = 3.7 \pm 0.2$ K. The magnetic entropy and energy content were again determined by numerical integration of

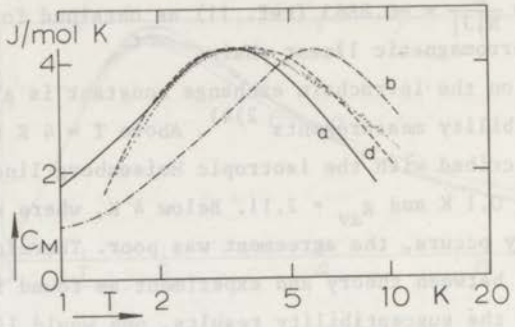

Fig. 9. *The magnetic specific heat, C_M, of $Ni(N_2H_5)_2(SO_4)_2$ as a function of temperature (semi logarithmic plot).*

..... *experimental results.*

——— *a) Heisenberg linear chain model, as calculated by Weng* [15] *for S=1; J/k = -2.4 K.*

-.-.- *b) Heisenberg linear chain model, as calculated by Weng* [15] *for S=1; J/k = -3.3 K* [2]

- - - *d) Ising linear chain model with uniaxial single-ion anisotropy as calculated by Kowalski* [18] *for S=1; J/k (Ising, S=1) = -1.4 K and D/k = -12.3 K.*

the C_M data with respect to temperature. For the extrapolation to high temperatures it was assumed that the specific heat is adequately described by a single term $C_M = b/T^2$, where b = 340 ± 20 JK/mol, which is obtained from a C_pT^2 versus T^5 plot. In the low-temperature region we made use of the fact that a plot of $\ln(C_MT^2)$ versus 1/T (see fig. 11) results in a straight line in the temperature range 1.25 K< T< 2.5 K. This corresponds to the exponential relation, $C_M = AT^{-2} \exp(-B/T)$ with A = 320 JK/mol and B = 6.4 K. The total magnetic entropy for $Ni(N_2H_5)_2(SO_4)_2$ obtained in this way is 9.1 ± 0.1 J/mol K which is close to the theoretical value Rln(2S + 1) = Rln3 = 9.13 J/mol K for a spin S=1 system. In the same fashion the total magnetic energy has been determined as ΔE = 67 ± 3 J/mol. The broad maximum of the C_M vs. T

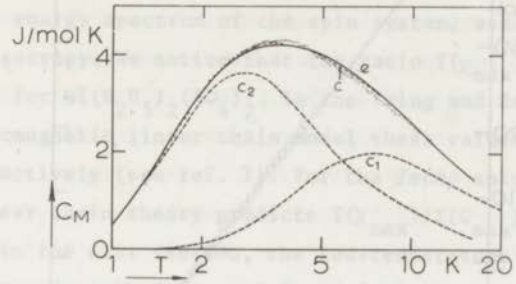

Fig. 10. *The magnetic specific heat, C_M, of $Ni(N_2H_5)_2(SO_4)_2$ as a function of temperature (semi logarithmic plot).*

..... *experimental results.*

----- c_1: *Schottky anomaly for independent ions with single-ion anisotropy; D/k = -15.3 K.*

- - - c_2: *Ising linear chain model, S=½; $|J/k(S=½)| = 6.3$ K.*

---- *c : The sum of c_1 and c_2. This curve coincides for the greater part with the full line (e).*

——— *e : Heisenberg linear chain model with uniaxial single-ion anisotropy as calculated by Blöte* [19] *for S=1; J/k(S=1) = -1.56 K and D/k = -15.6 K.*

curve, together with the absence of a λ-like anomaly above T = 1.3 K indicates a high degree of short-range order in this material. In fact, the entropy variation between T = 1.25 K (i.e. $T > T_c$) and T = ∞ amounts to 8.7 J/mol K which corresponds to a very large value, 93 per cent of Rln3.

From susceptibility measurements [2], an asymptotic Curie-Weiss constant of -9.5 ± 0.5 K was derived. Thus it appears that antiferromagnetic exchange interactions predominate in this compound. The experimental susceptibility data in the temperature range 2 K < T < 80 K were fitted within experimental error to the calculations of Weng [15] for the S=1 antiferromagnetic isotropic Heisenberg linear chain model,

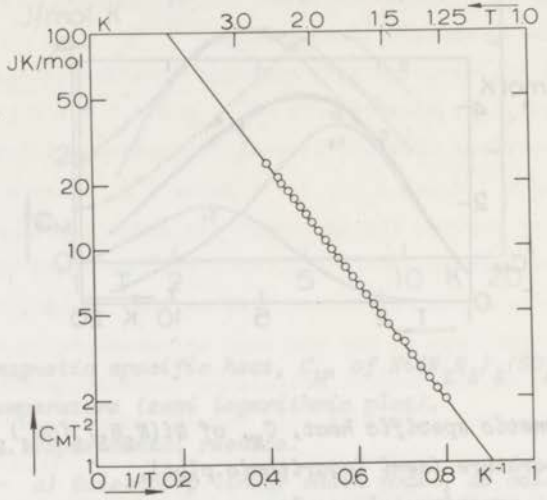

Fig. 11. *The low-temperature magnetic specific heat of* $Ni(N_2H_5)_2(SO_4)_2$ *plotted as* $C_M T^2$ *versus* $1/T$. *The straight line represents the fit* $C_M = AT^{-2}\exp(-B/T)$ *with* $A = 320$ *JK/mol and* $B = 6.4$ *K.*

yielding values for the intrachain exchange constant and the spectroscopic splitting factor of $J/k = -3.3 \pm 0.1$ K and $g = 2.17$, respectively. Weng [15] also calculated the specific heat as a function of temperature for this model. He finds for the relation between $T(C_{max})$ and J/k

$$\frac{kT(C_{max})}{|J|} \simeq 1.5 \qquad (4.1)$$

Using the experimental value of $T(C_{max}) = 3.7 \pm 0.2$ K we obtain $J/k = -2.4 \pm 0.1$ K, which differs considerably from the value derived from the susceptibility measurements. Full curves with values for J/k of -3.3 K and -2.4 K are shown in fig. 9. From this figure it is clear that neither curve fits the experimental C_M data within the experimental accuracy. Agreement is obtained only for the values of C_{max}: calculated $C_{max} = 4.3$ J/mol K, experimental $C_{max} = 4.30 \pm 0.05$ J/mol K.

The spin wave theory calculations [16] predict for an antiferro-

magnetic linear chain system a linear temperature dependence of C_M in the low-temperature region. It, therefore, seems probable that the exponential temperature dependence of C_M, as experimentally observed in the temperature range 1.25 K < T < 2.5 K, implies the existence of a gap in the energy spectrum of the spin system, associated with magnetic anisotropy. We notice that the ratio $T(\chi_{max})/T(C_{max})$ amounts to 2.5 ± 0.1 for $Ni(N_2H_5)_2(SO_4)_2$. In the Ising and Heisenberg spin S=1 antiferromagnetic linear chain model these values are 1.83 (for $\chi_{//}$) and 1.5 respectively (see ref. 3). For the *Ising* spin S=½ antiferromagnetic linear chain theory predicts $T(\chi_{max})/T(C_{max}) = 2.3$ [3]. In fact, as is shown in the next section, the low-temperature specific heat is probably better described by an Ising spin ½ linear chain model. It appears reasonable to attribute the anisotropy in the exchange to the presence of single-ion anisotropy in this compound.

4.2.1 Ni^{2+} single-ion anisotropy. The Ni^{2+} ion has the electronic configuration $3d^8$. The ^3F ground state of the free Ni^{2+} ion splits in an octahedral co-ordination into an orbital singlet, $^3A_{2g}$, and two triplets, $^3T_{2g}$ and $^3T_{1g}$, with the $^3A_{2g}$ state lowest. Through the combined action of spin-orbit coupling and non-cubic symmetry of the crystalline field the triply degenerate $^3A_{2g}$ level is split through second-order perturbation with higher states. For axial distortion of the crystalline field the anisotropy may be described by a term DS_z^2 in the spin hamiltonian. When the symmetry is lower (rhombic) a term $E(S_x^2 - S_y^2)$ has to be added. From infrared spectroscopic results on the $M(N_2H_5)_2(SO_4)_2$ compounds Nieuwpoort and Reedijk [1] conclude that the rhombic distortions are small in comparison with the tetragonal distortions of the crystalline field in these materials. For $Ni(N_2H_5)_2(SO_4)_2$ these authors arrived at a compressed octahedral co-ordination structure, which would give rise to a non-Kramers spin doublet ground state. From the existing optical data the doublet-singlet separation was calculated to be less than 8 K [17].

4.2.2 Single-ion anisotropy and exchange interaction. We will consider here only the special case of J/k < 0 and D/k < 0, which is relevant for $Ni(N_2H_5)_2(SO_4)_2$. We will treat the limiting case that $|J/k| \ll |D/k|$. The specific heat of an assembly of isolated Ni^{2+} ions with only single-ion anisotropy results in the usual Schottky curve.

At temperatures lower than $|D/k|$, only the $S_z = \pm 1$ components have an appreciable expectation value. Hence, the introduction of exchange interactions with $|J/k| << |D/k|$ yields anisotropic exchange interactions (Ising) between ions with an effective spin $S'=\frac{1}{2}$. When we consider linear chain exchange interactions the specific heat of such a system may be approximated by the sum of two independent contributions: the Schottky term and an Ising $S'=\frac{1}{2}$ linear chain curve. Interpretation of the specific heat data in this manner yields a best fit for J/k ($S'=\frac{1}{2}$) = -6.38 K and D/k = -15.3 K (see fig. 10). In this figure the separate contributions (curves c_1 and c_2), as well as the sum (curve c) are shown.

Although the agreement between the experimental data and theory (curve c) is quite satisfactory, it is not clear *a priori* that $|J/k|$ is in fact sufficiently small to be able to treat the contributions separately. A complete treatment starts from the hamiltonian,

$$H = -2J\Sigma_{i=1}^{N}\{a(S_{i,x}S_{i+1,x}+S_{i,y}S_{i+1,y})+b\,S_{i,z}S_{i+1,z}\}+D\Sigma_{i=1}^{N}(S_{i,z}^{2}-\tfrac{1}{3}S(S+1)). \quad (4.2)$$

The only calculations based on this hamiltonian for S=1 with $J/k < 0$, thus far reported, are for the Ising limit, i.e. with a = 0, b = 1. Kowalski [18] has obtained results for the correlation function, susceptibility and specific heat within this model. From a fit of our data to both the maximum of the experimental curve and $T(C_{max})$, one obtains J/k (Ising, S=1) = -1.4 K and D/k = -12.6 K. The agreement with the experimental data is poor at high temperatures (see fig. 9) which is not surprising because one would expect the situation a = b = 1 to prevail for the orbital singlet, $^3A_{2g}$. We, therefore, suggested to perform calculations for the hamiltonian of eq. (4.2) with a = b = 1. Blöte [19] has obtained results for infinite chains by means of a suitable extrapolation of the results on finite chains (for rings N up to 7). The best fit with the experimental data was obtained for J/k(S=1) = -1.56 K and D/k = -15.6 K (see curve e, fig. 10). We notice that this curve, obtained for the S=1 isotropic Heisenberg linear chain model with uniaxial single-ion anisotropy and the curve which represents the sum of an Ising $S'=\frac{1}{2}$ linear chain and a Schottky anomaly are in close agreement; also the values for J/k and D/k agree quite well; J/k(Heis., S=1) = -1.56 K, D/k = -15.6 K and J/k(Ising, $S'=\frac{1}{2}$) = -6.38 K,

which corresponds with J/k(S=1) = -1.58 K, and D/k = -15.3 K.

The observed D/k value is quite large in comparison with the values generally observed in inorganic Ni^{2+} compounds, of 1 K to 10 K [20], although recently values up to D/k ≈ -30 K have been reported [21]. In order to have an independent experimental verification for the D/k value, spin-lattice relaxation measurements have been performed in the Kamerlingh Onnes Laboratory by Van Duyneveldt [22]. Preliminary results corroborate the large single-ion anisotropy in $Ni(N_2H_5)_2(SO_4)_2$.

4.3 $Co(N_2H_5)_2(SO_4)_2$. The discussion of the magnetic specific heat will be divided into two parts corresponding to the two temperature regions of interest.

4.3.1 Low temperature region (T < 20 K). The magnetic specific heat of $Co(N_2H_5)_2(SO_4)_2$, obtained after subtraction of the lattice contribution from the experimental C_p data, is shown in fig. 12 as a function of temperature. The curve displays two distinct features: a broad peak that

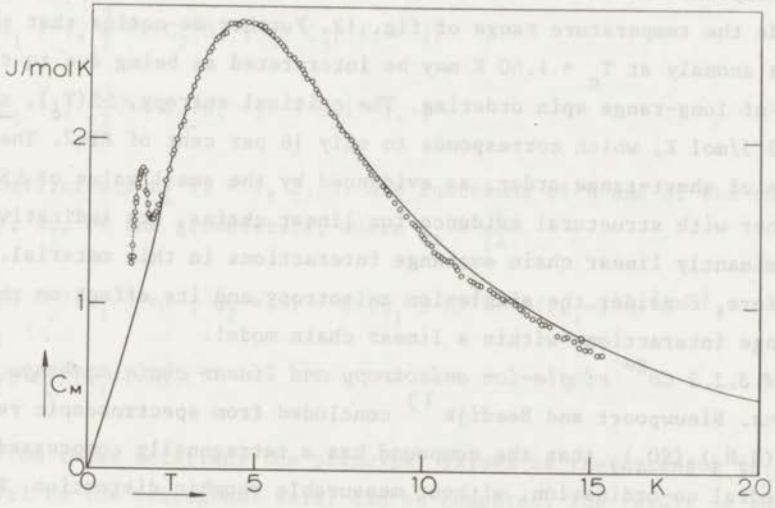

Fig. 12. *The magnetic specific heat, C_M, of $Co(N_2H_5)_2(SO_4)_2$ as a function of temperature.*
oooo experimental results.
—— Transverse coupled linear chain model ($J_{//} = 0$; $J_\perp = J$) as calculated by Katsura [25] for S=½; |J/k| = 7.05 K.

attains a maximum value of C_M = 2.70 ± 0.05 J/mol K at $T(C_{max})$ = 4.8 ± 0.1 K and an additional narrow peak, resembling a λ-like anomaly, at T_c = 1.60 K.

In order to draw, from these experiments, conclusions about the effective spin value of the Co^{2+} ion, the magnetic entropy has been determined. The entropy variation between T = 1.26 K and T = 15 K has been obtained by numerical integration of the C_M/T data with respect to temperature. The entropy content above T = 15 K has been calculated using the result of a C_pT^2 versus T^5 plot: C_MT^2 = 168 ± 5 JK/mol. The entropy content below T = 1.26 K has been determined by means of an extrapolation to T = 0 K, using a best fit to the data in the 1.26 K to T = 1.4 K temperature range. A value of ΔS = 0.58 J/mol K has been calculated for the entropy content below 1.26 K. The total entropy thus amounts to 5.7 ± 0.1 J/mol K. This value is sufficiently close to Rln2 = 5.76 J/mol K, the theoretical value for a spin ½ system, to conclude that the real spin $\frac{3}{2}$ of the Co^{2+} ions can be replaced by an effective spin S'=½ in this temperature region. The S'=½ effective spin value shows that this compound exhibits a crystalline field splitting which substantially exceeds the temperature range of fig. 12. Further we notice that the λ-like anomaly at T_c = 1.60 K may be interpreted as being due to the onset of long-range spin ordering. The critical entropy, $\Delta S(T_c)$, amounts to to 0.9 J/mol K, which corresponds to only 16 per cent of Rln2. The high degree of short-range order, as evidenced by the small value of $\Delta S(T_c)$, together with structural evidence for linear chains, are indicative of predominantly linear chain exchange interactions in this material. We, therefore, consider the single-ion anisotropy and its effect on the exchange interactions within a linear chain model.

4.3.1.1 Co^{2+} single-ion anisotropy and linear chain exchange interactions. Nieuwpoort and Reedijk [1] concluded from spectroscopic results on $Co(N_2H_5)_2(SO_4)_2$ that the compound has a tetragonally compressed octahedral co-ordination, without measurable rhombic distortion. From E.S.R. measurements, carried out at liquid hydrogen temperature on a sample of the compound $Zn(N_2H_5)_2(SO_4)_2$ doped with approximately 1% Co^{2+}, the values of the components of the spectroscopic splitting factor g_1 = 2.20 ± 0.01, g_2 = 4.40 ± 0.02 and g_3 = 5.45 ± 0.02 were found [2], from which one would conclude that a small rhombic distortion is present. Neglecting the small rhombic distortion we take

$g_{//}$ (= g_1) = 2.20 and $g_{\perp}$ (= $\frac{g_2 + g_3}{2}$) = 4.9.
Theoretical investigations of the effect of the crystalline field on a Co^{2+} ion have been carried out by several authors (e.g. see ref. 23). The lowest orbital state of the free Co^{2+} ion is a ^4F state and the next higher state, ^4P, is more than 14000 cm^{-1} higher. For a cubic octahedrally co-ordinated Co^{2+} ion the ^4F state is split into an orbital singlet, $^4A_2$, and two orbital triplets, $^4T_1$ and $^4T_2$, with the $^4T_1$ state lowest. Under the combined action of a tetragonal crystalline field and of the spin-orbit coupling, the 12-fold degenerate $^4T_1$ state splits into six Kramers doublets. In fig. 13 the energies of the $^4T_1$ state levels are represented graphically as a function of the reduced tetragonal field strength $\eta = \delta/(\frac{3}{4}\lambda)$ with λ = spin-orbit coupling constant (see ref. 22). The same energy level remains lowest for all values of η (fig. 13). The wave functions of this ground state doublet are, written in terms of a representation of spin angular momentum $S=\frac{3}{2}$ and a fictitious orbital angular momentum $l = 1$:

$$\psi_1 = C_1 \,|-1, \tfrac{3}{2}\rangle + C_2|0, \tfrac{1}{2}\rangle + C_3|\,1, -\tfrac{1}{2}\rangle \qquad (4.3)$$

$$\psi_2 = C_1 \,|1, -\tfrac{3}{2}\rangle + C_2|0, -\tfrac{1}{2}\rangle + C_3|\,-1, \tfrac{1}{2}\rangle \qquad (4.4)$$

The coefficients C_i ($i = 1, 2, 3$) are functions of η and of the reduced energy, x_1, of the groundstate, where $x_1 = \frac{E}{\frac{3}{4}\lambda}$

$$C_1 = \sqrt{6}\, C_2/(x_1-3-\eta)\ ,\ C_2 = \{\,1 + 6/(x_1-3-\eta)^2 + 8/(x_1-1-\eta)^2\}^{-\frac{1}{2}},$$

$$C_3 = \sqrt{8}\, C_2/(x_1-1-\eta). \qquad (4.5)$$

From these relations the principal values of the g-tensor ($g_{//}$, parallel to the tetragonal axis) can be computed. The result is shown in fig. 14. It is seen that in terms of the effective spin $S'=\frac{1}{2}$, the g-value is appreciably anisotropic if $\eta \neq 0$. The value of η is obtained from the E.S.R. result on Co^{2+} in a $Zn(N_2H_5)_2(SO_4)_2$ lattice. It seems quite reasonable to assume that the value for η, $\eta = -6$, found for the dope Co^{2+} is also a good value for $Co(N_2H_5)_2(SO_4)_2$ because of the very similar co-ordination in the two compounds. Inspection of fig. 13 shows

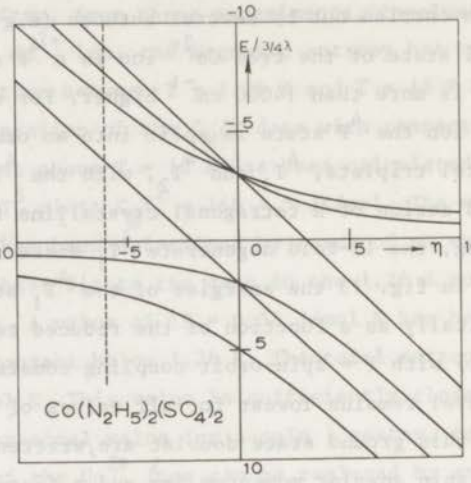

Fig. 13. *The energy level scheme of the ground triplet, $^4T_1$, of the Co^{2+} ion in a tetragonal field as a function of the reduced tetragonal field strength $\eta = \delta / |\frac{3}{4}\lambda|$ (after Kambe et al.* [23]).

δ : *tetragonal field strength.*

λ : *spin-orbit coupling constant which has a value of $-180\ cm^{-1}$ for the free ion. The dashed line indicates the value of η obtained for Co^{2+} ions in $Zn(N_2H_5)_2(SO_4)_2$ using $g_{//} = 2.2$ and $g_{\perp} = 4.9$.*

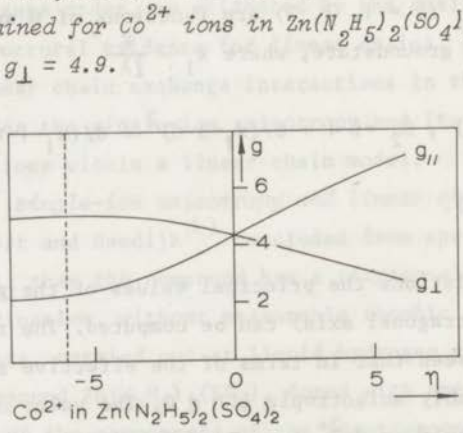

Fig. 14. *The principal g-values of Co^{2+} in a tetragonal crystalline field as a function of η, which is defined similarly as in fig. 13. The dashed line shows the result for η as obtained for Co^{2+} in $Zn(N_2H_5)_2(SO_4)_2$.*

that for $\eta = -6$ the energy difference between the ground level and the next higher level is $1.44 \times |3\lambda/4|$. Provided that λ has its free ion value, $\lambda = -180\ cm^{-1}$, this energy difference amounts to $195\ cm^{-1}$. If, as is usual, λ has a lower value (e.g. 25 per cent less) the energy difference is still approximately $150\ cm^{-1}$. We may, therefore, safely assume that in the temperature region considered the ions are predominantly in the groundstate, which is in accordance with the results of the entropy argument. It can be shown (see e.g. Lines [24]) that in the doublet groundstate the true spin $S=\frac{3}{2}$ may be replaced by a spin $S'=\frac{1}{2}$ operator with the property:

$$S_x = 2q\ S'_x\ ;\ S_y = 2q\ S'_y\ ;\ S_z = 2p\ S'_z. \qquad (4.6)$$

Here p and q are functions of the C_i's given in eq. (4.5):

$$p = \frac{3}{2} C_1^2 + \frac{1}{2} C_2^2 - \frac{1}{2} C_3^2 \text{ and } q = C_2^2 + \sqrt{3}\, C_1 C_2. \qquad (4.7)$$

In case of covalency and configuration interaction effects, however, these relations are somewhat more involved.

When we suppose that for the real spin $S=\frac{3}{2}$ the exchange hamiltonian can be written as:

$$H = -2J \sum_{i=1}^{N} \vec{S}_i . \vec{S}_{i+1}\ , \qquad (4.8)$$

we derive from eq. (4.6) and eq. (4.8)

$$H = -2J \sum_{i=1}^{N} \{(2q)^2 (S'_{i,x}\, S'_{i+1,x} + S'_{i,y}\, S'_{i+1,y}) + (2p)^2 S'_{i,z} S'_{i+1,z}\} \qquad (4.9)$$

We may conclude that, in terms of the effective spin $S'=\frac{1}{2}$, the exchange interactions will be anisotropic.

4.3.1.2 Comparison of the experimental results with theory. Using the afore-mentioned value of $\eta = -6$ for $Co(N_2H_5)_2(SO_4)_2$ we obtain $x_1 = 2.2$ and the values of C_1, C_2 and C_3 can be calculated with eq. (4.5). Using eq. (4.7) we find for the anisotropy of the hamiltonian (eq. 4.9), $\frac{q^2}{p^2} \simeq 3.5$. This large anisotropy in the exchange is of a special nature, since it corresponds to a preferential spin alignment in a plane, whereas

Co^{2+} compounds often show a preference for an axial spin alignment, corresponding to an Ising type of anisotropy. As we have seen, however, the Ising model does not fit the specific heat data satisfactorily. It, therefore, seems reasonable to try to interpret the specific heat results with the transversally coupled linear chain model (XY model) for spin $\frac{1}{2}$ with the hamiltonian

$$H = -2J \sum_{i=1}^{N} (S'_{i,x} S'_{i+1,x} + S'_{i,y} S'_{i+1,y}) \qquad (4.10)$$

The partition function according to this hamiltonian has been obtained by Katsura [25] who also has given the expression for the specific heat,

$$C/R = \frac{4(2J/kT)^2}{\pi} \int_0^{\pi} \frac{\cos^2 \omega}{\cosh(\frac{4J}{kT} \cos\omega)} \, d\omega \qquad (4.11)$$

The best fit to the experimental data above T = 2.3 K with eq. (4.11) has been obtained for $|J/k| = 7.05$ K. The full curve corresponding to this value is shown in fig. 12. The agreement between the experimental data and the calculated curve is quite satisfactory above T = 2.3 K. Below 2.3 K we observe a gradually increasing deviation. We attribute these differences to the presence of a weak coupling between the chains which causes long-range spin ordering below 1.60 K, i.e. the temperature at which the additional anomaly in the specific heat has been observed.

Since the specific heat calculated according to eq. (4.11) yields identical results for antiferromagnetic and ferromagnetic exchange interactions, we cannot determine the sign of the exchange constant from these measurements. Susceptibility measurements [2] on a powdered sample of $Co(N_2H_5)_2(SO_4)_2$, however, supply an asymptotic Curie-Weiss constant of -22 ± 1 K. This result points to antiferromagnetic exchange interactions in this compound. Summarizing we may conclude that predominantly antiferromagnetic transverse coupled linear chain exchange interactions exists among ions having effective spins $S'=\frac{1}{2}$ and $J/k = -7.05 \pm 0.02$ K in $Co(N_2H_5)_2(SO_4)_2$.

4.3.2 High temperature region (20 K < T < 80 K). While the high temperature specific heats of $Cu(N_2H_5)_2(SO_4)_2$, $Ni(N_2H_5)_2(SO_4)_2$ and $Mn(N_2H_5)_2(SO_4)_2$ could be well described as lattice specific heats only, this is not the case for $Co(N_2H_5)_2(SO_4)_2$. In fact, while for the first

three compounds the corresponding states argument is valid, i.e. the ratio $b(M_I)/b(M_{II})$ is constant (M_I, M_{II} are Cu, Ni or Mn), one finds that for $Co(N_2H_5)_2(SO_4)_2$ the ratio $b(Co)/b(M_{II})$, where M_{II} = Cu, Ni and Mn. is not temperature independent. This can be explained on the basis of an excess specific heat, caused by the thermal occupation of the higher single-ion Kramers doublet states. This excess specific heat can be determined from the experimental data. The lattice specific heat of $Co(N_2H_5)_2(SO_4)_2$ at high temperatures was calculated by means of the corresponding states ratio determined at low temperatures. We found the low-temperature ratio b(Co)/b(Cu) to be 1.027. Using this ratio and the high-temperature data on $Cu(N_2H_5)_2(SO_4)_2$ we could calculate the lattice specific heat for $Co(N_2H_5)_2(SO_4)_2$. Subtracting this from the total specific heat, C_p, the excess specific heat data, shown in fig. 15, were obtained. For $\eta = -6$ the energy differences (in units $|3\lambda/4|$) between the ground state and the five Kramers doublets are: 1.44, 5.90, 8.86, 10.0, 11.1 (see fig. 13).

Since the reduced energy of the single-ion levels for a given value of η is known, the excess Schottky specific heat can be calculated as a function of temperature with λ as a parameter. The calculated specific heat with $\lambda = -180$ cm^{-1}, the free ion value, is shown in fig. 15 as a dashed line. The fit is rather poor for this value of λ. A better fit to the experimental data has been obtained with $\lambda = -135$ cm^{-1} (fig. 15, full line). This points to a reduction of the spin-orbit coupling constant, relative to its free ion value. Such a reduction is a commonly observed phenomenon for Co^{2+} ions in a crystal and is ascribed mainly to covalency effects [26]. Although these results seem quite plausible it should be noticed that the values of the energy levels are determined from calculations based upon a g-tensor for which deviations from the tetragonal symmetry have been disregarded.

The more general problem of Co^{2+} ions in a crystalline field due to tetragonal and rhombic distortions of the cubic octahedral co-ordination has been treated by Uryû *et al.* [27]. The number of adjustable parameters in this approach, however, becomes too large to be resolved by heat capacity measurements alone.

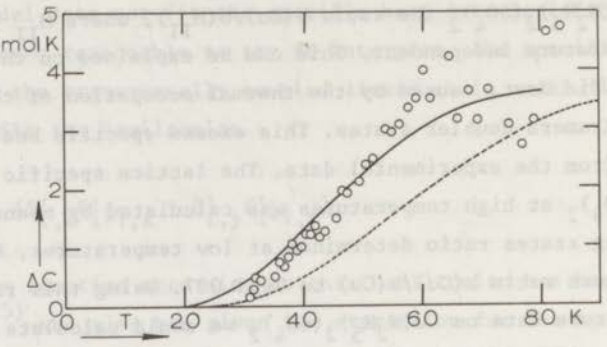

Fig. 15. *The excess specific heat, ΔC, for $Co(N_2H_5)_2(SO_4)_2$ obtained by subtraction of the lattice specific heat (see text) from the C_p data.*
- - - - specific heat, calculated for η = -6 and λ = -180 cm^{-1}.
——— specific heat, calculated for η = -6 and λ = -135 cm^{-1}.

4.4 $Fe(N_2H_5)_2(SO_4)_2$. The magnetic specific heat obtained after subtraction of the lattice contribution from the experimental data, is shown in fig. 16 as a function of temperature. The subtracted portion is essentially the lattice specific heat of $Cu(N_2H_5)_2(SO_4)_2$, scaled with the corresponding-states ratio b(Fe)/b(Cu) = 1.020, which is obtained from the high-temperature data of the two compounds. Some features of fig. 16 are noteworthy. A broad maximum occurs at $T(C_{max})$ = 11.7 ± 0.2 K with C_{max} = 7.95 ± 0.05 J/mol K. At a lower temperature, T = 6.02 ± 0.05 K, an additional λ-like anomaly is found. At this temperature the susceptibility versus temperature curve reported by Witteveen [2] displays a sharp decrease. Hence, it is very likely that long-range spin ordering is established below T_N = 6.02 K. Information concerning the effective spin value of the Fe^{2+} ions (involved in the anomalous low-temperature specific heat) may be obtained from entropy considerations.

In the temperature range between T = 1.26 K and T = 22 K numerical integration of the C_M/T data with respect to temperature yields an entropy

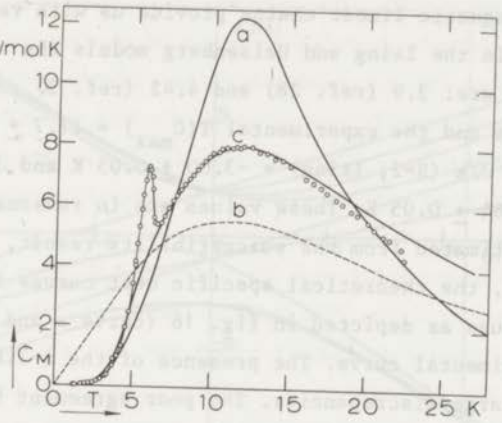

Fig. 16. *The magnetic specific heat of* $Fe(N_2H_5)_2(SO_4)_2$ *as a function of temperature.*

o o o o experimental results.

a:—— *Ising linear chain model as calculated by Obokata and Oguchi* [28] *for S=2:* $|J/k| = 3.0$ *K.*

b:- - - *Heisenberg linear chain model, for S=2:* $J/k = -2.64$ *K. The specific heat has been calculated using Weng's* [15] *interpolation scheme and the results for the* $S=\frac{1}{2}$ [10], $S=1$ [15] *and* $S=\infty$ [33] *Heisenberg linear chain model.*

c:—— *Schottky anomaly for a singlet-doublet-doublet energy level scheme.*

content of 10.6 J/mol K. For an estimate of the entropy above 22 K the value $C_M T^2 = 1300$ JK/mol is used. The calculated entropy below T = 1.26 K, 0.13 J/mol K, is negligible. The total magnetic entropy amounts to $\Delta S = 13.2 \pm 0.2$ J/mol K. This value agrees within experimental error with R ln 5 = 13.37 J/mol K, the theoretical value for a spin 2 system. The critical entropy, $\Delta S(T_N)$, is 1.7 J/mol K. This corresponds to only 12 per cent of R ln 5 and is indicative of a high degree of short-range order in this material. This result together with the structural evidence of linear chains in this compound and the reported Curie-Weiss constant

of -13 ± 1 K (ref. 2) points to predominantly antiferromagnetic linear chain exchange interactions in $Fe(N_2H_5)_2(SO_4)_2$.

The available theoretical calculations for the specific heat of spin 2 antiferromagnetic linear chains provide us with relations between $T(C_{max})$ and J/k. In the Ising and Heisenberg models the values for $\frac{kT(C_{max})}{J}$ reported are: 3.9 (ref. 28) and 4.42 (ref. 3) respectively. Using these values and the experimental $T(C_{max}) = 11.7 \pm 0.2$ K, we obtain the values J/k (S=2, Ising) $= -3.00 \pm 0.05$ K and J/k (S=2, Heisenberg) $= -2.64 \pm 0.05$ K. These values are in reasonable agreement with the value estimated from the susceptibility result, $J/k = -2.2 \pm 0.5$ K. On the other hand, the theoretical specific heat curves for the above mentioned J/k values as depicted in fig. 16 (curve a and b), do not at all fit the experimental curve. The presence of the λ-like anomaly cannot account for the large discrepancies. The poor agreement between theory and experiment is most probably caused by the presence of important single-ion anisotropy in this compound.

4.4.1 Single-ion anisotropy. Nieuwpoort and Reedijk [1] could explain their spectroscopic and Mössbauer results on $Fe(N_2H_5)_2(SO_4)_2$ by means of a temperature dependent tetragonal field strength, δ, and a value of the spin-orbit coupling constant $\lambda = -75$ cm^{-1}. The reduced tetragonal field strength, δ/λ, was found to increase slowly with decreasing temperature, reaching a value of about 11 at T = 80 K.

The lowest orbital state of the free Fe^{2+} ion is a ^5D state. In a crystalline field with cubic symmetry the ^5D state is split into a lower orbital triplet, t_{2g}, and an orbital doublet, e_g. Through the combined action of a tetragonal field component and the spin-orbit coupling, the 15-fold degeneracy of the t_{2g} state is partially lifted. The energy of these levels is represented in fig. 17 as a function of δ/λ (refs. 29, 30). The ground state is a singlet or a doublet according to whether δ/λ is positive or negative. Since $|\lambda| > T(C_{max})$ and S=2 for $Fe(N_2H_5)_2(SO_4)_2$ the energy level scheme in fig. 17 indicates that δ/λ has to be positive.

To obtain an estimate of the energy differences between the ground state singlet and the closest doublets, the experimental C_M data have been fitted assuming that the ions are independent. The data could be fitted reasonably well with a level scheme consisting of two doublets situated respectively 25.4 K and 56.4 K above the singlet ground state

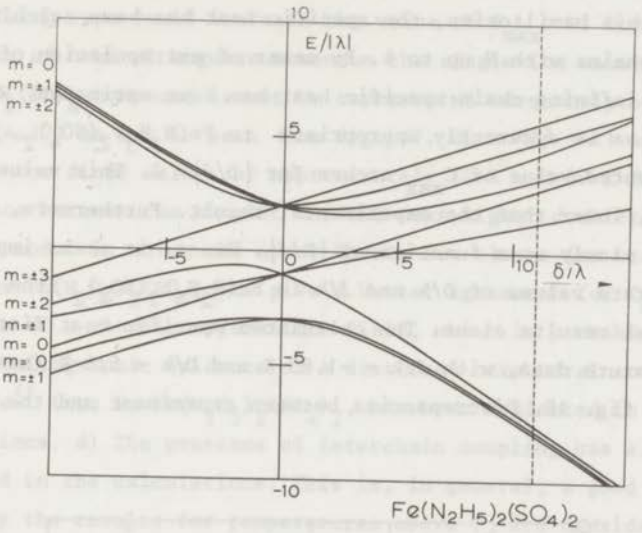

Fig. 17. *The energy level scheme of the ground orbital triplet t_{2g} of the Fe^{2+} ion (after Inomata and Oguchi [29]). Both the spin-orbit coupling (λ) and the tetragonal field (δ) have been taken into account. The dashed line in this figure indicates the value of δ/λ, obtained by Nieuwpoort and Reedijk [1] from spectroscopy and Mössbauer experiments on $Fe(N_2H_5)_2(SO_4)_2$.*

(see fig. 16). This energy level scheme is consistent with the results obtained by Nieuwpoort and Reedijk [1]. We notice, however, that in spite of the reasonable fit a single-ion picture alone is not sufficient to explain the thermal and magnetic behaviour of $Fe(N_2H_5)_2(SO_4)_2$.

4.4.2 Single-ion anisotropy and exchange interactions. To explain the specific heat behaviour of $Fe(N_2H_5)_2(SO_4)_2$ we assume that a) the exchange interactions between the Fe^{2+} ions are isotropic and b) the zero-field splitting of the Fe^{2+} ions can be described in terms of an axial zero-field splitting parameter $D > 0$ (yielding a singlet ground state with two higher lying doublets at energies of D and 4D). The linear chain hamiltonian can then be written as:

$$H = -2J \sum_{i=1}^{N} \vec{S}_i . \vec{S}_{i+1} + D \sum_{i=1}^{N} \{S_{i,z}^2 - \frac{1}{3} S\,(S+1)\}. \qquad (4.12)$$

Using this hamiltonian, the specific heat has been calculated [19] for finite chains with N up to 4. By means of extrapolation of these results the infinite chain specific heat has been estimated. With $D/k > 0$ and $J/k < 0$, as is apparently appropriate to $Fe(N_2H_5)_2(SO_4)_2$, the largest computed value of C_{max} occurs for $|D/J| \simeq 2$. This value of C_{max} is, however, lower than the experimental result. Furthermore, C_{max} varies only slowly as a function of $|D/J|$. Hence, it seems impossible to obtain accurate values of D/k and J/k in $Fe(N_2H_5)_2(SO_4)_2$ from the specific heat results alone. The calculated specific heat fitted to the high-temperature data, with J/k = -1.85 K and D/k = 5.6 K (see eq. (4.12)) is shown in fig. 18. Discrepancies between experiment and the theoretical

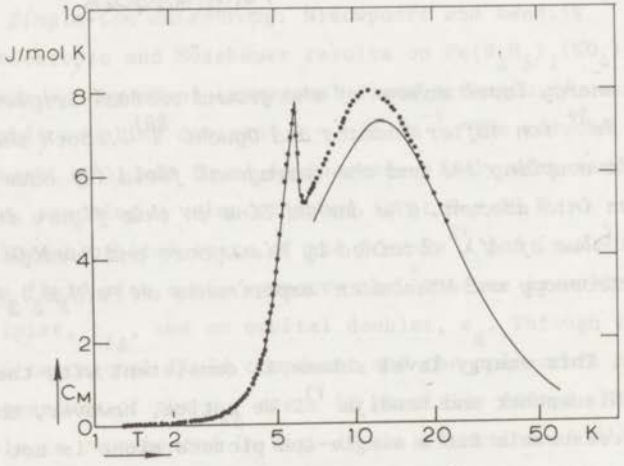

Fig. 18. *The magnetic specific heat of $Fe(N_2H_5)_2(SO_4)_2$ as a function of temperature.*

. . . . *experimental results*

——— *Heisenberg linear chain model with uniaxial single-ion anisotropy as calculated by Blöte [19] for S=2; J/k = -1.85 K and D/k = 5.6 K.*

results can be attributed to various effects. a) The admixture of orbital angular momentum in the lowest levels could give rise to anisotropy in the exchange interaction of eq. (4.12). An anisotropy of the Ising type would increase the value of C_{max}. b) Due to the admixture of orbital angular momentum the single-ion anisotropy of the $Fe(N_2H_5)_2(SO)_4$ compound cannot be represented adequately by a D-term in eq. (4.12) as can be seen from fig. 17. With $\delta/\lambda \simeq 11$ and $\lambda = -75$ cm^{-1} (ref. 1) one finds values of approximately 10 K and 30 K for the energy difference between the singlet and the next higher doublets. One should expect a model in which the upper levels are closer (as one would conclude for $Fe(N_2H_5)_2(SO_4)_2$) to give a better agreement for C_{max}. c) The influence of a rhombic crystalline field, which is probable in view of the crystallographic evidence of a distorted octahedral co-ordination of the Fe^{2+} ions in $Fe(N_2H_5)_2(SO_4)_2$, has been neglected in the calculations. d) The presence of interchain coupling has also been neglected in the calculations. This is, in general, a good approximation when only the results for temperatures above T_c are considered and $|J'/J| \ll 1$. For $Fe(N_2H_5)_2(SO_4)_2$ the ratio $T_N/T(C_{max})$ is as large as 0.5. However, we do not expect that an appreciable part of the discrepancy (10 per cent) at $T(C_{max})$ can be attributed to the presence of interchain coupling.

4.5 $Mn(N_2H_5)_2(SO_4)_2$. The magnetic specific heat of $Mn(N_2H_5)_2(SO_4)_2$, obtained after subtraction of the lattice contribution from the experimental data, is shown in fig. 19. At $T = 2.155 \pm 0.005$ K a large λ-like anomaly occurs which is associated with the onset of long-range spin ordering. Above the anomaly C_M passes through a flat region before a decrease sets in. It should be noticed that the susceptibility results, obtained by Witteveen [2], on a powdered $Mn(N_2H_5)_2(SO_4)_2$ specimen display a broad maximum at $T = 4.8 \pm 0.2$ K. These results can be associated either with a large single-ion anisotropy [31] or with predominantly low dimensional, viz. 1-d or 2-d, magnetic interaction. Nieuwpoort and Reedijk [1] determined by means of E.S.R. measurements, the zero-field splitting parameter, D/k, of Mn^{2+} ions substituted in both $Cd(N_2H_5)_2(SO_4)_2$ and the isomorphous $Zn(N_2H_5)_2(SO_4)_2$ compounds (D/k = 0.030 cm^{-1} and 0.025 cm^{-1}, respectively). They found the rhombic distortion to be small: $|E/D| \simeq 0.2$. A single-ion anisotropy of this order of magnitude

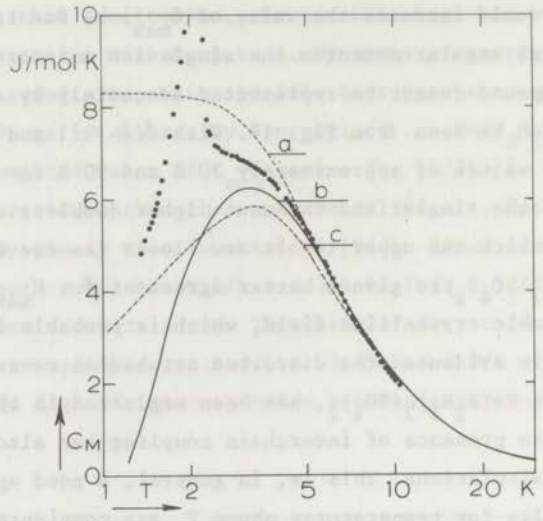

Fig. 19. *The magnetic specific heat of* $Mn(N_2H_5)_2(SO_4)_2$ *as a function of temperature.*

. . . . *experimental results.*

– – – *a: Heisenberg linear chain model as calculated by Fisher* [33] *for* $S=\infty$, *scaled to* $S=\frac{5}{2}$; $J/k(S=\frac{5}{2}) = -0.54$ K.

——— *b: Quantum corrected version of curve b;* $J/k(S=\frac{5}{2}) = -0.54$ K.

– – – *c: Heisenberg linear chain model for* $S=\frac{5}{2}$ *as calculated according to Weng's* [15] *interpolation scheme;* $J/k(S=\frac{5}{2}) = -0.54$ K.

is insufficient to explain the broad maximum that occurs in the specific heat of $Mn(N_2H_5)_2(SO_4)_2$ at a temperature as high as $T \approx 2.5$ K. We conclude, therefore, that the large peak is caused by magnetic exchange interactions. Susceptibility results yield an asymtotic Curie-Weiss constant of -5.5 K, which points to antiferromagnetic exchange interaction. From these results and the crystallographic evidence we conclude that predominantly antiferromagnetic linear chain exchange interactions occur in $Mn(N_2H_5)_2(SO_4)_2$. Further support for this conclusion may be

obtained from entropy considerations.

The total magnetic entropy has been obtained from a numerical integration of the C_M/T data with respect to temperature in the range 1.3 K < T < 10 K and extrapolation of the results to both T = 0 K and T = ∞. For the high-temperature extrapolation we used the result $C_M T^2$ = 214 ± 4 JK/mol, obtained from the $C_p T^2$ versus T^5 plot (see fig. 7). For the low-temperature extrapolation we used the relation $C_M = AT^{-2} \exp(-B/T)$, which provides a fit to the data between T = 1.3 K and T = 1.65 K, with A = 500 JK/mol and B = 5.7 K. The total entropy is found to be 14.5 ± 0.3 J/mol K. This value is close to the theoretical value for an $S=\frac{5}{2}$ system, Rln6 = 14.89 J/mol K. Part of the 3 per cent discrepancy may be due to the fact that the entropy content below T = 1.3 K (approximately 10 per cent of the total value) could have been underestimated. The amount of entropy associated with the short-range order is quite large, as is evidenced by the small value of the critical entropy $\Delta S(T_c)$ = 5.3 J/mol K, which is only 35 per cent of Rln 6. This also shows the preponderance of linear chain exchange interactions in this compound, since for example for a simple cubic lattice structure with nearest neighbour interactions the entropy $\Delta S(T_c)$ in the Heisenberg model with spin $\frac{5}{2}$, amounts to 78 per cent of Rln6 (see ref. 32).

Exchange interactions in Mn^{2+} compounds are, in general, isotropic because the lowest level, of the Mn^{2+} ion, $^6A_1$, has no orbital angular momentum and crystalline field effects are usually quite small. Thus far no exact specific heat computations for the isotropic Heisenberg linear chain model with spin $S=\frac{5}{2}$ have been reported in the literature.

Therefore, we will compare the experimental data with several approximations. Fisher [33] has pointed out that in the classical limit (S=∞) the isotropic Heisenberg linear chain model is exactly soluble. He found for the partition function, Z_c,

$$Z_c = \{(\sinh K)/K\}^N, \text{ where } K = 2JS(S+1)/kT \qquad (4.13)$$

and for the specific heat

$$C_M/R = 1-K^2/\sinh^2 K \qquad (4.14)$$

As the spin of the Mn^{2+} ions ($S=\frac{5}{2}$) is quite large, it is reasonable to compare the experimental data with Fisher's result. Since one may, however, not expect a good agreement very near or below the maximum of the experimental curve, the fit has been made to the high-temperature data, which can be represented by

$$C_M = b/T^2 \text{ with } b = 214 \pm 4 \text{ JK/mol.} \quad (4.15)$$

The leading term of the high-temperature expansion of eq. (4.14) is

$$C_M/R = \frac{4}{3}(J/k)^2 S^2(S+1)^2 \frac{1}{T^2} \quad (4.16)$$

Setting $S=\frac{5}{2}$, and identifying $C_M T^2 = 214$ JK/mol (eq. (4.15)) with eq. (4.16) yields a value for $|J/k|$ of 0.502 K. As this classical spin model produces a finite specific heat at T = 0 K, this model cannot, however, describe the low-temperature data.

Recently Harrigan and Jones [34] have given non-trivial quantum corrections to second order in 1/S to the partition function of the classical spin isotropic Heisenberg linear chain model. From their partition function,

$$\ln Z_Q = \ln Z_c + \frac{\ln(2S+1)^N}{(4\pi)^N} - \frac{(N-1)}{12S(S+1)} K^2 \{1 + L(K) - \frac{3L(K)}{K} + L^2(K)\} \quad (4.17)$$

we calculated the internal energy and the specific heat. In eq. (4.17) Z_c is the classical spin partition function of eq. (4.13). Further, $L(K) = \coth K - 1/K$, where $K = \frac{2JS(S+1)}{kT}$, S = spin value and N is the number of atoms. Fitting of the experimental C_M data in the temperature range $7 < T < 10$ K to eq. (4.17) for $S=\frac{5}{2}$ yields a value $J/k = -0.54$ K. This curve is shown in fig. 19 along with the classical spin result scaled to $S=\frac{5}{2}$. The $S=\frac{5}{2}$ specific heat curve of the quantum corrected classical spin model reaches a maximum value of $C_M = 6.25$ J/mol K at

$$\frac{kT(C_{max})}{|J|} = 5.8 \quad (4.18)$$

for antiferromagnetic interactions. Since at low temperatures, i.e. below $T(C_{max})/2.8$, the calculated specific heat becomes negative, this

model overestimates the corrections to the classical spin. Probably part of the difference between the experimental and calculated curve near the maximum is due to this overestimation.

As a third approximation method we discuss a treatment that has been introduced by Weng [15]. He starts from an exchange hamiltonian written in the form

$$H = \frac{-2J \sum_{i=1}^{N} \vec{S}_i \cdot \vec{S}_{i+1}}{2S(S+1)} \qquad (4.19)$$

to determine the thermodynamic quantities for arbitrary spin values. It is assumed that each thermodynamic quantity, Y, a) depends only upon the spin value S and the reduced temperature $T^{\ast} = \frac{kT}{2JS(S+1)}$ and b) obeys the relation,

$$Y(S,T^{\ast}) = \frac{a(T^{\ast})S + b(T^{\ast})}{S + c(T^{\ast})} \qquad (4.20)$$

where $a(T^{\ast})$, $b(T^{\ast})$ and $c(T^{\ast})$ depend only upon the reduced temperature. Since for the isotropic Heisenberg linear chain model the thermodynamic properties are known for the spin values $S=\frac{1}{2}$ (ref. 10) and S=1 (ref. 15) (numerical results) and for $S=\infty$ (ref. 33) (exact results), the constants a, b and c can be calculated for each value of T . The thermodynamic quantities may then be calculated for any spin value with eq. (4.20). By means of this interpolation scheme one finds for the antiferromagnetic isotropic Heisenberg linear chain with $S=\frac{5}{2}$ the relations:

$$\frac{kT(C_{max})}{J} \simeq 6.3 \text{ and } C_{max} = 5.8 \text{ J/mol K.} \qquad (4.21)$$

Although the presence of the λ-like anomaly at $T_c = 2.155$ K prevents an unambiguous determination of $T(C_{max})$, a probable value is $T(C_{max}) = 2.4 \pm 0.2$ K. Substituting this value into eq. (4.21) we obtain $J/k = -0.38 \pm 0.04$ K.

We notice that the value J/k differs significantly from those obtained with the classical and quantum corrected classical spin models. Further, the theoretical maximum is about 25 per cent lower. For comparison the interpolation scheme result is also shown in fig. 19 with J/k = -0.54 K. The discrepancies between experiment and theory may,

however, also arise from the presence of a considerable interchain coupling in this compound, which is evidenced by the large peak very close to $T(C_{max})$. In fact, neutron scattering experiments on several antiferromagnetic, approximately linear chain compounds demonstrate that interchain interaction is noticeable up to temperatures of $2T_N$ or even higher (see refs. 35, 36). The effect of interactions between the linear chains on the specific heat above T_N is most probably an additional contribution to the specific heat. The compound $Mn(N_2H_5)_2(SO_4)_2$ is not as good an example of a linear chain system as are $CsMnCl_3 \cdot 2H_2O$ (ref. 37) and $\{(CH_3)_4N\}MnCl_3$ (refs. 38, 39), because the ratio $T(\chi_{max})/T_c$ is close to 1 ($\simeq$2.2), while it is appreciably larger for the other compounds: 6.5 and 65 respectively. On the other hand, however, no C_M data near to the short-range order maximum are available for these substances.

TABLE IV

Values of J/k, D/k and J'/k derived from the specific heat results

	Model	eff. spin	J/k K	D/k K	J/k K	D/k K	J/k K	J'/J
					Our estimate			
$Cu(N_2H_5)_2(SO_4)_2$	isotropic Heisenberg	$\frac{1}{2}$	-1.99		-1.99±0.02		-2.00±0.05 [a]	15×10^{-2}
$Ni(N_2H_5)_2(SO_4)_2$	isotropic Heisenberg	1					-3.3 ±0.1 [a]	
	Ising + D/k	1	-1.4	-12.3				
	Ising + D/k	$\frac{1}{2}$	-6.38	-15.3				
	isotropic Heisenberg + D/k	1	-1.56	-15.6	-1.56±0.02	-15.5 ±0.5		5×10^{-2}
$Co(N_2H_5)_2(SO_4)_2$	XY ($J_z = 0$; $J_\perp = J$)	$\frac{1}{2}$	-7.05		-7.05±0.05		-8.9 ±0.3 [a]	2×10^{-2}
$Fe(N_2H_5)_2(SO_4)_2$	isotropic Heisenberg	2	-2.64				-2.2 ±0.5 [a]	3×10^{-2}
	Ising	2	-3.0					
	isotropic Heisenberg + D/k	2	-1.85	+ 5.6	-2.0 ±0.5			
$Mn(N_2H_5)_2(SO_4)_2$	isotropic Heis. (eq. (4.16))	$\frac{5}{2}$	-0.502				-0.55±0.05 [a]	3×10^{-2}
	(eq. (4.18))	$\frac{5}{2}$	-0.43					
	(eq. (4.21))	$\frac{5}{2}$	-0.38					
	(eq. (4.17))	$\frac{5}{2}$	-0.54		-0.53±0.03	0.035±0.005 [b]		

[a] ref.2
[b] ref.1

5. Interchain exchange interaction. The heat capacities of the $Co(N_2H_5)_2(SO_4)_2$, $Fe(N_2H_5)_2(SO_4)_2$ and $Mn(N_2H_5)_2(SO_4)_2$ compounds display a λ-like anomaly. We interpret this λ-like anomaly as a transition to a long-range ordered state, due to a coupling between the chains, where the transition temperature is mainly determined by the magnitude of the interchain interactions. To obtain values of the interchain coupling

constant, J'/k, in these compounds we apply the relation derived by Oguchi [40] that relates the ratio $|J'/J|$, the transition temperature T_c and the spin value. This numerical relation, however, has been derived for a tetragonal lattice structure and isotropic interactions. Because this series of compounds does not satisfy the conditions for this model, only an order of magnitude result can be expected.

From the experimental T_c's (table II) and the values of the intrachain exchange constants with the corresponding spin values (table IV), the $|J'/J|$ values, also given in table IV, have been calculated. Since the specific heat of the $Cu(N_2H_5)_2(SO_4)_2$ and $Ni(N_2H_5)_2(SO_4)_2$ compounds does not show the evidence of the onset of long-range spin ordering down to T = 1.3 K we can only estimate a maximum value of $|J'/J|$ for these salts. These results are also collected in table IV.

6. Concluding remarks. The heat capacity of a series of compounds with general formula $M(N_2H_5)_2(SO_4)_2$ with M = Cu, Ni, Co, Fe, Mn has been measured in the temperature range 1.3 to 80 K. Reliable lattice contributions to the specific heat have been obtained for each of these compounds by means of the conventional C_pT^2 versus T^5 plot or the application of the corresponding states argument for the lattice heat capacity, which has been checked experimentally for several compounds (Cu, Ni and $Mn(N_2H_5)_2(SO_4)_2$) of this series of powder X-ray isomorphs. The low-temperature anomalous magnetic specific heat data have been explained by linear chain exchange interactions, which are apparently antiferromagnetic for all these investigated compounds. The λ-like anomalies found at $T_c = 1.60 \pm 0.03$ K; 6.02 ± 0.05 K and 2.155 ± 0.005 K for $Co(N_2H_5)_2(SO_4)_2$, $Fe(N_2H_5)_2(SO_4)_2$ and $Mn(N_2H_5)_2(SO_4)_2$ respectively, have been interpreted as due to the onset of long-range spin ordering. The absence of such anomalies in the specific heats of $Cu(N_2H_5)_2(SO_4)_2$ and $Ni(N_2H_5)_2(SO_4)_2$ above 1.3 K is indicative of very weak interchain interaction as compared with the intrachain exchange interaction in these compounds.

Estimated values for the ratio $|J'/J|$, which is a measure for the magnetic isolation of the linear chains, have been obtained. The small values of $|J'/J|$, about 10^{-2} (see table IV), show that these compounds

may be considered as nearly isolated linear chain compounds.

An interesting result from the specific heat and magnetic susceptibility measurements is the observation of the presence of relatively strong superexchange interactions in these $M(N_2H_5)_2(SO_4)_2$ compounds in spite of the large number of intervening ligands. The most probable intrachain superexchange pathway is via the three diamagnetic ions O-S-O. A few compounds having strong superexchange interactions with a large number of intervening ligands have been reported, e.g., $GeCo_3O_4$ [41] and $CuVO_4$ [42].

From table V, where the metal-metal distances within the chains (for Cu, Ni and $Co(N_2H_5)_2(SO_4)_2$) (ref.5) and the estimated values of J/k with the corresponding spin value are collected, it can be seen that the values of J/k and the spin values are not related in a simple way, in spite of the approximately equal intrachain metal-metal separations.

TABLE V

Comparison of the values of $|J/k|S^2$ for the various compounds

	b-axis Å	J/k K	S	$\|J/k\|S^2$ K
$Cu(N_2H_5)_2(SO_4)_2$	5.402 [a]	-1.99	$\frac{1}{2}$	0.50
$Ni(N_2H_5)_2(SO_4)_2$	5.35 [a]	-1.56	1	1.56
$Co(N_2H_5)_2(SO_4)_2$	5.37 [a]	-7.05	$\frac{1}{2}$	1.76
$Fe(N_2H_5)_2(SO_4)_2$		-2	2	8
$Mn(N_2H_5)_2(SO_4)_2$		-0.54	$\frac{5}{2}$	3.37

a) ref. 5

Anderson [43] has shown that if only one orbital is involved in the superexchange mechanism and all other factors are equal, the exchange constants should be proportional to $1/S^2$. Only in the case of $Ni(N_2H_5)_2(SO_4)_2$ and $Co(N_2H_5)_2(SO_4)_2$ are the values of $|J/k|S^2$ approximately equal. For $Cu(N_2H_5)_2(SO_4)_2$ the value of $|J/k|S^2$ is smaller while for $Mn(N_2H_5)_2(SO_4)_2$ and $Fe(N_2H_5)_2(SO_4)_2$ much larger values of $|J/k|S^2$ have been found. This points to a more complicated superexchange mechanism in which probably

more than one orbital is involved. The nearly equal metal-metal separations within the chains and the large differences in the values of $|J/k|S^2$ in these compounds possibly indicate that the contribution of the superexchange interaction is mainly determined by the bridging angles in the superexchange pathway. Mc Gregor *et al.* [44] found evidence of a dependence of the exchange constant upon the bridging angle for a series of dimeric Cu compounds. A relatively small variation of the bridging angle could even cause a reversal of the sign of the intradimer exchange constant.

References

1 Nieuwpoort, A. and Reedijk, J., Inorg. Chim. Acta 7 (1973) 323.
2 Witteveen, H.T., Thesis, University at Leyden (1973).
3 De Jongh, L.J. and Miedema, A.R., Advances in Physics, 23 (1974) 1.
4 Mermin, N.D. and Wagner, H., Phys. Rev. Letters 17 (1966) 1133.
5 Hand, D.W. and Prout, C.K., J. Chem. Soc. A (1966) 168.
6 Prout, C.K. and Powell, H.M., J. Chem. Soc.,(1961) 4177.
7 Star, W.M., van Dam, J.E. and van Baarle,C., J. Phys. E2 (1969) 257.
8 Klaaijsen, F.W. *et al.*, this thesis ch. II, to be published.
9 Stout, J.W. and Catalano, E., J. Chem. Phys.,23 (1955) 2013.
10 Bonner, J.C. and Fisher, M.E., Phys. Rev.,135 (1964) A 640.
11 Hulthén, L., Arkiv. Mat. Astron. Fysik 26 A, No 11 (1938).
12 Hillaert, J.G.A., private communication.
13 Dzyaloshinski, I., J. Phys. Chem. Solids 4 (1958) 241.
14 Moriya,T., Phys. Rev.,120 (1960) 91.
15 Weng, C.Y., Thesis, Carnegie-Mellon University (1968).
16 Kubo, R., Phys. Rev.,87 (1952) 568.
17 Vermaas, A., private communication.
18 Kowalski, J.M., Acta Phys. Pol.,A 41 (1972) 763.
19 Blöte, H.W.J., Physica, to be published.
20 Mc Elearney, J.N., Losee, D.B., Merchant, S. and Carlin, R.L., Phys. Rev.,B 7 (1973) 3314;
Polgar, L.G. and Friedberg, S.A., Phys. Rev.,B 4 (1971) 3110;
Klaaijsen, F.W., Reedijk, J. and Witteveen, H.T., Z. Naturf. 27a (1972) 1532;

Reedijk, J., Witteveen, H.T. and Klaaijsen, F.W., J. Inorg. Nucl. Chem., 35 (1973) 3439;
Kopinga, K. and de Jonge, W.J.M., Phys. Lett., 43 A (1973) 415.
21 **Klaaijsen**, F.W., Blöte, H.W.J. and Dokoupil, Z., Solid State Commun., 14 (1974) 607.
22 Van Duyneveldt, A.J., private communication.
23 Kambe, K., Koide, S. and Usui, T., Progr. Theor. Phys., 7 (1952) 15.
24 Lines, M.E., Phys. Rev., 131 (1963) 546.
25 Katsura, S., Phys. Rev., 127 (1962) 1508.
26 see for example, Owen, J., Proc. Roy. Soc., 227 (1954) 183.
27 Uryû, N., Skalyo Jr, J. and Friedberg, S.A., Phys Rev., 144 (1966) 689.
28 Obokata, T. and Oguchi, T., J. Phys. Soc. Japan 25 (1968) 322.
29 Inomata, K. and Oguchi, T., J. Phys. Soc. Japan 23 (1967) 765.
30 Griffith, J.S., 'The theory of transition metal ions' Cambridge University Press, 1961.
31 Reedijk, J., Klaaijsen, F.W. and Witteveen, H.T., J. Chem. Soc. Faraday II (1973) 1537.
32 Blöte, H.W.J. and Huiskamp, W.J., Physica 53 (1971) 445.
33 Fisher, M.E., Am. J. Phys., 32 (1964) 343.
34 Harrigan, M.E. and Jones, G.L., Phys. Rev., B 7 (1973) 4897.
35 Skalyo Jr. J., and Shirane, G., Phys. Rev., B 2 (1970) 4632.
36 Minckiewicz, V.J., Cox, D.E. and Shirane, G., Solid State Commun. 8 (1970) 1001.
37 Smith, T. and Friedberg, S.A., Phys. Rev., 176 (1968) 660.
38 Dingle, R., Lines, M.E. and Holt, S.L., Phys. Rev. 187 (1969) 648.
39 Haseda, T., Int. Conf. on Magnetism, Moscow, 1973.
40 Oguchi, T., Phys. Rev., 133 (1964) A 1098.
41 Saji, H., Phys. Lett., 45 A (1973) 469.
42 Saji, H., J. Phys. Soc. Japan 33 (1972) 671.
43 Anderson, P.W., Phys. Rev., 115 (1959) 2.
44 Mc Gregor, K.T., Watkins, N.T., Lewis, D.L., Drake, R.F., Hodgson, D.J. and Hatfield, W.E., Inorg. Nucl. Chem. Lett. 9 (1973) 423.

CHAPTER IV

MAGNETIC SPECIFIC HEATS OF SPIN 1 LINEAR CHAIN COMPOUNDS. AN EXPERIMENTAL STUDY OF THE ANISOTROPIC FERROMAGNETIC S=1 LINEAR CHAIN INTERACTIONS IN NiX_2L_2 COMPOUNDS (X = Cl, Br; L = PYRAZOLE, PYRIDINE)

Abstract. The heat capacities of NiX_2L_2 with X = Cl, Br; L = pyrazole (pz = $N_2C_3H_4$), pyridine (py = NC_5H_5) have been measured between 1.3 and 80 K. These nickel compounds can be considered as consisting of ferromagnetic linear chains with a weak antiferromagnetic coupling between the chains. The Ni^{2+} ions exhibit a large single-ion anisotropy. Calculations for the isotropic Heisenberg spin 1 linear chain model with uniaxial single-ion anisotropy are found to provide a good description of the experimental specific heat results. Information has been obtained on the intrachain exchange constants and on the crystal field splitting parameters of the Ni^{2+} ions in these materials. For $NiCl_2$.2pz, $NiBr_2$.2pz and $NiBr_2$.2py, a sharp peak in the specific heat has been found at T = 6.05 K, 3.35 K and 2.85 K, respectively. These peaks are apparently associated with the onset of three dimensional long-range spin ordering. For $NiCl_2$.2py, two peaks have been observed at 6.41 K and 6.75 K. From heat capacity measurements in external magnetic field and from susceptibility measurements evidence for metamagnetic behaviour of these compounds has been obtained. Estimated values for the interchain exchange constants in these materials are presented.

1. Introduction. As part of a research program on magnetic compounds of various spin values in which the exchange interaction is predominantly along chains we have investigated a series of compounds of general formula MX_2L_2, where M = Cu, Ni, Fe and Mn; X = Cl, Br; L = pyrazole (pz = $N_2C_3H_4$), pyridine (py = NC_5H_5), by means of specific heat measurements. A preliminary report on Ni has appeared [1]. In this chapter we shall discuss four spin 1 compounds of this series, viz. two *bis*(pyrazole)Ni(II)halides ($NiCl_2$.2pz and $NiBr_2$.2pz) and two *bis*(pyridine)Ni(II)halides ($NiCl_2$.2py and $NiBr_2$.2py).

Experimental data for (approximately) linear chain compounds with spin 1 are rare. Theoretically the thermal and magnetic properties of the spin 1 linear chain system have been studied for two models. The Ising linear chain model has been treated by Suzuki *et al.* [2] and by Obokata and Oguchi [3]. Recently also for the S=1 isotropic Heisenberg linear chain model the thermodynamic properties have been calculated [4]. By means of computer calculations on finite chains Weng [4] estimated the infinite chain results.

The theories show that the specific heat of a linear chain system displays a broad peak in the specific heat, associated with short-range interactions. Evidently, in real crystals deviations from one-dimensional (1-d) behaviour occur due to the finite coupling between the chains, that is always present experimentally. Whereas the ideal chain system thus does not possess a transition to long-range order at a finite temperature, the interchain coupling will give rise to a finite transition point T_c, corresponding with a sharp peak in the specific heat. On the other hand, it has been shown that 1-d theories give a good description of the thermal properties above the transition temperature to long-range order, provided that the intrachain exchange constant J/k is much larger than the interchain exchange constant J'/k (see e.g. ref. 5.). Hence, in order to study the linear chain characteristics one should like compounds in which the linear chains are well separated.

The well-known compounds of the formula $MX_2.2H_2O$, where M = Cu, Ni, Co, Fe and Mn; X = Cl, Br exhibit a polymeric chain structure (e.g. refs. 6-8). The infinite chemical linear chains of dihalide bridged metal ions are separated by H_2O molecules. In order to increase the separation between the chains the water molecules can be replaced by large organic molecules, such as e.g. pyrazole, pyridine. In this class of Ni compounds, thus far only two X-ray structure determinations have been performed, viz. α-$CoCl_2.2py$ [9] and $MnCl_2.2pz$ [10]. Both compounds contain similar polymeric linear chains consisting of dihalide bridged metal ions and axial N-donor ligands, yielding a distorted octahedral co-ordination around the metal ions (see fig. 1). The metal - metal distances within the chain amount to 3.7 - 3.8 Å. From X-ray powder diagrams Gill *et al.* [11] concluded that $NiCl_2.2py$ belongs to the same class of compounds as α-$CoCl_2.2py$. Similarly from the X-ray powder

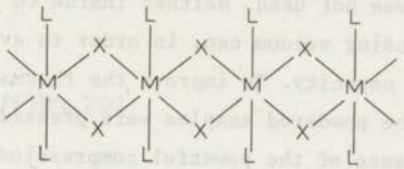

Fig. 1. *Probable chain structure of the NiX_2L_2 compounds, where X = Cl, Br and L = pyrazole, pyridine.*

diagrams and infrared spectra of the Ni compounds of this research, Reedijk [12] concluded that they were isomorphic with α-$CoCl_2$.2py, thus indicating that similar linear chains occur in the present compounds.

For a few compounds of the series MX_2L_2 i.e. $CuCl_2$.2py [13] [14], $CuBr_2$.2py [15], $CoCl_2$.2py [13] and $MnCl_2$.2pz [16] experimental evidence has been found for a better isolation of the chains in a comparison of the specific heat and susceptibility results with those of the dihydrated compounds [17] [18]. As will be shown below, the specific heat results on the NiX_2L_2 compounds are not only consistent with a chain structure as suggested from the isomorphism with α-$CoCl_2$.2py, but in fact require it. Furthermore, it will be shown that the presence of single-ion anisotropy greatly determines the magnetic and thermal properties of these linear chain compounds.

2. Experimental. 2.1 Sample preparation. The compounds were prepared as yellow-green powders by mixing alcoholic solutions of $NiX_2.6H_2O$ and the ligand in a 1:2 ratio, in the presence of diethylorthoformate for dehydration [19] [20]. The purity of the samples was checked by metal analysis and infrared spectroscopy. The compounds are quite stable in the air, except $NiBr_2$.2py, which is hygroscopic [12].

2.2 Apparatus. The heat capacity measurements have been performed on powdered samples, weighing about ten grams, in an adiabatic calorimeter set-up, using the standard heat pulse method. The sample holders were made mainly of copper and were gold plated to prevent chemical

reactions of the samples with the calorimeter can. A mechanical heat-switch provided thermal contact between the sample holder and the cooling liquids. Exchange gas was not used, neither inside to the calorimeter can, nor in the surrounding vacuum can, in order to avoid spurious contributions to the heat capacity. To improve the thermal contact within the calorimeter can, the powdered samples were pressed hydraulically into the sample holder. Because of the powerful compression of the samples it was impossible to re-use the calorimeter can. In each case the heat capacity of the empty calorimeter can has, therefore, been determined in a separate measuring run, prior to the sample measurement.

As a thermometer we used a carbon resistance [21], which was calibrated each run against the He^4, H_2 and O_2 bath temperatures. The details of the thermometry and of the electronic parts of the measuring apparatus will be published elsewhere [22].

3. Experimental results. 3.1 General. The specific heats of $NiCl_2.2pz$ and $NiBr_2.2pz$ are shown as a function of temperature between T = 1.3 K and T = 80 K in figs. 2 and 3, respectively. The specific heat curve

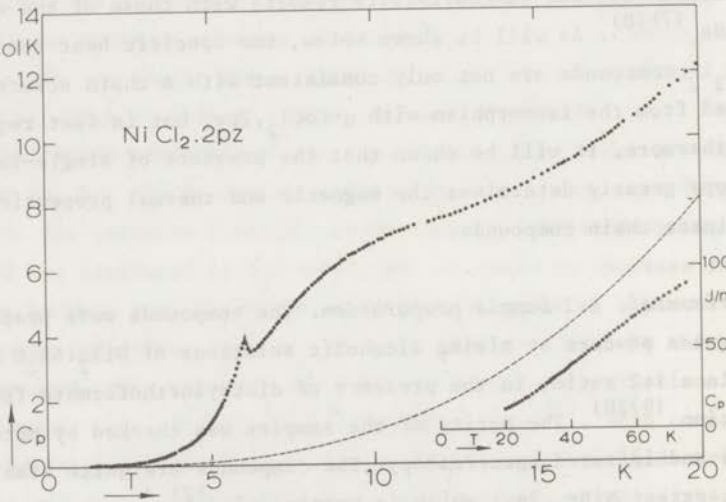

Fig. 2. *The specific heat of $NiCl_2.2pz$ as a function of temperature.*
..... *experimental results.*
- - - *estimated lattice heat capacity.*
The high temperature data, i.e. up to T = 80 K, are represented in the inset.

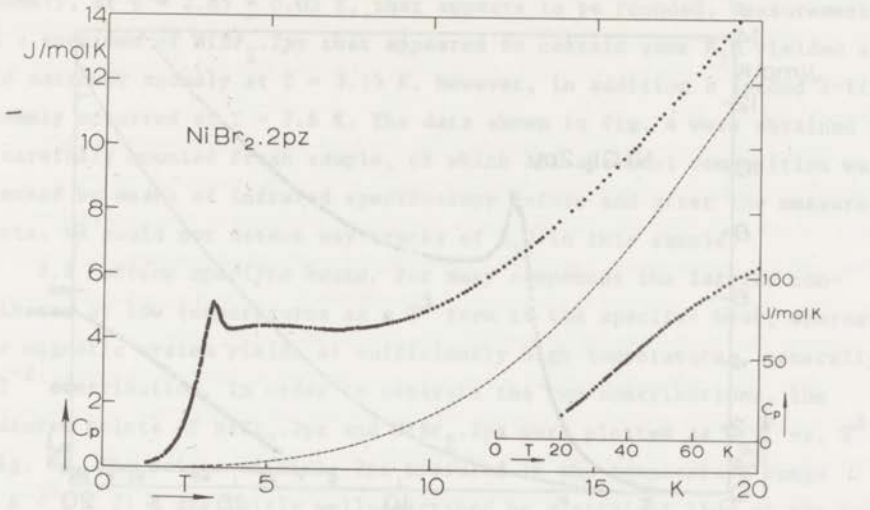

Fig. 3. *The specific heat of $NiBr_2.2pz$ as a function of temperature.*
..... *experimental results.*
- - - *estimated lattice heat capacity.*

of fig. 2 displays a broad shoulder between the liquid helium and hydrogen temperature regions with in addition a relatively small λ-like anomaly at T = 6.05 ± 0.05 K. We associate this sharp peak with the establishment of long-range ordering. Below the peak temperature the specific heat decreases rapidly, e.g. resulting in a C_p value of only 0.008 J/mol K at T = 1.3 K. A similar behaviour is found for $NiBr_2.2pz$ (fig. 3). However, for this compound the maximum of the shoulder occurs at a lower temperature and is less marked. The variation of C_p in the temperature region between T = 3.5 K and T = 8.5 K, amounts to only 4 per cent of the value of C_p. On the other hand the λ-like anomaly, at T = 3.35 ± 0.05 K is more pronounced than that for $NiCl_2.2pz$.

The specific heats of $NiCl_2.2py$ and $NiBr_2.2py$ are shown as a function of temperature in figs. 4 and 5, respectively. Although the features are generally similar to those in figs. 2 and 3, it should be noticed that the λ-like anomalies are more pronounced and that the total specific heats above the long-range ordering temperatures do not display the broad maxima, seen in figs. 2 and 3. For $NiCl_2.2py$ actually two peaks

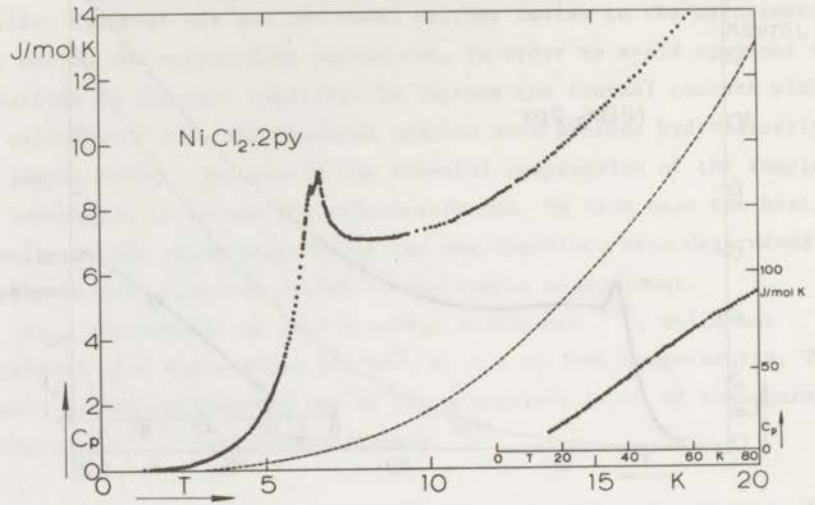

Fig. 4. *The specific heat of $NiCl_2.2py$ as a function of temperature.*
..... *experimental results.*
- - - *estimated lattice heat capacity.*

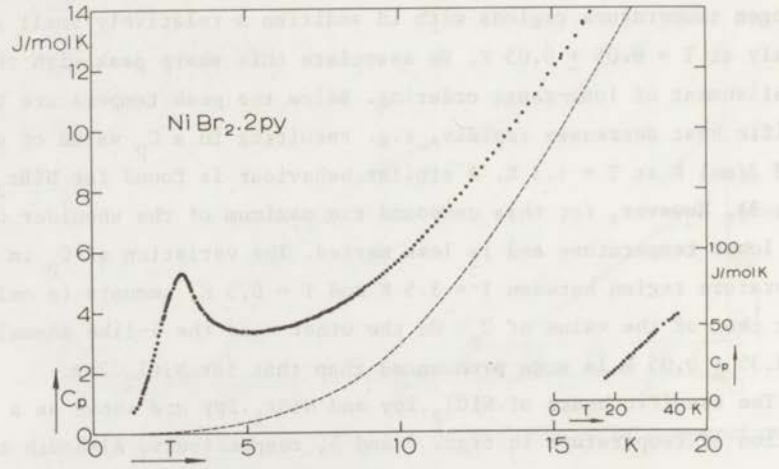

Fig. 5. *The specific heat of $NiBr_2.2py$ as a function of temperature.*
..... *experimental results.*
- - - *estimated lattice heat capacity.*

are observed which occur at T = 6.41 ± 0.01 K and T = 6.750 ± 0.005 K. For $NiBr_2.2py$ (fig. 4) the specific heat curve displays a rather symmetrical anomaly, at T = 2.85 ± 0.05 K, that appears to be rounded. Measurements on a specimen of $NiBr_2.2py$ that appeared to contain some H_2O yielded a higher and narrower anomaly at T = 3.15 K. However, in addition a second λ-like anomaly occurred at T = 7.6 K. The data shown in fig. 4 were obtained on a carefully mounted fresh sample, of which the chemical composition was checked by means of infrared spectroscopy before and after the measurements. We could not detect any traces of H_2O in this sample.

3.2 Lattice specific heats. For many compounds the lattice contributes at low temperatures as a T^3 term to the specific heat, whereas the magnetic system yields at sufficiently high temperatures, generally a T^{-2} contribution. In order to separate the two contributions, the measured points of $NiCl_2.2pz$ and $NiBr_2.2pz$ were plotted as C_pT^2 vs. T^5 (fig. 6). The points of $NiCl_2.2pz$ measured in the temperature range 18 K < T < 21 K are fairly well-described by a straight line of the form $C_pT^2 = b + a\,T^5$, with $a = 1.1 \times 10^{-3}$ J/mol K^4 and b = 1400 JK/mol. Interpretation of the T^3-coefficient in terms of a Debye Θ yields an acceptable value for Θ. In the case of $NiBr_2.2pz$, however, this method fails: the curvature of the C_pT^2 versus T^5 plot makes this method of separation of doubtful significance. Instead, in order to obtain a reliable estimate of the low-temperature lattice specific heat of $NiBr_2.2pz$, the corresponding states argument [23] has been used.

Since $NiCl_2.2pz$ and $NiBr_2.2pz$ are shown to be powder X-ray isomorphous and the only ions that are different are the halogen ions, the corresponding states argument should be applicable. Assuming

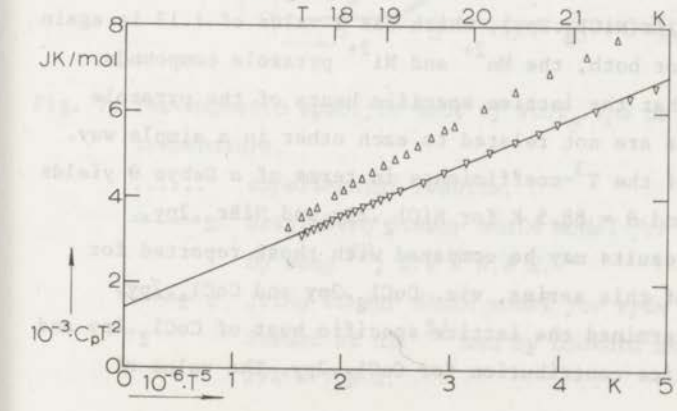

Fig. 6.
C_pT^2 *vs.* T^5 *plot*
∇ $NiCl_2.2pz$
Δ $NiBr_2.2pz$

that at high temperatures, i.e. T >50 K, the measured specific heat is due solely to the lattice contributions the ratio $r(NiBr_2.2pz)/r(NiCl_2.2pz)$ was determined in this range as 1.17. Using this value the low-temperature lattice specific heat of $NiBr_2.2pz$ (see fig. 3) has been calculated from that of $NiCl_2.2pz$.

Evidently it would be worthwhile to put the estimated lattice specific heats on a sounder base through a comparison with the specific heat of an isomorphous diamagnetic compound. Attempts to prepare such diamagnetic compounds, however, were unsuccessful. Nevertheless, the lattice specific heats have been compared with the corresponding results obtained for the isomorphous magnetic compounds $MnX_2.2pz$ [24] (X = Cl, Br). The C_pT^2 versus T^5 plots for these compounds exhibit straight lines over a larger temperature region and at lower temperatures than those for the $NiX_2.2pz$ compounds, so that one has greater confidence in the accuracy of the derived lattice contribution. The corresponding states ratio $r(MnBr_2.2pz)/r(MnCl_2.2pz)$ takes a value of 1.17 in both the high and the low-temperature regions. This is the same value as the ratio determined for the Ni compounds. Furthermore, the fact that the total magnetic entropy, as found for the Ni compounds is close to the theoretical value for a spin 1 system supports the reliability of the lattice specific heat estimates.

The lattice specific heats of the compounds $NiCl_2.2py$ and $NiBr_2.2py$, indicated in figs. 4 and 5, were determined along similar lines as for the pyrazole compounds. At low temperatures the values for the T^3 coefficients were obtained as: $a = 1.7 \times 10^{-3}$ J/mol K^4 and $a = 2.8 \times 10^{-3}$ J/mol K^4 for $NiCl_2.2py$ and $NiBr_2.2py$, respectively. The ratio $r(NiBr_2.2py)/r(NiCl_2.2py)$, which has a value of 1.17 is again equal to that found for both, the Mn^{2+} and Ni^{2+} pyrazole compounds. We notice, however, that the lattice specific heats of the pyrazole and pyridine compounds are not related to each other in a simple way.

Interpretation of the T^3-coefficients in terms of a Debye θ yields values of θ = 103 K and θ = 88.5 K for $NiCl_2.2py$ and $NiBr_2.2py$, respectively. These results may be compared with those reported for the other compounds of this series, viz. $CuCl_2.2py$ and $CoCl_2.2py$. Takeda *et al.* [13] determined the lattice specific heat of $CoCl_2.2py$ and assumed the same lattice contribution for $CuCl_2.2py$. The value of

θ = 84 K, of Takeda, differs considerably from the value obtained for $NiCl_2.2py$, θ = 103 K. On the other hand, however, similarly large differences have been found for the Ni and Mn compounds with both pyrazole and pyridine (chapter V).

4. Magnetic specific heat results. 4.1 General. The magnetic specific heat C_M of $NiCl_2.2pz$, obtained after subtraction of the lattice contribution from the experimental C_p data, is shown in fig. 7 as a function of temperature. The main features of the figure are the broad maximum in the C_M versus T curve (C_{max} = 5.8 $\pm$ 0.1 J/mol K and $T(C_{max})$ = 11 K) and the λ-like anomaly at T = 6.05 $\pm$ 0.05 K. Recalling the structural evidence for linear chains in this material, the broad maximum may be interpreted as being due to the presence of predominantly linear chain exchange interactions. We shall now discuss that a comparison of the entropy found above and below T_c supports this conclusion.

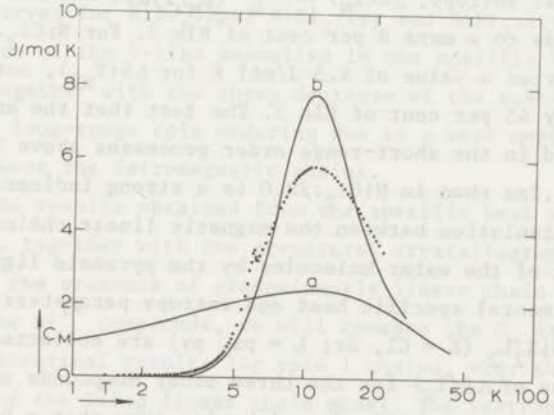

Fig. 7. *The magnetic specific heat of $NiCl_2.2pz$ as a function of temperature.*

..... *experimental results.*

——— a *Heisenberg linear chain model for S=1 as calculated by Weng [4]; J/k = 6.8 K.*

——— b *Ising linear chain model for spin 1 as calculated by Suzuki et al. [2] and by Obokata and Oguchi [3]; J/k = 7.9 K.*

Numerical integration of the C_M/T data with respect to temperature yields a value of 6.9 J/mol K for the entropy variation between 1.3 K and 20 K. Using the $C_M T^2$ value obtained from the $C_p T^2$ versus T^5 plot, we calculate by extrapolation a contribution of 1.75 J/mol K above 20 K. From the rapid decrease of C_M at low temperatures, together with the fact that C_p amounts to only 1×10^{-2} J/mol K at 1.3 K, we may safely assume that the entropy content below 1.3 K is much smaller than the estimated error in the ΔS determination (i.e. 0.1 J/mol K). Thus, the total magnetic entropy content $\Delta S = 9.0 \pm 0.1$ J/mol K, which is close to the theoretical value for a spin 1 system: $\Delta S = R\ln(2S + 1) = R\ln 3 = 9.13$ J/mol K. The estimated uncertainty in ΔS partly arises from the high-temperature extrapolation because a proper representation of $C_M(T)$ for T >20 K will probably require higher-order terms in the high-temperature series expansion of the specific heat, in addition to the T^{-2} term. Also the uncertainty of the C_1 estimate may influence the results.

The critical entropy, $\Delta S(T_N) = \int_0^{T_N} (C_M/T)dT$, amounts 0.73 J/mol K, which corresponds to a mere 8 per cent of R ln 3. For $NiCl_2.2H_2O$ Polgar *et al.* [25] reported a value of 4.3 J/mol K for $\Delta S(T_{N2})$, corresponding to approximately 45 per cent of R ln 3. The fact that the amount of entropy involved in the short-range order processes above T_N is much larger in $NiCl_2.2pz$ than in $NiCl_2.2H_2O$ is a strong indication of a more effective isolation between the magnetic linear chains through the replacement of the water molecules by the pyrazole ligands.

The experimental specific heat and entropy parameters obtained on the compounds NiX_2L_2 (X = Cl, Br; L = pz, py) are collected in table I. The small values of $\Delta S(T_N)$ for the three other compounds of this series, although larger than for $NiCl_2.2pz$, likewise show that a high degree of short-range order occurs at temperatures closely above T_N in all these materials.

Information about the sign of the magnetic exchange interactions in the NiX_2L_2 compounds has been obtained from susceptibility measurements [26a-b]. The asymptotic Curie-Weiss constants (θ) were found to lie in the range between 24 K ($NiCl_2.2pz$) and 9 K ($NiBr_2.2py$) [26b] From the positive θ values one concludes that the exchange along the chains is ferromagnetic for all of the Ni^{2+} compounds investigated.

TABLE I

Experimental results for the magnetic specific heat

	T_{N1}	T_{N2}	$T(C_{max})$	C_{max}	ΔS	$\Delta S(T_{N1})$	$\Delta S(T_{N2})$	$\Delta E(T_{N1})$
	K	K	K	J/mol K	J/mol K	J/mol K	J/mol K	J/mol
$NiCl_2$.2pz	6.05 ± 0.05		11	5.3	9.0 ± 0.1	0.73		3.6
$NiBr_2$.2pz	3.35 ± 0.05		4.6	4.2	9.0 ± 0.1	1.2		3.3
$NiCl_2$.2py	6.41 ± 0.01	6.750 ± 0.005			9.2 ± 0.1	1.4	1.83	7.5
$NiBr_2$.2py	2.85 ± 0.05		10	2.3	9.1 ± 0.1	2.4		5.0

For $NiCl_2$.2pz the susceptibility decreases drastically below 6 K; it may be recalled that the λ-like anomaly in the specific heat occurs at T_N = 6.05 K. Similar behaviour of the low-temperature susceptibility [26b] has been observed for $NiBr_2$.2pz, $NiCl_2$.2py and $NiBr_2$.2py. We attribute the occurrence of the λ-like anomalies in the specific heat of these compounds, together with the sharp decrease of the susceptibilities, to the onset of long-range spin ordering due to a weak *antiferromagnetic* coupling between the ferromagnetic chains.

Since the results obtained from the specific heat and susceptibility measurements, together with the structural crystallographic evidence, all point to the presence of predominantly linear chain exchange interactions in the Ni^{2+} compounds, we will compare the C_M data with the available theoretical results for spin 1 chains, viz. the isotropic Heisenberg and the Ising linear chain model. The isotropic Heisenberg linear chain model with spin 1 has been treated by Weng [4]. He calculated the thermodynamic properties in the limit of infinite chains by means of an extrapolation of his finite chain results, i.e. chains and rings, containing up to 7 atoms. The specific heat for this model which is described by the exchange hamiltonian

$$H = -2J\Sigma_{i=1}^{N} \vec{S}_i . \vec{S}_{i+1}, \qquad (4.1)$$

calculated for J/k = 6.8 K, is shown in fig. 7.

The specific heat for the Ising linear chain model with spin 1 has been reported by Suzuki *et al.* [2] and by Obokata and Oguchi [3]. With the exchange hamiltonian written as

$$H = -2J\Sigma_{i=1}^{N} S_{i,z} S_{i+1,z}, \qquad (4.2)$$

the specific heat has been calculated for J/k = 7.9 K (see fig. 7). The J/k values were chosen in such a way that the maxima of the theoretical and experimental curves occur at the same temperature. Neither of the theoretical curves, however, matches the experimental data, even qualitatively, on $NiCl_2$.2pz. In view of the position of the observed transition temperature with respect to that of the maximum, one may expect that the interchain coupling present in $NiCl_2$.2pz is sufficiently weak that its effect on the specific heat at temperatures as high as $T(C_{max})$ = 11 K cannot nearly account for the difference between the experimental and either of the two theoretical curves.

Similar differences between experiment and theory (i.e. eqs. (4.1) and (4.2)) were found for $NiBr_2$.2pz, $NiCl_2$.2py. A more likely explanation, therefore, seems to lie in the presence of single-ion anisotropy, in particular, since divalent nickel may have a large crystal field splitting. We will consider the single-ion anisotropy of the Ni^{2+} ions (sec. 4.1.1) and its interplay with the exchange interactions and the effect on the specific heat (sec. 4.1.2).

4.1.1 Single-ion anisotropy. The $3d^8$ electronic configuration of the Ni^{2+} ion gives rise to a ^3F ground orbital state for the free ion. In a cubic octahedral co-ordination the ^3F state is split into an orbital singlet $^3A_{2g}$ and two triplets $^3T_{1g}$ and $^2T_{2g}$, with $^3A_{2g}$ lowest. Through the combined action of a spin-orbit coupling and deviations from the cubic crystalline field symmetry the $^3A_{2g}$ level is split. This is demonstrated by second-order perturbation theory via higher states. When the distortion of the octahedral surrounding has axial symmetry the anisotropy may be described by a term DS_z^2 in the spin hamiltonian; when the symmetry is lower, i.e. rhombic, an additional term $E(S_x^2 - S_y^2)$ is required to describe the single-ion properties. The available crystallographic evidence indicates that the Ni^{2+} ions in the NiX_2L_2 compounds are surrounded by four equatorial halogen ions, while

two strong N-donor ligands complete the octahedral co-ordination. Reedijk [12] concluded from optical spectra that a tetragonally compressed octahedral co-ordination of the Ni^{2+} ions is present in the four compounds studied in this paper. In the absence of exchange or external fields such a structure would give rise to a non-Kramers spin doublet ground state and a higher lying singlet level. When the single-ion hamiltonian is written as

$$H = D\{S_z^2 - \frac{1}{3} S (S + 1)\}, \qquad (4.3)$$

the doublet-singlet separation corresponds to D negative.

4.1.2 Single-ion anisotropy and exchange interaction. We will consider here only the case $D/k<0$, as this will be shown to describe all the experimental data adequately. The decrease in the occupation of the single-ion singlet state with decreasing temperature has the consequence that the z-components of the spin angular momentum exclusively have an appreciable expectation value. Hence, the introduction of exchange interactions with the assumption that $|J/k| << |D/k|$ yields anisotropic, Ising type, exchange interactions between ions with an effective spin $S'=\frac{1}{2}$. When we consider only linear chain exchange interactions, the specific heat would then display two broad maxima, viz. at high temperatures ($T \simeq |D/k|$) a Schottky anomaly and at low temperatures ($T \simeq |J/k|$) an Ising $S'=\frac{1}{2}$ linear chain contribution.

However, in case $|D/k|$ and $|J/k|$ have comparable magnitude, the exchange interactions cannot be approximated as either Heisenberg ($D = 0$, $S = 1$) or purely Ising ($S'=\frac{1}{2}$), i.e. the full hamiltonian has to be used, which includes isotropic intrachain exchange interactions between ions with spin 1 and an uniaxial single-ion anisotropy term:

$$H = -2J \sum_{i=1}^{N} \vec{S}_i . \vec{S}_{i+1} + D \sum_{i=1}^{N} \{S_{i,z}^2 - \frac{1}{3} S(S+1)\} \qquad (4.4)$$

The specific heat according to eq. (4.4) has been obtained in new calculations by Blöte [27] by means of suitable extrapolation of computational results for a finite number of atoms in the chains. The finite chain results have been calculated for chains with N ranging up to 7. In addition, numerical computations on finite rings (up to N = 8)

have been utilized, which provide an estimate of the effect of boundary conditions on linear chain calculations and which, furthermore, offer computational advantages [27]. It will now be shown that the experimental data can be satisfactorily fit by this, more complete, model.

4.2 Comparison with theory. 4.2.1 $NiBr_2.2pz$. The magnetic specific heat of $NiBr_2.2pz$ is shown as a function of temperature in fig. 8. The curve displays two broad maxima (although they are not clearly separated) and in addition a λ-like anomaly at T_N = 3.35 K. The appearance of the two maxima makes an interpretation on the basis of a model with an effective spin $S'=\frac{1}{2}$ Ising linear chain and an independent Schottky anomaly quite plausible. The best fit, assuming simply the additivity of these contributions was obtained for $|J/k(S'=\frac{1}{2})|$ = 10.5 K and D/k = -31 K. In fig. 8 we show the separate contributions as well as the sum curve.

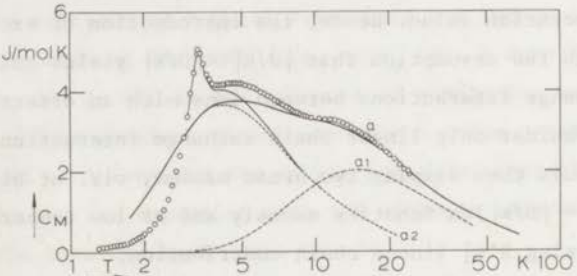

Fig. 8 *The magnetic specific heat of $NiBr_2.2pz$ as a function of temperature.*

o o o experimental results.

----- a1 : Schottky curve for independent Ni^{2+} ions with single-ion anisotropy parameter D/k = -31 K.

----- a2 : Ising linear chain model $S=\frac{1}{2}$; $J/k(S=\frac{1}{2})$ = 10.5 K.

——— a The sum curve of a1 and a2. This curve coincides for the greater part with the curve for the Heisenberg linear chain model with uniaxial single-ion anisotropy as calculated for spin 1 by Blöte [27]; J/k = 2.7 K, D/k = -33 K.

On the other hand, using the full hamiltonian, i.e. eq. (4.4), we found best agreement with experiment for D/J = -12 with J/k = 2.7 K, thus D/k = -33 K (fig. 8). The values for D/k as derived with the two different methods agree quite well. The values for the exchange are also in agreement, since the J/k obtained within the $S'=\frac{1}{2}$ formalism should be four times larger than that corresponding to the S=1 hamiltonian. Since both the specific heat curves and the values for D/k and J/k are in agreement one may conclude that the obtained ratio $|D/J| \simeq 12$ is apparently sufficiently large as to allow Schottky and exchange contributions to be added algebraically as if they were entirely independent. In other words, the behaviour of the compound at low temperatures is close to that of an ideal Ising system with $S=\frac{1}{2}$.

As is seen in fig. 8, the experimental results below T_N are not described with the one-dimensional model calculations. This can be explained on the basis of the three-dimensional long-range spin ordering that will disturb the one-dimensional characteristics drastically. From fig. 8 it can, however, be inferred that also above T_N, up to $T \simeq 8$ K, the experimental heat capacity of $NiBr_2.2pz$ exceeds the calculated curves. This contrasts with the specific heat results of Takeda *et al.* [13] on $CoCl_2.2py$, a compound belonging to the same class of compounds as $NiBr_2.2pz$.

Both compounds can be considered as consisting of anisotropic, Ising-coupled effective spins $\frac{1}{2}$ yielding ferromagnetic linear chains that are coupled by relatively weak antiferromagnetic interactions. Moreover, the intrachain exchange constants in the two compounds are approximately equal, i.e. J/k ($S'=\frac{1}{2}$) $\simeq$ 10 K, whereas the transition temperatures to a long-range ordered state are 3.35 K and 3.17 K for $NiBr_2.2pz$ and $CoCl_2.2py$, respectively. For comparison we show in fig. 9 the magnetic specific heat of $NiBr_2.2pz$ after the subtraction of the Schottky anomaly and that of $CoCl_2.2py$ [13], together with the Ising $S'=\frac{1}{2}$ linear chain curve for J/k = 10 K. Although the features in fig. 9 are generally similar a striking difference is observed above the Néel temperatures, where the experimental data for $NiBr_2.2pz$ are above the theoretical Ising $S'=\frac{1}{2}$ result, while for $CoCl_2.2py$ the experimental curve lies below it. We cannot offer an explanation for the differences in the experimental results. However, it should be noticed that the

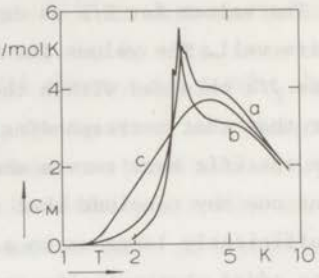

Fig. 9. *The magnetic specific heats of $NiBr_2.2pz$ and $CoCl_2.2py$.*
a. The magnetic specific heat of $NiBr_2.2pz$ after subtraction of a Schottky curve (D/k = -31 K).
b. The magnetic specific heat of $CoCl_2.2py$ after Takada et al. [13].
c. Ising linear chain model for S=½; J/k = 10 K

entropy of $CoCl_2.2py$, when extrapolated to T = ∞ according to the reported results does not reach Rln 2, the theoretical value for the entropy of an S'=½ spin system. Thus the evaluation of the lattice contribution may be somewhat in error. Furthermore, of course, the Ising model may not be realized in practice by these systems.

Exact calculations for the specific heat of a system of linear chains, weakly coupled in a three-dimensional array are thus far not available. However, one would conclude from the two dimensional analogue, i.e. the square S=½ Ising lattice with different couplings in the two directions as calculated by Onsager [28] that the presence of a weak coupling between the chains (besides yielding a finite T_c) will give rise to an additional short-range order contribution to the specific heat above T_c, so that the heat capacity is increased with respect to the curve of the fully isolated chains.

In a similar fashion the magnetic specific heats of $NiCl_2.2pz$, $NiCl_2.2py$ and $NiBr_2.2py$, shown in figs. 10, 11 and 12, respectively, are compared with the curves calculated according to eq. (4.4). The values for J/k and D/k, which give best agreement with the experimental results, are collected in table II along with the values obtained for

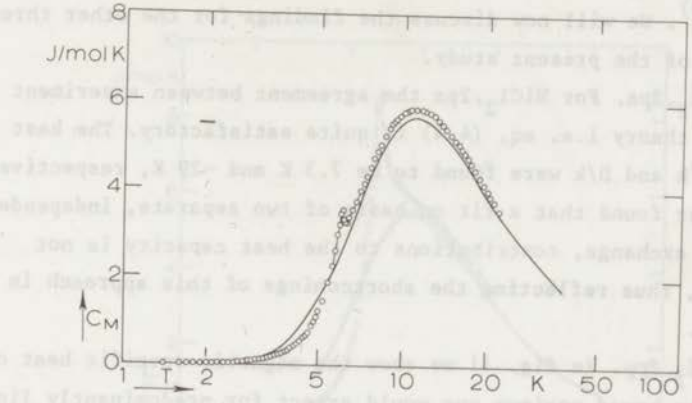

Fig. 10. *The magnetic specific heat of $NiCl_2.2pz$ as a function of temperature.*

o o o *experimental results.*

——— *isotropic Heisenberg linear chain model with uniaxial single-ion anisotropy as calculated by Blöte* [27] *for spin 1; J/k = 7.3 K, D/k = -29 K.*

TABLE II

Values of J/k and D/k derived from specific heat results

	J/k	D/k
	K	K
$NiCl_2.2pz$	7.3	-29
$NiBr_2.2pz$	2.7	-33
$NiCl_2.2py$	5.35	-27
$NiBr_2.2py$	1.9	-30
$NiCl_2.2H_2O$ [25]	-	-16
$NiBr_2.2H_2O$ [29]	1.2	-10

$NiBr_2.2pz$ and with the reported values for $NiCl_2.2H_2O$ [25] and $NiBr_2.2H_2O$ [29]. We will now discuss the findings for the other three nickel salts of the present study.

4.2.2 $NiCl_2.2pz$. For $NiCl_2.2pz$ the agreement between experiment and the complete theory i.e. eq. (4.4) is quite satisfactory. The best values for J/k and D/k were found to be 7.3 K and -29 K, respectively. It was further found that a fit on basis of two separate, independent Schottky and exchange, contributions to the heat capacity is not satisfactory, thus reflecting the shortcomings of this approach in case D/J is small.

4.2.3 $NiCl_2.2py$. In fig. 11 we show the magnetic specific heat of $NiCl_2.2py$. The broad maximum one would expect for predominantly linear chain exchange interactions is partially obscured ty the occurrence of the large peak at about 6.5 K. In order to determine the parameters J/k and D/k of eq. (4.4) from the specific heat data, the value of $T(C_{max})$ as well as the value of C_{max} have to be well defined. From fig. 11, however, it can be inferred that neither of these values can be determined accurately. Hence, for a proper interpretation of the data on $NiCl_2.2py$ one requires calculations on a model which includes the intrachain exchange interaction and single-ion anisotropy as well as the interchain exchange interaction. Since such calculations have not yet been reported in the literature one can only try to fit the experimental data far above T_N to theory. Two curves, calculated on the basis of eq. (4.4), using two sets of parameters, viz. J/k = 6.0 K, D/k = -24 K and J/k = 5.35 K, D/k =-27.0 K, are shown in fig. 11. We believe the latter choice (drawn curve) to be the most reliable one.

The fact that we observed two peaks, lying close together, needs some comment. Double peaks in the specific heat have been observed for quite a number of Ni compounds, e.g. $CsNiCl_3$ [30], $NiI_2[(NH_2)_2CS]_6$. As special examples we mention $NiCl_2.2H_2O$ [25] and $NiBr_2.2H_2O$ [29] in which the temperature intervals between the two peaks are approximately 1 K and 0.5 K, respectively. In the series of Ni compounds reported here, only the specific heat of $NiCl_2.2py$ was found to display two well-defined peaks. The temperature interval between them is smaller than for $NiCl_2.2H_2O$ or $NiBr_2.2H_2O$. On the other hand, the apparently rounded peak in $NiBr_2.2py$ (fig. 4) might be the result of two peaks lying so

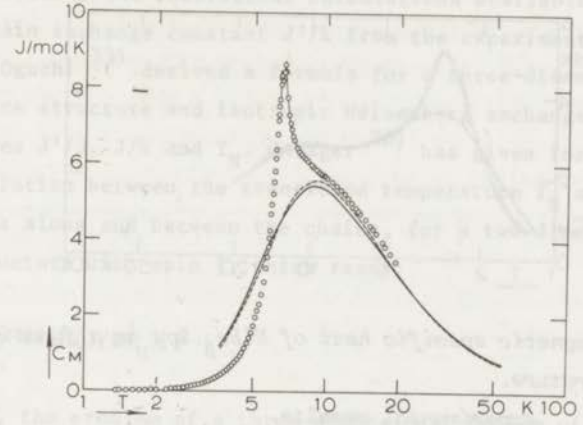

Fig. 11. *The magnetic specific heat of $NiCl_2.2py$ as a function of temperature.*

o o o *experimental results.*

——— *Isotropic Heisenberg linear chain model with uniaxial single-ion anisotropy for spin 1; J/k = 5.35 K, D/k = -27 K.*

------ *Isotropic Heisenberg linear chain model with uniaxial single-ion anisotropy for spin 1; J/k = 6.0 K, D/k = -24 K.*

close together that they are not separated within the experimental resolution or that the peaks are smeared out due to size effects in the powdered samples. Double peaks may result from a spin reorientation in the ordered state due to the presence of significant and complicated anisotropies [30]. From specific heat measurements alone, however, no conclusions can be drawn about the mechanism responsible for the occurrence of the double peaks in $NiCl_2.2py$.

4.2.4 $NiBr_2.2py$. The high-temperature magnetic specific heat of $NiBr_2.2py$ could be fitted on the basis of eq. (4.4), within the experimental error limits, with J/k = 1.9 K and D/k = -29.8 K (see fig. 12). Deviations become apparent near to the low-temperature anomaly. This is not surprising when one takes into account the absence of a

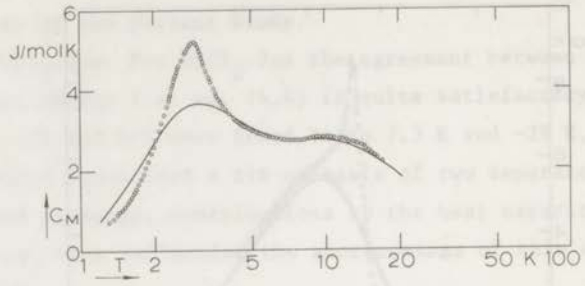

Fig. 12. *The magnetic specific heat of $NiBr_2.2py$ as a function of temperature.*

o o o *experimental results.*

——— *Isotropic Heisenberg linear chain model with uniaxial single-ion anisotropy for spin 1; $J/k = 1.9$ K, $D/k = -29.8$ K.*

pronounced linear chain specific heat maximum. Apparantly the interchain interactions are quite large in this material.

It is known theoretically that the critical entropy, $\Delta S(T_N)$, increases with increasing lattice dimensionality. Typical theoretical values for a 2-d simple quadratic and a 3-d simple cubic lattice with $S'=\frac{1}{2}$ and Ising exchange interactions are $\Delta S(T_c) = 2.42$ and 4.64 J/mol K respectively (e.g. ref. 32). The critical entropy found for $NiBr_2.2py$ amounts to 2.33 J/mol K, which is rather close to the value for the 2-d simple quadratic lattice. For structural reasons, however, significant 2-d ordering is improbable in this compound. Hence, the large value for $\Delta S(T_N)$ in comparison with the values found for the three other compounds of this series is most likely to be attributed to a less complete magnetic isolation of the linear chains in $NiBr_2.2py$. Because of this complication, the value obtained for J/k is less reliable.

5. *Interchain exchange interactions.* As we noticed before, the sharp peak in the specific heat is attributed to the onset of long-range spin ordering, which is due to the presence of a weak antiferromagnetic

coupling (interchain interaction) between the ferromagnetic chains. We mention briefly the theoretical calculations available to determine the interchain exchange constant J'/k from the experimental specific heat data. Oguchi [33] derived a formula for a three-dimensional tetragonal lattice structure and isotropic Heisenberg exchange interactions which relates J'/J, J/k and T_N. Onsager [28] has given for the Ising model an exact relation between the transition temperature T_N and the exchange interactions along and between the chains, for a two-dimensional square lattice structure with spin ½, which reads:

$$\sinh(J'/kT_N)\ \sinh(J/kT_N) = 1 \qquad (4.5)$$

Furthermore, the problem of a three-dimensional system of Ising linear chains with interactions between the chains has been treated by Stout and Chisholm [34] in a molecular field approximation. Within this model the interactions between atoms belonging to adjacent chains would, if acting alone, produce long-range order at a temperature T_c^*, which temperature is related to the actual transition temperature T_c in the coupled linear chain system as:

$$T_c^* = T_c \exp\ (-|J|/kT_c). \qquad (4.6)$$

In the general molecular field approximation the expression for the transition temperature of a spin ½ three-dimensional system with an exchange constant $\tilde{J}/k$ between z nearest neighbours reads [35]:

$$\tilde{T}_c = |z\tilde{J}/2k| \qquad (4.7)$$

Identifying in our case $\tilde{T}_c = T_c^*$, $|\tilde{J}/k| = |J'/k|$ and z with the number of next nearest neighbours, the resulting expression for the weakly coupled Ising S=½ linear chain system may then be written:

$$|zJ'/k| = 2\ T_c \exp\ (-J/kT_c) \qquad (4.8)$$

Because, however, none of the rather simple models mentioned above fully describes the interactions in the investigated Ni^{2+} compounds, only an

order of magnitude result for $|J'/J|$ can be anticipated.

Using the experimentally determined values of T_N (table I) and the values of J/k (table II), the ratio's J'/J (Oguchi), J'/J (2-d square Ising lattice) and zJ'/J (M.F. approximation) were calculated (table III).

TABLE III

Values of J'/J and zJ'/J derived from specific heat and susceptibility [38] results

	$\lvert J'/J\rvert$ [a]	$\lvert J'/J\rvert$ [b]	$\lvert zJ'/J\rvert$ [c]	$\lvert zJ'/J\rvert$ [d]
$NiCl_2.2pz$	2×10^{-2}	0.3×10^{-2}	0.3×10^{-2}	0.35×10^{-2}
$NiBr_2.2pz$	$5 \times$ "	$2.5 \times$ "	$2.5 \times$ "	$2.5 \times$ "
$NiCl_2.2py$	$6 \times$ "	$3 \times$ "	$3 \times$ "	$3 \times$ "
$NiBr_2.2py$	$9 \times$ "	$5 \times$ "	$4 \times$ "	$10 \times$ "

a) Oguchi, b) eq. (4.5), c) eq. (4.8), d) eq. (4.12)

In order that we may use the molecular field approximation in the form expressed before and the Onsager solution, the exchange constants J/k (S=1) were transformed to the values in the spin ½ form, i.e. $J/k(S=\frac{1}{2}) = 4\ J/k(S=1)$. The Ising properties of the exchange interactions at low temperatures were demonstrated in the case of $NiBr_2.2pz$, whereas for $NiCl_2.2py$ the possible Ising properties of the exchange interactions are less clear than for $NiBr_2.2pz$.

In the last column of table III the ratio zJ'/J is given, as calculated from the field-dependent transitions in these compounds, to be discussed in sec. 6.2.

6. Metamagnetic behaviour. 6.1 General. The application of an external magnetic field to an antiferromagnetic substance is expected to affect the ordered arrangement of the spins. The effects depend on the orientation of the field with respect to the easy axis as well as the strength of the field compared with the internal exchange and anisotropy fields. In particular when the anisotropy is not large, a field applied parallel to the easy axis will cause the phenomenon of spin-flop (e.g. ref. 36). On the other hand, when the anisotropy energy is

large in comparison with the exchange energy, another situation occurs which is conducive to the existence of metamagnetic behaviour. The application of an external magnetic field along the easy spin direction of a metamagnetic system produces, when $T<T_{tricritical}$, at a critical field strength $H_c(T)$ an abrupt transition from the antiferromagnetic to a paramagnetic phase with a parallel spin alignment. This phenomenon is particularly well studied in the series of anhydrous iron dihalides (e.g. ref. 37). Since for the present compounds $J/k>0$ and $J'/k<0$, while $|D| > |J'|$ it was thought that the basic conditions necessary for metamagnetism to occur might be fulfilled. We decided, therefore, to measure the heat capacity of the most likely candidate in an external magnetic field. The compound $NiBr_2.2pz$ was chosen because it has the largest single-ion anisotropy and is at low-temperatures satisfactorily described by an Ising $S'=\frac{1}{2}$ system. Furthermore, the measured field dependence of the ferromagnetic linear chain specific heat can be compared with theoretical calculations. The hamiltonian for an Ising $S'=\frac{1}{2}$ linear chain system with an external magnetic field applied along the easy axis of spin orientation can be written as:

$$H = -2J \sum_{i=1}^{N} S_{i,z} S_{i+1,z} + g\mu_B H_z \sum_{i=1}^{N} S_{i,z}. \qquad (4.9)$$

Since we are for $NiBr_2.2pz$ dealing with a random orientation of the powdered sample grains, an averaging procedure has been applied in order to account for the different orientations of the spins with respect to the external field direction. Due to the large single-ion anisotropy, the g-value becomes anisotropic at low temperatures, i.e. $T<<D/k$, yielding $g_{//} \simeq 2g$ and $g_{\perp} \simeq 0$, where g is the high-temperature g-value. This is generally found to take a value of about 2.2 for Ni^{2+} ions in octahedral surroundings. Since, to a first approximation, the perpendicular term can be neglected, we arrive at eq. (4.9) with $g = g_{//}$.

6.2 Specific heat of $NiBr_2.2pz$ in an external magnetic field. The magnetic specific heat of $NiBr_2.2pz$ measured in a field of 5 kOe, C(H), is shown in fig. 13. The λ-like anomaly has disappeared within experimental error which result probably implies that the critical field for $NiBr_2.2pz$ is smaller than 5 kOe. Furthermore, the maximum of

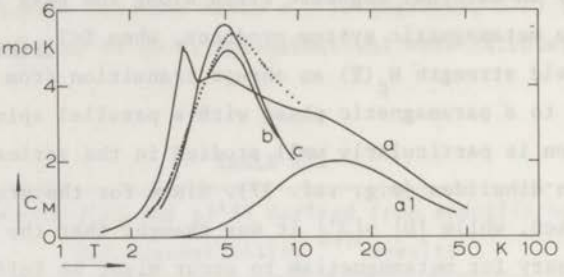

Fig. 13. *The magnetic specific heat of $NiBr_2.2pz$ in an external magnetic field as a function of temperature.*

..... *experimental results.*

a : *experimental results in zero field.*

a1: *Schottky curve for D/k = -31 K.*

b : *experimental results in external field, after subtraction of curve a1.*

c : *Ising linear chain model in an external field; J/k = 10 K, $g_{//}$ = 4.5 and H_{ext} = 5 kOe.*

the magnetic specific heat increased to 5.4 J/mol K and shifted to a higher temperature, $T(C_{max})$ = 5.4 K. At temperatures sufficiently high, i.e. T > 14 K, the C(H) curve approximately coincides with the C(0) curve. We will use eq. (4.9) to calculate C(H). Using $g_{//}$ = 4.5 and H = 5 kOe, together with J/k ($S'=\frac{1}{2}$) = 10.5 K, as determined from the C(0) results, we obtain C(H) as shown in fig. 13. The general features are satisfactorily described, although the calculated curve attains a maximum value which is approximately 10 per cent larger than the experimental result. A better result for the powder measurements and this simple model is not to be expected. In fact, we notice that when $g_{\perp}$ is unequal to zero, which may occur due to e.g. the presence of a rhombic distortion of the crystalline field at the Ni ions, the maximum of the calculated specific heat will be lower. The overall agreement between the calculated and experimental results corroborates the proposed presence of a large zero-field splitting of the nickel ions in $NiBr_2.2pz$.

Specific heat measurements, however, cannot procure sound conclusions about the metamagnetic behaviour. Even a determination of the magnetic phase diagram (H-T) by means of external field measurements is hard to obtain because the energy involved in the 3-d long-range order peak is small in comparison with the magnetic field energy involved in the short-range order processes. Therefore, to obtain values for the critical field in these Ni-compounds both the real and the imaginary components of the complex susceptibility $\chi = \chi' - i\chi''$ have been measured at low temperatures ($1.3\ K < T < 4.2\ K$) by Rutten *et al.* [38] with the aid of a twin-T-bridge [39]. Frequencies between 100 kHz and 30 MHz were used and the radiofrequent field was parallel to the external magnetic field. Signals proportional to χ' and χ'' were recorded directly as a function of magnetic fields up to 5 kOe.

While for $NiCl_2.2pz$ and $NiBr_2.2pz$ a single critical field value, H_c, has been observed, for $NiCl_2.2py$ the magnetization reaches its saturation stepwise. Similar stepwise behaviour of the magnetization has been reported earlier, e.g. in $CoCl_2.2H_2O$ [40], $CoBr_2.2H_2O$ [41] and $NiCl_2.2H_2O$ [42]. These compounds also consist of ferromagnetic linear chains mutually linked by antiferromagnetic interactions and the behaviour of the magnetization has been explained by assuming the presence of different interchain interactions, yielding competing anisotropy energies.

The fact that no sign of spin-flopping was found supports the conclusion of the metamagnetic character, whereas due to the small values of $|J'/J|$ it is expected that the tricritical point lies closely below T_N. However, since only powder measurements have been performed thus far, no firm conclusions can be given. Except for the case of $NiBr_2.2py$ the critical field values were always found to be smaller than 5 kOe. We recall that the interchain coupling is found to be weak in these compounds, which explains the small critical field values. In order to obtain an estimate for the interchain coupling from the experimental H_c-values, we assume the compounds, at temperatures $T < T_N$ and in zero external field, to consist of a two-sublattice antiferromagnetic structure. Because of the large values of D/k ($D/k < 0$) we may at low temperatures regard the system as having effective spins $S' = \frac{1}{2}$ and Ising exchange interactions. For the magnetic energy at $T = 0\ K$

and H = 0 we then find:

$$E_I = -N\,S'^2(2J + z|J'|) \tag{4.10}$$

In an external field $H > H_c$ half of the spins reverse their direction so as to attain a parallel spin alignment. The energy at T = 0 K, and $H > H_c$ may then be written as:

$$E_{II} = -N\,S'^2(2J - z|J'|) - \frac{N}{2} g_{//} \mu_B S'H \tag{4.11}$$

At $H = H_c$ we obtain

$$2N\,S'^2\, z|J'| = N\, g_{//} \mu_B H_c S' \tag{4.12}$$

which can be written as

$$z|J'| = g_{//} \mu_B H_c/2S' \tag{4.12}$$

Using $g_{//} = 4.4$, $S' = \frac{1}{2}$ and the experimental H_c-values we obtain from eq. (4.12) the values for $z|J'|$ (or $|\frac{zJ'}{J}|$) as collected in table III. Naturally, we notice that for $NiCl_2.2py$ the largest critical field value was used for the calculation of $z|J'|$. Now we suppose that z = 4, which is from the crystal structure a reasonable value for these compounds. Then the values for $|J'/J|$ using Oguchi's formula are approximately a factor ten larger than those found with the two experimental methods mentioned above. This difference is quite understandable because Oguchi's calculations are performed for isotropic exchange interactions, whereas the present Ni^{2+} compounds exhibit anisotropic exchange interactions at temperatures of the order T_N. The close results obtained using the two dimensional Ising model approximation might be reasonable because the difference between the 2-d and 3-d model with respect to kT_c/J can, to a good approximation, be reduced to the number of nearest neighbours. On the other hand, the close agreement of the $|J'/J|$ values found for the molecular field approximation method of the 3-d weakly mutually coupled Ising linear chains is rather unexpected in view of the approximations made to arrive at the relation between T_c, J/k and J'/k.

7. Concluding remarks. The experimental magnetic specific heat results of the Ni^{2+} compounds can, for temperatures $T > T_N$, be adequately described by an isotropic S=1 exchange hamiltonian with an additional uniaxial single-ion anisotropy and neglecting the interchain coupling. The small values for $|J'/J|$ as derived from both the kT_c/J values and the field-dependent transitions, in conjunction with the large values of short-range order entropy, show a predominance of the intrachain exchange interactions in these Ni-compounds. From the comparison of the values for the critical entropy we may conclude that, by replacing the water molecules in $NiX_2.2H_2O$ by the larger ligands, such as pyrazole and pyridine, the isolation of the magnetic linear chains is greatly improved.

The magnetic specific heat above T_N in these compounds is mainly due to a combination of the exchange interactions along the chains and the large zero-field splitting of the divalent nickel ions. The intrachain exchange constants, which are apparently all ferromagnetic in the investigated compounds, have smaller values in both the pyrazole and pyridine compounds than in $NiBr_2.2H_2O$ [29] (see also table II). We notice the large difference between the J/k values in the Cl and Br compounds. Whereas in isomorphous compounds the J/k values are usually larger for the Br than for the Cl compounds, in this series of Ni salts the J/k values in the Cl compounds are a factor three larger than those of the corresponding Br compounds. From susceptibility measurements on dimeric nickel compounds Ginsberg *et al.* [43] found evidence for a similar decrease of the J/k value in the sequence of the bridging ligands $Cl^- > Br^- > NCS^-$, which has been ascribed to the increasing size of the expanded magnetic orbital of the bridging group. Accurate crystal structure determinations of these crystals could prove interesting in finding a relation between exchange and crystallographic parameters.

The crystal-field splittings of the divalent nickel ions, as determined from the specific heat results, are quite large (see table II). From the band splittings in the optical spectra and using the usual methods to determine the zero-field splitting (see e.g. Ballhausen [44]), it was found that $|D/k|$ has a much smaller value [45]. This discrepancy remains unexplained. A possible source may be the different temperature regions of the two experiments. Because of the cooling of the sample a contraction of the crystal may give rise to an increase of the tetragonal

crystal field, yielding an increase of $|D/k|$ at the lower temperatures. On the other hand preliminary calculations of D/k from the band splittings, introducing anisotropic spin-orbit coupling, yields quite good agreement with the results from the thermal measurements [45].

In principle, specific heat measurements can give information about rhombic distortions of the crystalline field at the Ni^{2+} ion sites. Calculations for the exchange hamiltonian given in eq. (4.4) with an additional rhombic term $E\ (S_x^2 - S_y^2)$ on finite chains (N up to 3), however, indicate that the introduction of a small E/k value, i.e. $E/k < |J/k|$, does not significantly alter the heat capacity curve.

Estimates for the interchain coupling constants in the Ni compounds are given in table III. From table III it can be concluded that an increase of the interchain interactions between the ferromagnetic linear chains is found in the sequence of compounds, $NiCl_2$.2pz, $NiBr_2$.2pz, $NiCl_2$.2py and $NiBr_2$.2py. The smaller values for $|J'/J|$ found for the pyrazole as compared to the pyridine compounds is probably due to hydrogen bonding between the anions and the pyrazole ligands within the chain [10]. In summarizing the results we can say that these measurements have shown that, notwithstanding the fact that theoretical calculations for the S=1 isotropic Heisenberg linear chain model show a large difference between the C_{max} value for an antiferromagnetic and a ferromagnetic linear chain, no conclusions can be drawn about the sign of the exchange constant from the experimental C_{max} value for Ni^{2+} linear chain compounds alone; the presence of single-ion anisotropy may greatly enhance the C_{max} value.

References

1 Klaaijsen, F.W., Blöte, H.W.J. and Dokoupil, Z., Solid State Commun., 14 (1974) 607.

2 Suzuki, M., Tsujiyama, B. and Katsura, S., J. Math. Phys., 8 (1967) 124.

3 Obokata, T. and Oguchi, T., J. Phys. Soc. Jap., 25 (1968) 322.

4 Weng, C.Y., Thesis, Carnegie - Mellon University, Pittsburg (1968).

5 De Jongh, L.J. and Miedema, A.R., Adv. in Phys., 23 (1974) 1.

6 Morosin, B., Acta Cryst., 23 (1967)630.

7 Morosin, B. and Graeber, J., Acta Cryst., 16 (1963) 1176.
8 Morosin, B. and Graeber, J., J. Chem. Phys., 42 (1965) 898.
9 Dunitz, J.D., Acta Cryst., 10 (1957) 307.
10 Gorter, S., Acta Cryst., submitted.
11 Gill, N.S., Nyholm, R.S., Barclay, G.A., Christie, T.I. and Pauling, P.J., J. Inorg. Nucl. Chem., 18 (1961) 88.
12 Reedijk, J., private communication.
13 Takeda, T., Matsukawa, S. and Haseda, T., J. Phys. Soc. Japan, 30 (1971) 1330.
14 Takeda, T., Yamamoto, Y. and Haseda, T., Phys. Lett., 45 A (1973) 419.
15 Jeter, D.Y. and Hatfield, W.E., J. Inorg. Nucl. Chem., 34 (1972) 3055.
16 Witteveen, H.T. and Reedijk, J., Solid State Commun., 12 (1973) 557. Witteveen, H.T., Thesis, Leiden (1973).
17 Shinoda, T., Chihara, H. and Seki, S., J. Phys. Soc. Japan 19 (1963)1176.
18 Mc Elearny, J.N., Merchant, S. and Carlin, R.L., Inorg. Chem., 12 (1973) 906.
19 Nicholls, D. and Warburton, B.A., J. Inorg. Nucl. Chem., 32 (1970) 3871.
20 We thank Mr. J.A. Smit for kindly providing us with the specimens.
21 Star, W.M., Van Dam, J.E. and Van Baarle, C., J. Phys., E2 (1969) 257.
22 This thesis, chapter II; Klaaijsen, F.W. et al., to be published.
23 Stout, J.W. and Catalano, E., J. Chem. Phys., 23 (1955) 2013.
24 Klaaijsen, F.W., to be published in Physica.
25 Polgar, L.G., Herweyer, A. and De Jonge, W.J.M., Phys. Rev., B5 (1972) 1957.
26a Goldstein, M., Taylor, F.B. and Unsworth, W.D., J. Chem. Soc., Dalton, (1972) 418.
26b Witteveen, H.T., Reedijk, J. and Rutten, W.L., to be published.
27 These calculations have been performed by H.W.J. Blöte (see also ref. 1). Details of the machine calculation procedure will be published in Physica.
28 Onsager, L., Phys. Rev., 65 (1944) 117.
29 Kopinga, K. and De Jonge, W.J.M., Phys. Lett., 43 A (1973) 415.
30 Adachi, K. and Mekata, M., J. Phys. Soc. Japan 34 (1973) 269. Mekata, M., Adachi, K., Takaki, H. and Achiwa, H., Proc. 12th Intern. Conf. Low Temp. Phys., Kyoto, Japan (1971) p. 691.

31 Forstat, H., Love, N.D. and Mc Elearney, J.N., J. Phys. Soc. Japan 23 (1967) 229.

32 Domb, C. and Miedema, A.R., "Progress in Low Temperature Physics", vol. IV (Ed. Gorter, C.J., Amsterdam, North Holland).

33 Oguchi, T., Phys. Rev., 133 (1964) A1098.

34 Stout, J.W. and Chisholm, R.C., J. Chem. Phys., 36 (1962) 979.

35 Smart, J.S., in "Effective Field Theories of Magnetism" (1966) W.B. Saunders Co.

36 Morrish, A.H., "The Physical Principles of Magnetism" p. 470, John Wiley & Sons Inc. (1965).

37 Jacobs, I.S. and Lawrence, P.E., Phys. Rev., 164 (1967) 866.

38 Rutten, W.L. and Verstelle, J.C., private communication.

39 Hillaert, J.G.A., Thesis, Leiden (1973).

40 Narath, A. and Barham, D.C., Bull. Am. Phys. Soc., II 9 (1964) 112.

41 Narath, A., J. Phys. Soc. Japan 19 (1964) 2244.

42 Motokawa, M., Proc. Twelfth Int. Conf. Low Temperature Physics, Kyoto (1970) p. 703.

43 Ginsberg, A.P., Martin, R.L., Brookes, R.W. and Sherwood, R.C., Inorg. Chem., 11 (1972) 2884.

44 Ballhausen, C.J., "Introduction to Ligand Field Theory", Mc Graw - Hill, London (1962).

45 Vermaas, A., private communication.

CHAPTER V

MAGNETIC SPECIFIC HEAT OF FOUR CLOSELY RELATED $S=\frac{5}{2}$ LINEAR CHAIN COMPOUNDS MnX_2L_2, WHERE X = Cl, Br; AND L = PYRAZOLE, PYRIDINE.

Abstract. The intrachain exchange constants have been determined in four manganese linear chain compounds of general formula MnX_2L_2, where X = Cl, Br and L = pyrazole (pz = $N_2C_3H_4$), pyridine (py = NC_5H_5), with the aid of heat capacity measurements in the temperature region between 1.3 K and 80 K. The well-resolved broad maxima in the specific heats can be explained in terms of linear chain interactions, with, in addition, a moderately large single-ion anisotropy. A good agreement of theory with experiment is obtained, using recent calculations for the spin $\frac{5}{2}$ isotropic Heisenberg linear chain model with uniaxial single-ion anisotropy.

For the compounds $MnBr_2.2pz$, $MnCl_2.2py$ and $MnBr_2.2py$ additional λ-like anomalies were found at T = 1.930 $\pm$ 0.005 K, 1.380 $\pm$ 0.005 K and 2.055 $\pm$ 0.005 K, respectively, which are associated with long-range spin ordering. For $MnCl_2.2pz$ evidence for the onset of long-range spin ordering has not been observed down to T = 1.3 K.

The values obtained for the intrachain exchange constants are all in the range $0.5\ K < |J/k| < 1\ K$, while for the ratio of interchain to intrachain exchange constants we estimate $|J'/J| \simeq 0.01$. The axial single-ion anisotropy constant D/k, for the various compounds lies between $0.2\ K < |D/k| < 0.5\ K$.

1. Introduction. Calculations of the thermodynamic properties of magnetic linear chain systems are relatively simple as compared to those on higher dimensional systems. Analytical expressions for the free energy in zero field of linear chain systems with exchange interactions that are fully *anisotropic* (i.e. Ising interaction) have been obtained for several spin values [1-3]. Exact solutions to the linear chain model with *isotropic* exchange interactions (i.e. Heisenberg interaction) have thus far only been obtained on chains containing a *finite* number of atoms.

These results are, moreover, confined to $S=\frac{1}{2}$ [4] and $S=1$ [5]. On the other hand, extrapolations of the finite chain results for either $S=\frac{1}{2}$ or $S=1$ to the infinite linear chain yield fairly accurate estimates of the thermodynamic behaviour. Furthermore, Fisher [6] has pointed out that the isotropic Heisenberg linear chain model becomes exactly soluble in the classical limit, i.e. $S=\infty$. The specific heat corresponding to this model, however, maintains a finite value at T = 0 K, which is an unrealistic result. More recently, Harrigan and Jones [7] have given non-trivial quantum corrections up to second order in 1/S to the partition function of the classical spin model. As will be shown later on, however, these results are also unrealistic at low temperatures, since the specific heat becomes negative. As an approximation at low temperatures it is more appropriate to consider spin wave theory [8] which predicts a linear temperature dependence of the specific heat for an antiferromagnetic linear chain system with isotropic exchange interactions. Qualitatively the spin wave result is in agreement with that predicted by means of finite chain calculations [4)5)]. Quantitatively, however, the low-temperature results of both methods differ by a factor 3 for the $S=\frac{1}{2}$ and 2.3 for the S=1 antiferromagnetic linear chains. This may suggest that with increasing spin value the spin wave results become more reliable. Thus for the isotropic Heisenberg linear chain with large spin, spin wave theory should be a reasonable approximation at low temperatures, whereas at higher temperatures the classical spin results should be applicable. In the intermediate temperature region the specific heat of such a system possesses a broad maximum brought about by the short-range exchange interactions along the chain. This feature of the specific heat is characteristic for a system that ideally does not possess a transition to long-range order at a finite temperature, and thus cannot have a divergence in the heat capacity. The temperature corresponding to this maximum in the heat capacity is of the order JS^2/k. Theoretical results for the temperature at which the maximum occurs and for the height of the maximum for various S have been obtained by Weng [5]. He developed an interpolation scheme by means of which C_{max} and $T(C_{max})$ could be estimated for any spin value on the basis of the results for $S=\frac{1}{2}$ [4], $S=1$ [5] and $S=\infty$ [6].

For an experimental study of the thermal properties of an

isotropic linear chain system with large spin value, compounds containing isolated chains of Mn^{2+} ions are an obvious choice. The Mn^{2+} ion has the largest spin value of the 3d transition-metal ion group; furthermore, interactions between Mn^{2+} ions are generally highly isotropic.

Evidently, in real crystals there will always be a small but finite coupling between the chains, which will affect the 1-d behaviour in the lowest temperature range. Although some Mn^{2+} compounds consisting of highly isolated linear chains are already known [9)10)], there exists a gap in the experimental knowledge of the *thermal* properties of large spin linear chain compounds, in particular through the temperature region of the broad maximum. This arises because in the compounds studied up till now the exchange interactions are so large that the broad peak in the heat capacity associated with the interactions along the chain will occur in a temperature range in which the lattice contribution greatly exceeds the magnetic contribution. This makes it nearly impossible to separate the latter from the lattice specific heat in a reliable way. By way of contrast, the present Mn^{2+} salts were expected to have a considerably smaller intrachain exchange.

In order to investigate experimentally the thermal properties of an isolated linear chain system conclusions about the effect of the interchain coupling, which is always present, on the specific heat of real crystals have to be drawn. For this purpose we have selected four closely related manganese compounds viz. two *bis*(pyrazole)Mn(II)halides, i.e. $MnCl_2.2N_2C_3H_4$ and $MnBr_2.2N_2C_3H_4$ and two *bis*(pyridine)Mn(II)halides, i.e. $MnCl_2.2NC_5H_5$ and $MnBr_2.2NC_5H_5$. In the following we will abbreviate the ligands pyrazole and pyridine as pz and py, respectively.

These Mn^{2+} compounds belong to the series MX_2L_2 where M = Cu, Ni, Fe and Mn; X = Cl, Br and L = pz, py. The investigation of this series of compounds is carried out in collaboration with the Chemistry Department at the University of Leyden and the Technological University at Delft, where related properties of these salts have been studied by Reedijk [11)] (I.R. spectroscopy, E.S.R.) and by Witteveen [12)] (susceptibility), whereas the crystal structure of $MnCl_2.2pz$ was determined by Gorter *et al.* [13)]. This compound crystallizes in the monoclinic system, space group C2/c (fig. 1). The reported dimensions of the crystallographic axes are given in table I. The $MnCl_2.2pz$ structure consists of

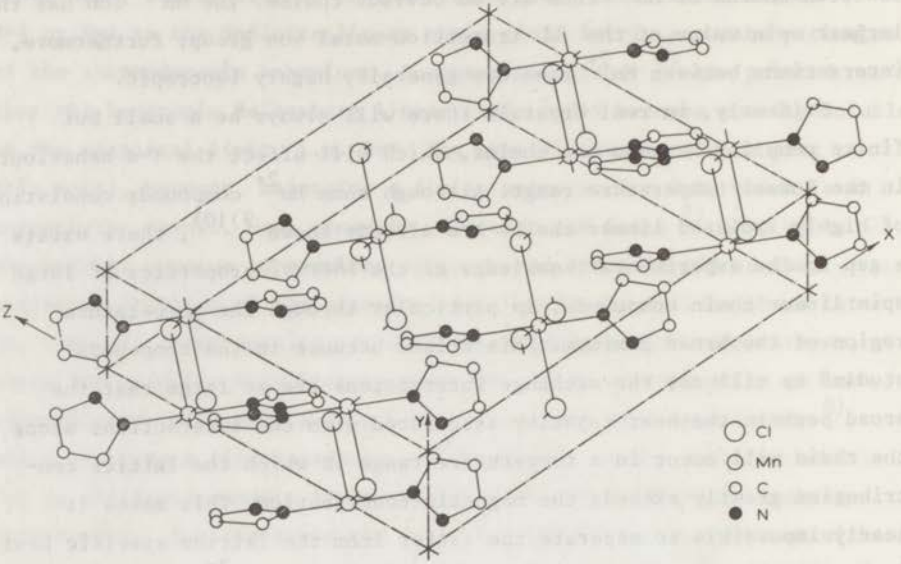

Fig. 1. *Structure of $MnCl_2.2pz$ (taken from ref. 13). The manganese ions along the b-axis are linked by bridges involving two chlorine ions (see fig. 1a). The structure of $MnCl_2.2py$ is very similar. Also in $MnCl_2.2py$ the manganese ions are bridged by two chlorine atoms, which together with the two N-donor ligands from the py groups, lead to an octahedral co-ordination. The compounds $MnBr_2.2pz$ and $MnBr_2.2py$ probably exhibit a similar chain structure.*

edge sharing *trans*- $MnCl_4(pz)_2$ octahedra, yielding infinite chains of $Mn\langle^{Cl}_{Cl}\rangle Mn$-units that lie parallel to the crystallographic b-axis. The distance between the dichloride-bridged Mn^{2+} ions, i.e. within the chains, is 3.761 $\pm$ 0.002 Å, which is close to the value reported for $MnCl_2.2H_2O$ [14] (see also table I). The compound $MnCl_2.2H_2O$ consists of similar dichloride-bridged Mn^{2+} ions yielding chains that lie along the crystallographic c-axis. The superexchange pathway between two Mn^{2+} ions within the chain has an approximately 90° pathway in $MnCl_2.2pz$ and is also very similar to that in $MnCl_2.2H_2O$. In the two

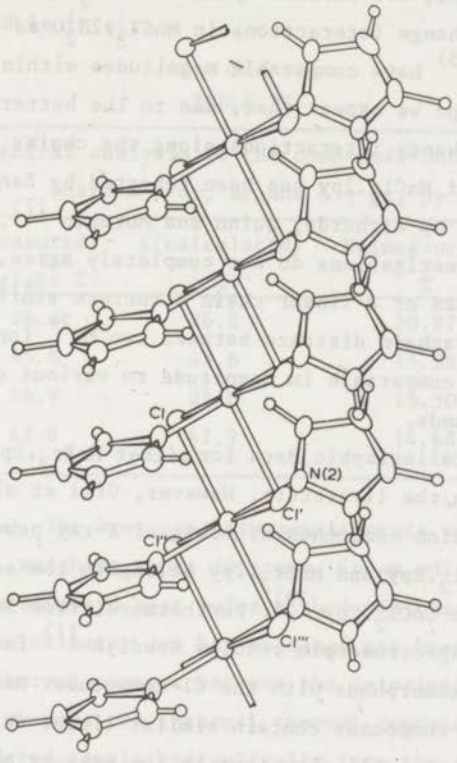

Fig. 1a.

TABLE I

Crystallographic data of $MnCl_2L_2$ where L = pz, py and H_2O

	a Å	b Å	c Å	degrees	Z	space group
$MnCl_2.2pz$ [13]	18.26 ± 0.02	3.761 ± 0.002	13.839 ± 0.002	94.78	4	C_2/c
$MnCl_2.2py$ [16]	17.40	8.75	3.76	91	2	P_{2_1}/m
$MnCl_2.2py$ [17]	19.508	3.738	15.543	116.64	4	P_2/c
$MnCl_2.2H_2O$ [14]	7.409	8.80	3.691	98.67	2	C_2/m

compounds the chains are mutually linked by hydrogen bonds, but due to the larger pz ligands, are further apart in $MnCl_2.2pz$ than in $MnCl_2.2H_2O$. Thus, while the exchange interactions in $MnCl_2.2H_2O$ as reported by Mc Elearny *et al.* [15] have comparable magnitudes within and between the chains, for $MnCl_2.2pz$ we expect that, due to the better isolation of the chains, the exchange interactions along the chains predominate. The crystal structure of $MnCl_2.2py$ has been reported by Zanetti *et al.* [16] and, more recently, by Richards, Quinn and Morosin [17]. Although the results of both investigations do not completely agree, it is clear that $MnCl_2.2py$ is composed of a linear chain structure similar to that of $MnCl_2.2pz$. The intrachain distance between two Mn^{2+} ions in $MnCl_2.2py$ is 3.7 Å, which is comparable in magnitude to various other dichloride-bridged Mn^{2+} compounds.

Detailed crystallographic data for either $MnBr_2.2pz$ or $MnBr_2.2py$ are not yet reported in the literature. However, Gill *et al.* [18] have examined a series of dipyridine compounds by means of X-ray powder photography and found that $MnCl_2.2py$ and $MnBr_2.2py$ belong to the same class of polymeric compounds as α-$CoCl_2.2py$ [19]. Furthermore, from X-ray powder diagrams and from infrared spectroscopic results Reedijk [11] found that the Br-compounds are isomorphous with the Cl-compounds. Hence, it is very likely that the Br-compounds contain similar linear chains.

In this paper we shall show that in the present manganese compounds linear chain exchange interactions are predominant, and moreover, that the exchange constants are small enough for the characteristic specific heat maxima to occur in a temperature region where a reliable estimate of the lattice specific heat can be made. The experimental methods are mentioned briefly in section 2 and the results of the measurements are given in sec. 3. The analysis of the heat capacity in terms of linear chain models are discussed in sec. 4, while the estimated values for the interchain coupling are given in sec. 5. The general conclusions are summarized in sec. 6.

2. Experimental. 2.1 Sample preparation. The compounds MnX_2L_2 (X = Cl, Br and L = pz, py) were prepared as slightly pink coloured powders by mixing alcoholic solutions of $MnX_2.4H_2O$ and the ligand in a ratio 1 : 2 (ref. 20). The precipitates were filtered, washed with alcohol and ether,

and finally dried in vacuo at room temperature. The samples were checked by chemical analysis (see table II) and infrared spectroscopy. The compounds are stable in air.

TABLE II

Chemical analysis of the compounds MnX_2L_2 where X = Cl, Br and L = pz, py

	X(measured) weight %	X(calculated) %	Mn(measured) %	Mn(calculated) %
$MnCl_2.2pz$	26.8	26.8	20.97	20.98
$MnBr_2.2pz$	45.0	45.6	15.58	15.66
$MnCl_2.2py$	24.9	25.0	19.30	19.34
$MnBr_2.2py$	42.9	42.9	14.68	14.73

2.2 Apparatus. The heat capacity measurements were performed on powdered samples, weighing about 10 grams, in an adiabatic calorimeter set-up, using the standard heat pulse method. Neither external, nor internal to the calorimeter can has exchange gas been used. A mechanical switch provided thermal contact between the calorimeter can and the cooling liquids, whereas the internal thermal contact was improved by pressing the powdered sample hydraulically into the sample holder which contains many copper vanes. The contribution of the sample holder to the measured heat capacity was determined in separate runs on the empty calorimeter can.

As a thermometer a carbon resistance [21] was used that was calibrated against the vapour pressure of liquid helium, hydrogen and oxygen. A complete description of the apparatus and experimental procedure will be published elsewhere [22].

3. Experimental results. 3.1 General. The experimental specific heat data for $MnCl_2.2pz$, $MnBr_2.2pz$, $MnCl_2.2py$ and $MnBr_2.2py$ are shown in figs. 2, 3, 4 and 5, respectively. The curves for $MnCl_2.2pz$, $MnBr_2.2pz$ and $MnCl_2.2py$ display a large broad peak. The specific heat maxima range from 7.2 $\pm$ 0.1 J/mol K for $MnCl_2.2py$ up to 8.55 $\pm$ 0.05 J/mol K for $MnBr_2.2pz$. In addition to the broad peaks, λ-like anomalies were observed

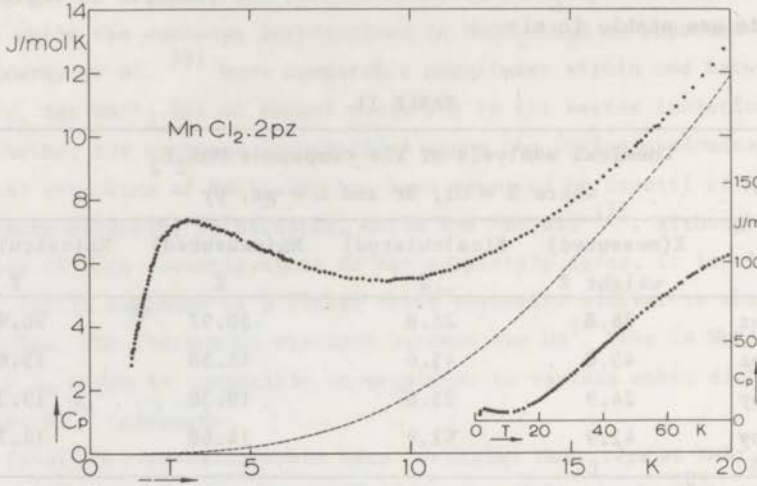

Fig. 2. *The experimental specific heat of $MnCl_2.2pz$ as a function of temperature. The dashed line represents the estimated lattice contribution. The high-temperature data, i.e. up to T = 80 K, are indicated in the inset.*

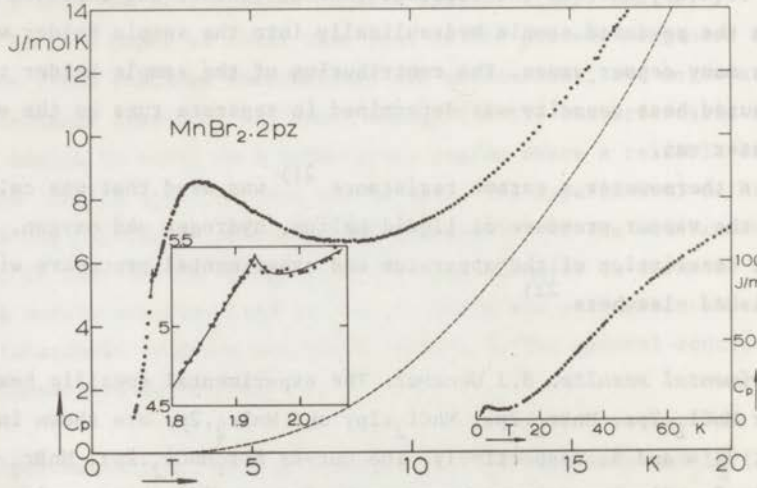

Fig. 3. *The experimental specific heat of $MnBr_2.2pz$ as a function of temperature. The dashed line represents the lattice estimate.*

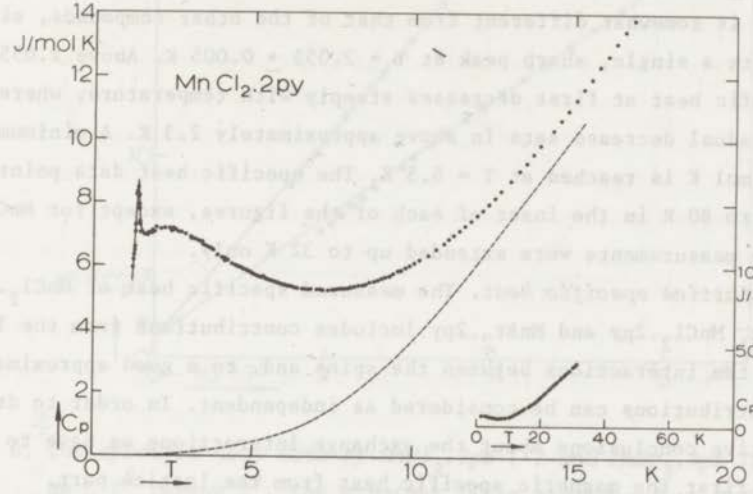

Fig. 4. *The experimental specific heat of $MnCl_2.2py$ as a function of temperature. The estimated lattice specific heat is indicated by a dashed line.*

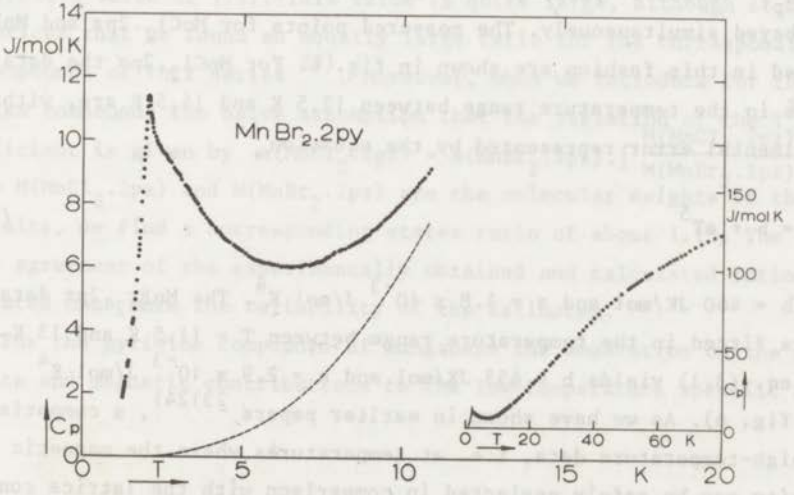

Fig. 5. *The experimental specific heat of $MnBr_2.2py$ as a function of temperature. The dashed line corresponds with the estemated lattice specific heat.*

for $MnBr_2.2pz$ at T = 1.930 ± 0.005 K and for $MnCl_2.2py$ at T = 1.380 ± 0.005 K. The low-temperature specific heat behaviour of $MnBr_2.2py$ is somewhat different from that of the other compounds, since it exhibits a single, sharp peak at T = 2.055 ± 0.005 K. Above 2.055 K the specific heat at first decreases steeply with temperature, whereas a more gradual decrease sets in above approximately 2.3 K. A minimum value of 6.0 J/mol K is reached at T = 6.5 K. The specific heat data points are shown up to 80 K in the inset of each of the figures, except for $MnCl_2.2py$ where the measurements were extended up to 32 K only.

3.2 Lattice specific heat. The measured specific heat of $MnCl_2.2pz$, $MnBr_2.2pz$, $MnCl_2.2py$ and $MnBr_2.2py$ includes contributions from the lattice and from the interactions between the spins and, to a good approximation, these contributions can be considered as independent. In order to draw quantitative conclusions about the exchange interactions we have to separate first the magnetic specific heat from the lattice part.

The low-temperature lattice specific heat should be well represented by a term aT^3 while at temperatures high compared to the exchange, the magnetic specific heat of a magnetic insulator varies as T^{-2}. Hence, it is often possible to separate the two contributions adequately by means of a C_pT^2 versus T^5 plot for a temperature region where the two power laws are obeyed simultaneously. The measured points for $MnCl_2.2pz$ and $MnBr_2.2pz$ plotted in this fashion are shown in fig. 6. For $MnCl_2.2pz$ the data points in the temperature range between 12.5 K and 14.5 K are, within experimental error represented by the equation,

$$C_pT^2 = b + aT^5 \qquad (3.1)$$

with b = 460 JK/mol and a = 1.8×10^{-3} J/mol K^4. The $MnBr_2.2pz$ data points fitted in the temperature range between T = 11.5 K and 13 K with eq. (3.1) yields b = 455 JK/mol and a = 2.9×10^{-3} J/mol K^4 (see fig. 6). As we have shown in earlier papers [23)24)], a comparison of the high-temperature data, i.e. at temperatures where the magnetic heat capacity may be safely neglected in comparison with the lattice contribution, in terms of the corresponding states argument [25)] supplies a check on the low-temperature lattice specific heat estimates as obtained from the low-temperature data. The corresponding states ratios

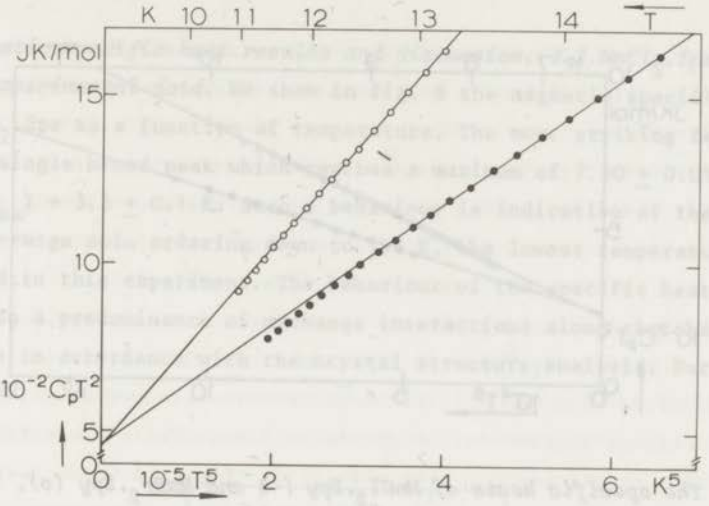

Fig. 6. *The specific heat data of $MnCl_2.2pz$ (·) and $MnBr_2.2pz$ (o) plotted as C_pT^2 versus T^5. The straight lines correspond to $C_pT^2 = b + aT^5$ with b = 460 JK/mol and $a = 1.8 \times 10^{-3}$ J/mol K^4 for $MnCl_2.2pz$ and with b = 445 JK/mol and $a = 2.9 \times 10^{-3}$ J/mol K^4 for $MnBr_2.2pz$.*

in both the high and the low-temperature regions are in perfect agreement and yield a value of 1.17. This value is quite large, although it may be noticed that we found an equally large ratio for the corresponding Ni compounds of this series [23]. Moreover, when we introduce for these complex compounds the naive assumption that the variation of the T^3 coefficient is given by $a(MnCl_2.2pz) = a(MnBr_2.2pz).\left[\frac{M(MnCl_2.2pz)}{M(MnBr_2.2pz)}\right]^{\frac{3}{2}}$ where $M(MnCl_2.2pz)$ and $M(MnBr_2.2pz)$ are the molecular weights of the two salts, we find a corresponding states ratio of about 1.15. The close agreement of the experimentally obtained and calculated ratios indicates once more the reliability of the estimates.

For the pyridine compounds of manganese the separation of the lattice and magnetic contributions to the low-temperature specific heats

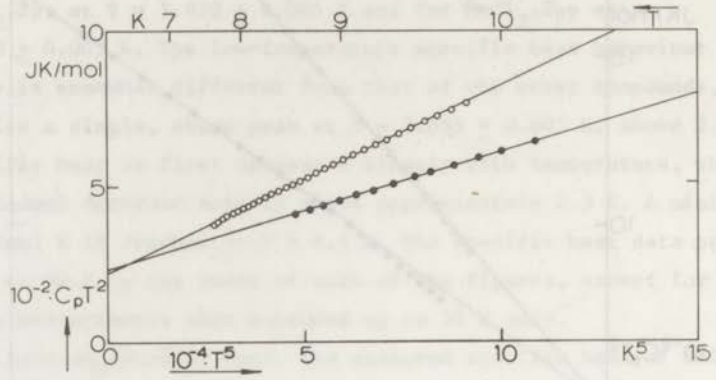

Fig. 7. *The specific heats of $MnCl_2.2py$ (•) and $MnBr_2.2py$ (o). The data points are plotted as C_pT^2 versus T^5. The straight lines correspond to $C_pT^2 = b + aT^5$ with b = 235 JK/mol and $a = 3.75 \times 10^{-3}$ J/mol K^4 for $MnCl_2.2py$ and with b = 220 JK/mol and $a = 6.1 \times 10^{-3}$ J/mol K^4 for $MnBr_2.2py$.*

was performed in a manner generally similar to that for the Mn bispyrazole compounds. From the best fits according to eq. (3.1), which are indicated in fig. 7 by solid lines, we find for $MnCl_2.2py$: b = 235 JK/mol and $a = 3.75 \times 10^{-3}$ J/mol K^4, and for $MnBr_2.2py$: b = 220 JK/mol and $a = 6.1 \times 10^{-3}$ J/mol K^4. Thus the corresponding states ratio for $MnCl_2.2py$ and $MnBr_2.2py$ also takes a value of approximately 1.17, which is in accordance with the Mn dipyrazole compounds, since the molecular weights of the two series are very similar.

We notice that the lattice specific heats of the Mn dipyrazole and Mn dipyridine compounds are not related in a simple way, except in the trivial T^3 - low-temperature region. In view of the X-ray powder isomorphism we might have expected otherwise. It should, however, be noted that the Cl^- and Br^- compounds within each of the two series apparently are quite similar, except for a scaling factor ratio. Hence, we attribute the above effects to the differences between the pyrazole and the pyridine ligands.

4. Magnetic specific heat results and discussion. 4.1 $MnCl_2$.2pz.

4.1.1 Experimental data. We show in fig. 8 the magnetic specific heat of $MnCl_2$.2pz as a function of temperature. The most striking feature is the single broad peak which reaches a maximum of 7.30 ± 0.05 J/mol K at $T(C_{max})$ = 3.1 ± 0.1 K. Such a behaviour is indicative of the absence of long-range spin ordering down to 1.3 K, the lowest temperature attained in this experiment. The behaviour of the specific heat indeed points to a predominance of exchange interactions along the chain, which is in accordance with the crystal structure analysis. Furthermore,

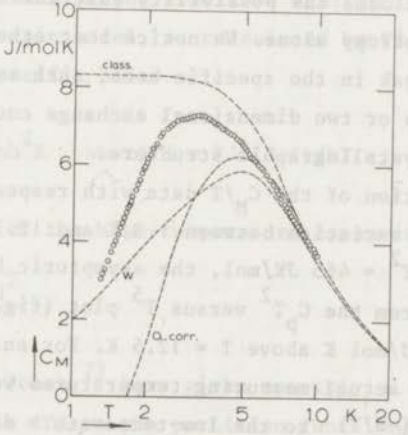

Fig. 8. *The magnetic specific heat, C_M, of $MnCl_2$.2pz as a function of temperature (semi logarithmic plot).*

o o o *experimental results*

--- Class: *classical isotropic Heisenberg linear chain model as calculated by Fisher for S=∞, scaled to $S=\frac{5}{2}$; $J/k\ (S=\frac{5}{2}) = -0.78$ K.*

--- Q corr: *second order quantum corrected version of the isotropic classical spin model: $J/k\ (S=\frac{5}{2}) = -0.78$K.*

--- W : *isotropic Heisenberg linear chain model for $S=\frac{5}{2}$ as calculated according to Weng's interpolation scheme: $J/k\ (S=\frac{5}{2}) = -0.78$K.*

the absence of a λ-like anomaly in the specific heat of $MnCl_2.2pz$ indicates that the chains in this compound have a very small interchain interaction.

On the other hand, the presence of single-ion anisotropy (i.e. crystalline field splitting) can, even in the absence of exchange and dipole interaction etc., give rise to a broad peak in the specific heat. Such a feature has been observed in e.g. $Mn(pz)_4I_2$ [26]. However, since the single-ion energy levels of a divalent manganese ion are Kramers degenerate, the entropy content for such a system of isolated spins would amount to Rln3. As will be shown below, the experimentally obtained magnetic entropy content equals the value Rln6 within the experimental error, which result excludes the possibility that the broad peak is due to the single-ion anisotropy alone. We notice that other possible origins of the broad peak in the specific heat, such as magnetic clustering of Mn^{2+} ions or two dimensional exchange coupling, are not consistent with the crystallographic structure.

Numerical integration of the C_M/T data with respect to temperature yields for the entropy variation between 1.3 K and 12.5 K a value of 12.6 J/mol K. Using $C_M T^2$ = 465 JK/mol, the asymptotic high-temperature relation as obtained from the $C_p T^2$ versus T^5 plot (fig. 6), we calculate a contribution of 1.5 J/mol K above T = 12.5 K. For an estimate of the contribution below the actual measuring temperatures we fitted the relation $C_M = AT^{-2} \exp(-B/T)$ to the low-temperature data in order to extrapolate the C_M versus T curve to T = 0 K. From fig. 9 it is seen that the data points in the temperature region between T = 1.3 K and T = 2.2 K can be fitted within experimental error by the exponential relation with A = 445 JK/mol and B = 5.9 K. Adding a calculated entropy contribution of 0.8 J/mol K below 1.3 K, the total magnetic entropy content amounts to 14.9 $\pm$ 0.1 J/mol K. This value for ΔS is, in fact, very close to the theoretical entropy for a $S=\frac{5}{2}$ system, i.e. Rln(2S + 1) = Rln 6 = 14.89 J/mol K. The entropy content below 1.3 K amounts to only 5 per cent of Rln 6.

4.1.2 Inadequacy of isotropic exchange interactions to describe the heat capacity of $MnCl_2.2pz$. Exchange interactions in Mn^{2+} compounds are generally isotropic because the lowest single-ion orbital state of Mn^{2+} in a cubic octahedral co-ordination structure has orbital angular

momentum zero and crystalline field effects are usually quite small. As a first attempt to explain the specific heat results we, therefore, assume isotropic linear chain exchange interactions. In view of the crystal structure it is reasonable, as a first approximation, to consider only nearest neighbour exchange interactions. The exchange hamiltonian may then be written as:

$$H = -2J \sum_{i=1}^{N} \vec{S}_i \cdot \vec{S}_{i+1}. \qquad (4.1)$$

As we mentioned before, exact calculations for the isotropic Heisenberg linear chain model for spin $\frac{5}{2}$ have not yet been reported in the literature. The calculations available are:

i) The classical spin model, as calculated by Fisher [6]. This model yields for the specific heat:

$$C_M/R = 1 - K^2/\sinh^2 K \quad \text{where } K = 2JS(S+1)/kT. \qquad (4.2)$$

The leading term of the high-temperature expansion of eq. (4.2) reads:

$$C_M/R = \frac{4S^2(S+1)^2J^2}{3k^2T^2} . \qquad (4.3)$$

ii) Harrigan and Jones [7] have given non-trivial quantum corrections to second order in 1/S to the partition function of the classical spin isotropic Heisenberg linear chain model. They find for the partition function Z_Q:

$$\ln Z_Q = \ln Z_c + \ln(2S+1)^N/(4\pi)^N - (N-1)/12S(S+1)K^2 \{1+L(K)-3L(K)/K+L^2(K)\}, \qquad (4.4)$$

where Z_c is the classical partition function [6], $L(K) = \coth K - 1/K$ and $K = 2J\,S(S+1)/kT$ and N is the number of atoms. Applying this to the $S=\frac{5}{2}$ antiferromagnetic isotropic Heisenberg linear chain model one finds that the specific heat for this model reaches a maximum of 6.25 J/mol K at

$$kT(C_{max})/J = -5.8. \qquad (4.5)$$

iii) As a third approximation method we mention Weng's [5] interpolation scheme, yielding for the specific heat of the $S=\frac{5}{2}$ antiferromagnetic Heisenberg linear chain the relation

$$kT(C_{max})/J \simeq -6.3 \text{ and } C_{max} \simeq 5.8 \text{ J/mol K} \qquad (4.6)$$

These results have been used earlier in the analysis of the specific heat results on another linear chain compound, $Mn(N_2H_5)_2(SO_4)_2$ [24]. When identifying the experimental value $T(C_{max}) = 3.1$ K for $MnCl_2.2pz$ with the theoretical results of eq. (4.5) and eq. (4.6) we get $J/k = -0.535$ K and -0.49 K, respectively (see also table V). On the other hand, if we substitute $C_M T^2 = 460$ JK/mol, the asymptotic high-temperature variation of C_M, into eq. (4.3) we obtain $|J/k| = 0.755$ K. Thus, the various methods yield widely different J/k values.

A comparison of the $|J/k|$-values from the specific heat results with those which have been obtained by means of susceptibility and E.S.R. measurements, i.e. $J/k \simeq -0.8$ K [12)27)], indicates that close to $T(C_{max})$ the theoretical approximations for the specific heat are probably in error. As the theoretical approximations are expected to be better at higher temperatures, we have chosen the temperature region between 7 K and 10 K to fit the theoretical curve corresponding to eq. (4.4) with $S=\frac{5}{2}$ to the experimental C_M-data, yielding $J/k = -0.78$ K. In this temperature range the lattice contribution to the specific heat is still relatively small in comparison with the magnetic part, whereas the temperatures are about $3T(C_{max})$, i.e. sufficiently far from $T(C_{max})$. For comparison we showed in fig. 8 the curve for the quantum corrected classical spin model (eq. (4.5)) together with the classical spin model (eq. (4.2)) and the interpolation scheme result, all for $S=\frac{5}{2}$ and $J/k = -0.78$ K.

As another method for estimating the exchange constant J/k, which is independent of the choice of a temperature region over which the fit is made, we will equate the experimental magnetic energy ΔE (table III) with the theoretical results for the magnetic energy at T = 0 K for a $S=\frac{5}{2}$ antiferromagnetic Heisenberg linear chain system with antiferromagnetic interactions between nearest neighbours only. Theoretical calculations for the magnetic energy, E_o, of such a system have been

TABLE III

Experimental results for the *magnetic* specific heat and related quantities.

	T_c K	$T(C_{max})$ K	C_{max} J/mol K	ΔS J/mol K	$\Delta S(T_c)$ J/mol K
$MnCl_2.2pz$	< 1.3	3.1 ±0.1	7.30±0.05	14.9±0.1	< 0.8
$MnBr_2.2pz$	1.930±0.005	3.35±0.05	8.45±0.05	14.9±0.1	1.3
$MnCl_2.2py$	1.380±0.005	2.25±0.05	7.15±0.05	15.0±0.2	2.4
$MnBr_2.2py$	2.055±0.005			14.5±0.3	3.1

	ΔE J/mol	$\Delta E(T_c)$ J/mol	$T(\chi_{max})$ K	$T(\chi_{max})/T_c$	$T(\chi_{max})/T(C_{max})$
$MnCl_2.2pz$	98	< 0.8	6.5±0.2 [a]	> 5.1	2.1±0.1
$MnBr_2.2pz$	102	2.1	6.3±0.2 [a]	3.2±0.1	1.9±0.1
$MnCl_2.2py$	73	2.7	4.0±0.2 [a]	2.9±0.1	1.8±0.1
$MnBr_2.2py$	72	5.8	4.7±0.2 [a]	2.3±0.1	-

a) ref. 12

performed by many authors. Rigorous bounds for E_o have been given by Anderson [28]. He determined $-15 < E_o/N|J| < -12.5$ where J/k in the exchange constant defined according to eq. (4.1) and N is Avogadro's number. Using a second-order correction in the antiferromagnetic spin wave theory Kubo [8] arrived at $E_o/N|J| = -14.6$. Weng [5] has proposed an empirical formula for E_o that should hold for general spin. Using the known results for $S=\frac{1}{2}$ [29], $S=1$ [5] and $S=\infty$ [6] we obtained a value of -14.6 for $E_o/N|J|$. Davis [30] derived $E_o/N|J| = -13.9$ and recently Scales and Gersch [31] obtained by means of a second order Greens' function theory $E_o/N|J| = -13.5$. For convenience we shall put these results on an equal basis and take the mean value for $E_o/N|J|$, i.e.

$$E_o/N|J| = -14.0 \qquad (4.7)$$

Using the experimental result, $\Delta E = 98$ J/mol we thus obtain $|J/k| = 0.84$ K. This result is, in fact, close to the J/k values deduced from susceptibility and E.S.R. experiments [27], while it is also in

fair agreement with the J/k value determined from the high-temperature specific heat results (see table V).

Although we may conclude that the various methods yield J/k values that are similar, there still remains a discrepancy between experiment and theory at the experimental maximum, C_{max}, which is about 18 per cent higher that the quantum corrected classical spin model result and approximately 25 per cent higher than the interpolation scheme result (see fig. 8). As will be shown in the next section, a still larger value for C_{max} is observed for $MnBr_2.2pz$. Now, for the antiferromagnetic isotropic Heisenberg linear chain model the value of C_{max} should be independent of the value of J/k. Hence, the large differences between experiment and theory on the one hand, and those between the results for $MnCl_2.2pz$ and $MnBr_2.2pz$ on the other hand, cannot be attributed to the approximate character of the calculations for the $S=\frac{5}{2}$ isotropic Heisenberg linear chain model. These are independent of the model chosen. Therefore, we will now consider the possible origins for the deviations from the ideal chain model. As one of these we mention interchain coupling which causes a transition to a long-range spin ordered state at $T \neq 0$ K. The $MnCl_2.2pz$ specific heat, however, does not display such a transition down to T = 1.3 K, whereas the short-range order maximum occurs at T = 3.1 K. Although the specific heat of a system of weakly coupled antiferromagnetic $S=\frac{5}{2}$ linear chains has not yet been treated theoretically, a comparison with experimental results on similar systems with lower spin values shows that we may safely deduce that this effect cannot be responsible for the large deviations from the ideal 1-d behaviour which occurs at temperatures as high as $T(C_{max}) = 3.1$ K, when $T_c < 1.3$ K. Moreover, it may be seen in fig. 8 that C_M still decreases *exponentially* with temperature. According to spin wave theory [8], however, C_M should have a linear temperature dependence at sufficiently low temperatures when the antiferromagnetic exchange interactions are isotropic. The exponential dependence of $C_M(T)$ can be explained by the existence of a gap in the energy spectrum of the spin system. This may be associated with anisotropy in the magnetic coupling. As possible origins we mention dipole-dipole and single-ion anisotropy. of which we believe the latter is the most important one for $MnCl_2.2pz$. We will, therefore, consider the single-ion anisotropy in more detail.

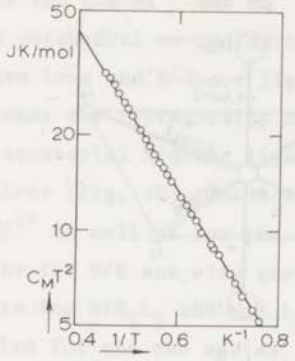

Fig. 9. *The low-temperature magnetic specific heat of* $MnCl_2.2pz$ *plotted as* $C_M T^2$ *versus 1/T (semi logarithmic plot). The straight line corresponds with the relation* $C_M = AT^{-2}.\exp(-B/T)$ *in which* $A = 445$ *JK/mol and* $B = 5.9$ *K.*

Independent measurements to determine the crystal field splitting parameter of the divalent manganese ions in $MnCl_2.2pz$ have not been obtained unfortunately. Therefore, we will first present arguments for the presence of large crystal field splittings in the compounds MnX_2L_2 where X = Cl, Br and L = pz, py; we also explain the reason why we expect the $S_z = \pm \frac{5}{2}$ doublet to be lowest in the absence of exchange or external fields (sec. 4.1.3). The effect of single-ion anisotropy on the specific heat of a $S=\frac{5}{2}$ linear chain system will be discussed in sec. 4.1.4.

4.1.3 Zero-field splitting parameters in MX_2L_2 *and* MX_2L_4 *compounds (M = Ni, Mn; X = Cl, Br, I and L = pz, py).* In order to get some idea about the zero-field splittings and the related parameters in the MnX_2L_2 compounds, we will compare the reported zero-field splitting parameters of two series of compounds, MX_2L_2 and MX_2L_4, that are similar in some respects. Of the compounds MX_2L_2 where X = Cl, Br and L = pz, py the nickel and manganese compounds are X-ray powder isomorphous [18]. The distorted octahedral configuration of the metal ions is formed by four equatorial halogen ions and two strong N-donor ligands (see fig. 10). Thus far the crystal field splitting parameters have been determined only for the Ni^{2+} compounds. The values for D/k, according to the single-ion hamiltonian

$$H = D\{S_z^2 - \tfrac{1}{3} S(S+1)\}, \qquad (4.8)$$

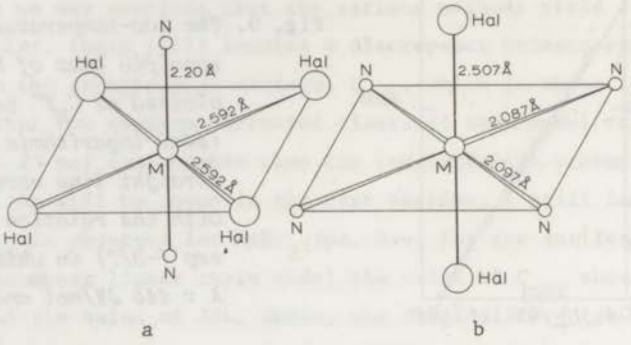

Fig. 10. *The octahedral co-ordination structure of the metal ions of the two series of compounds: MX_2L_2 (fig. 10a) and MX_2L_4 (fig. 10b). (M = Ni, Mn; X = Cl, Br, I; L = pz, py). The distances shown in fig. 10a correspond to $MnCl_2.2pz$ [13], whereas those in fig. 10b correspond to $NiCl_2.4pz$ [40].*

where D/k is the axial crystal-field splitting parameter, have been obtained by means of heat capacity measurements [23] and are collected in table IV.

TABLE IV

Comparison of the zero-field splitting parameters (in K), according to the single-ion hamiltonian $H = D\{S_z^2 - \frac{1}{3} S(S+1)\}$, for NiX_2L_4, NiX_2L_2 and MnX_2L_4 where X = Cl, Br, I and L = pz, py

	Cl^-		Br^-		I^-		method
$NiX_2.4pz$	10	a)	7.5	a)	5.4	b)	specific heat, susceptibility
$NiX_2.2pz$	-29	c)	-33	c)			specific heat
$NiX_2.2py$	-27	c)	-30	c)			specific heat
$MnX_2.4py$	0.11	d)	0.60	d)	1.4	e)	E.S.R., specific heat

a) ref. 34
b) ref. 32
c) ref. 23
d) ref. 35
e) ref. 26

For several compounds of formula MX_2L_4, isomorphism frequently occurs for the Ni^{2+} and Mn^{2+} compounds [32]. In this case also the distorted cubic octahedral co-ordination structure of the metal ions is formed by halogen ions and N-donor ligands. However, in contrast to the MX_2L_2 compounds the tetragonally distorted structure of MnX_2L_4 consists of four equatorial N-donor ligands and the halogen atoms are on the axial positions (fig. 10). The D/k values (eq. (4.8)) have been reported for the Ni^{2+} as well as for the Mn^{2+} compounds (refs. 26, 32, 34-36). The results for D/k are also given in table IV. From a comparison of the results for NiX_2L_2 and NiX_2L_4 it is seen that the signs of D/k are opposite for the two series. Hence, presumably the distorted octahedral co-ordination structure of the divalent nickel ions changes from a compression in NiX_2L_2 to a spectrochemically tetragonally elongated structure in NiX_2L_4. Furthermore, the absolute values of D/k are much larger in the dipyrazole than in the tetrapyrazole nickel compounds.

In very much the same fashion we expect opposite signs for D/k in MnX_2L_2 and MnX_2L_4. Thus, according to eq. (4.8) we anticipate negative values for D/k in the MnX_2L_2 compounds. We notice further that the values for D/k reported for MnX_2L_4 (X = Cl, Br, I; L = pz, py) are already quite large in comparison with the values generally reported for divalent manganese in inorganic compounds [36]. From the comparison with the two nickel series, one thus tentatively expects relatively large values for the crystal field splitting parameters for Mn^{2+} in MnX_2L_2, with $D/k < 0$.

4.1.4 Linear chain exchange interactions and uniaxial single-ion anisotropy. In order to investigate theoretically whether the discrepancies between the experimental results for $MnCl_2.2pz$ and the isotropic Heisenberg linear chain model could be attributed to single-ion anisotropy, we have performed calculations for this model with additional single-ion anisotropy. The exchange hamiltonian may then be written as

$$H = -2J\sum_{i=1}^{N} \vec{S}_i.\vec{S}_{i+1} + D\sum_{i=1}^{N}\{S_{iz}^2 - \frac{1}{3}S(S+1)\} \qquad (4.9)$$

Due to the axial single-ion term, the asymptotic T^{-2} term will be enlarged $\{C_M T^2/R\} \simeq 6.2(D/k)^2$ for $S=\frac{5}{2}$ which consequently will result in a smaller value of J/k, when determined from the high-temperature specific

heat data. Preliminary results for the specific heat of finite chains, i.e. N = 2 and N = 3 and various values of J/k and D/k appear to be quite promising, as the maximum value of the specific heat proved to be very sensitive to the ratio D/J for values of J/k and D/k that are quite plausible for the present series of manganese compounds in view of the above discussion.

The calculations according to eq. (4.9) were subsequently extended by Blöte [37] to chains containing a larger number of atoms, i.e. N = 2, 3, 4 and furthermore to rings consisting of a like number of atoms. The specific heat of "infinite" chains, i.e. $N \to \infty$, was obtained by means of an extrapolation of the finite chain results, using the same procedure as reported earlier for the calculations on spin 1 chains with additional single-ion anisotropy [37]. In that case the extrapolated results proved to be sufficiently accurate.

The preliminary infinite chain results indicate that for D/k = 0, i.e. the isotropic Heisenberg linear chain model, the calculations according to eq. (4.9) are for $|kT/J| > 7$ in perfect agreement with the quantum corrected classical spin model result (eq. (4.4)). Below $|kT/J| \simeq 7$ the C_M values calculated according to eq. (4.9) remain larger than those according to eq. (4.4), and a maximum of $C_{max} \simeq 6.4$ J/mol K is calculated when $kT(C_{max})/J \simeq -5.4$. This result is quite understandable because the quantum corrected classical spin model, eq. (4.4), produces a negative specific heat below $|kT/J| \simeq 2$, which indicates that the second order quantum correction is insufficient to describe the low-temperature specific heat.

New results are obtained in these calculations when D/k is allowed to be non-zero. The preliminary computational results for various values of $|D/J|$ with $D/k < 0$ and J/k = -1 K are plotted in fig. 11 on a double logarithmic scale. In the case where $|D/J|$ is small, i.e. $|D/J| < 0.2$, of course only small differences with the D/k = 0 results are found. However, when $|D/J|$ takes values as large as approximately 2, the calculated C_{max} values are about twice as large as those obtained with D/k = 0. When the single-ion anisotropy energy becomes large in comparison with the exchange energy, i.e. $|D/k| \gg 1$, the calculations yield two broad peaks in the specific heat curve, as one would expect.

4.1.5. Comparison between theory and experiment. In principle, the

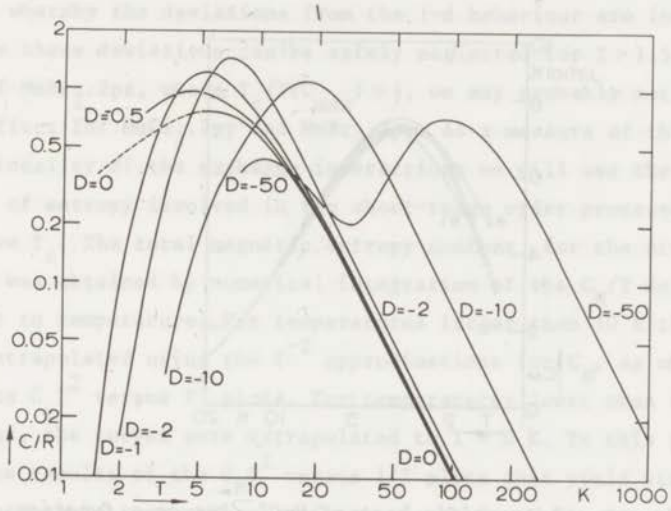

Fig. 11. *Preliminary results for the specific heat, in dimensionless units C/R, (R = gas constant) as a function of temperature for the isotropic Heisenberg linear chain model with uniaxial single-ion anisotropy as calculated by Blöte [37] for S=5/2; J/k = -1 K and D/k< 0. For D/k = 0 the calculations are, down to kT/J ≈ 7 in perfect agreement with those for the quantum corrected classical spin model (see text).*

experimental values for C_{max} and $T(C_{max})$ are sufficient to determine the J/k and D/k values, when the interactions can be described with eq. (4.9). At low temperatures and for small values of the ratio D/J it was, however, found that convergence to N = ∞ is less good than in the case $|D/J| > 1$. The estimated ratio $|D/J|$ for $MnCl_2.2pz$ amounts to only 0.3. In fig. 12 we show two curves for J/k = -0.78 K and D/k = -0.30 K, obtained by different extrapolation methods. The full curve (B1) represents the extrapolation using the finite chain result for N = 2,3 and 4 spins, while curve B2 corresponds to an extrapolation of the finite chain results for N = 3 and N = 4 only. As can be seen from comparing figs. 8 and 12, the description of the experimental data

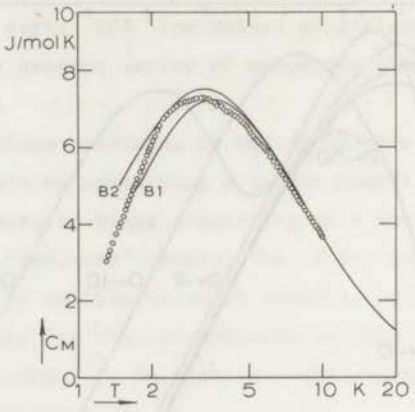

Fig. 12. *The magnetic specific heat of $MnCl_2.2pz$ as a function of temperature.*
o o o experimental results.
——— *isotropic Heisenberg linear chain model with uniaxial single-ion anisotropy (eq. (4.9)) as calculated by Blöte for $S=\frac{5}{2}$; (B1) extrapolation result using chains of N = 2, 3 and 4 spins with J/k = -0.78 and D/k = -0.30 K; (B2) as B1, but with the N = 3 and N = 4 results only.*

with this model is, in fact, much better than with the calculations on the isotropic Heisenberg linear chain model mentioned above. Furthermore, the D/k value for $MnCl_2.2pz$ as obtained from the present fit, seems to be quite plauxible in view of the results found for NiX_2L_2 and NiX_2L_4.

4.2 $MnBr_2.2pz$, $MnCl_2.2py$ and $MnBr_2.2py$. 4.2.1 Magnetic specific heats of $MnBr_2.2pz$, $MnCl_2.2py$ and $MnBr_2.2py$. The magnetic specific heat curves of $MnBr_2.2pz$ (fig. 13), $MnCl_2.2py$ (fig. 14) and $MnBr_2.2py$ (fig. 15) are somewhat different from that of $MnCl_2.2pz$ in that each of the curves displays a λ-like anomaly of which the energy content increases in the sequence of compounds given above. The sharp peaks are ascribed to the onset of long-range spin

ordering. Within this picture, the increasing energy content of the peaks would indicate that the chains become less isolated from each other, whereby the deviations from the 1-d behaviour are increased. Whereas these deviations can be safely neglected for $T > 1.5$ K in the case of $MnBr_2.2pz$, where $T_c/T(C_{max}) \simeq \frac{1}{2}$, we may probably not neglect this effect for $MnCl_2.2py$ and $MnBr_2.2py$. As a measure of the lattice dimensionality of the exchange interactions we will use the relative amount of entropy involved in the short-range order processes, that is above T_c. The total magnetic entropy content for the present compounds was obtained by numerical integration of the C_M/T data with respect to temperature. For temperatures larger than 10 K the curves were extrapolated using the T^{-2} approximations for C_M, as obtained from the C_pT^2 versus T^5 plots. For temperatures lower than those actually measured, the curves were extrapolated to T = 0 K. To this purpose we used the results of the C_MT^2 versus 1/T plots that yield straight lines over acceptable temperature regions, except for $MnCl_2.2py$ where the number of measured points is rather small below T_c. Nevertheless, the C_MT^2 versus 1/T plot for $MnCl_2.2py$ yields values which compare favourably with those obtained on the other compounds.

The data on the magnetic entropy content of the compounds so far investigated are collected in table III. The magnetic energies were found in a similar fashion and they are also tabulated in table III. The entropy content for each of the compounds differs by less than 3 per cent from the theoretical value. From table III it is seen that only a small amount of the total magnetic entropy change takes place below T_c. In other words, the critical entropy, denoted as $\Delta S(T_c)$ in table III, is small, even for $MnBr_2.2py$ where $\Delta S(T_c)$ amounts to 3.1 J/mol K, i.e. only 20.5 per cent of $R\ln 6$. This may be compared with the entropy change below T_c for a spin $\frac{5}{2}$ three-dimensional isotropic Heisenberg antiferromagnet, e.g. a simple cubic lattice structure, where $\Delta S(T_c)$ amounts to approximately 78 per cent of $R\ln 6$ (ref. 38). Thus, although the magnetic specific heat of $MnBr_2.2py$ does not exhibit the characteristic broad peak, associated with predominantly linear chain exchange interactions, this material still shows a pronounced low-dimensional behaviour as will be shown in section 4.2.4.

4.2.2 $MnBr_2.2pz$. The occurrence of magnetic linear chains in $MnBr_2.2pz$

has already been inferred from the temperature dependence of the susceptibility [12], measured on a powdered sample. The paramagnetic susceptibility displays a broad maximum, indicating that the dominant exchange interactions are antiferromagnetic. The intrachain exchange constant was found to be $J/k = -1.00 \pm 0.04$ K [12]. This result was obtained from the high-temperature ($T > 20$ K) fits to the classical spin model scaled to $S=\frac{5}{2}$ and to Weng's interpolation scheme result for $S=\frac{5}{2}$. In order to determine J/k from the specific heat results we shall again fit the data to: a) the classical spin model (scaled to $S=\frac{5}{2}$) and to b) the quantum corrected classical spin model, c) the interpolation scheme result (both for $S=\frac{5}{2}$). The J/k values obtained are collected in table V.

TABLE V

Values for J/k (in K) derived from the specific heat results

	eq.(4.3)	eq.(4.5)	eq.(4.6)	eq.(4.4) best fit	eq.(4.10)	from X-exp.	from E.S.R.-exp.
$MnCl_2.2pz$	- 0.755	-0.535	-0.49	-0.78	-0.84	-0.89±0.04 [a]	-0.81±0.10 [a]
$MnBr_2.2pz$	- 0.748	-0.58	-0.53	-0.825	-0.88	-1.00±0.32 [a]	-0.75±0.10 [a]
$MnCl_2.2py$	- 0.54	-0.39	-0.36	-0.59	-0.62	-0.69±0.02 [a] -0.59±0.04 [b]	-0.43±0.05 [a]
$MnBr_2.2py$	- 0.53			-0.55	-0.62	-0.86±0.02 [a]	-0.50±0.05 [a]

[a] ref. 12
[b] ref. 17

The specific heat curves for each of the approximations to the spin $\frac{5}{2}$ isotropic Heisenberg linear chain model with $J/k = -0.825$ K are shown in fig. 13, along with the experimental results.

Since for the classical spin isotropic Heisenberg linear chain model C_{max} equals R (= 8.31 J/mol K) and since all the calculations mentioned above are based on this model, producing values for C_{max} smaller than R, the data near the maximum cannot be described by any of these calculations. The difference between the C_{max} values for the two compounds $MnBr_2.2pz$ and $MnCl_2.2pz$ is too large to be due to the interchain coupling, although this is probably somewhat larger in $MnBr_2.2pz$ than in $MnCl_2.2pz$. Since furthermore dipole-dipole anisotropy in $MnBr_2.2pz$ is, due to the large Br^- ions, expected to be even smaller

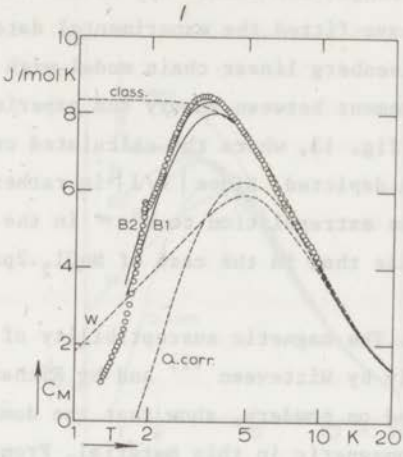

Fig. 13. *The magnetic specific heat of $MnBr_2.2pz$ as a function of temperature.*

o o o : *experimental results*

------ class : *isotropic Heisenberg linear chain model as calculated by Fisher for S=∞ , scaled to $S=\frac{5}{2}$: J/k ($S=\frac{5}{2}$) = -0.825 K.*

------ Q. corr.: *second order quantum corrected version of the isotropic classical spin model: J/k ($S=\frac{5}{2}$) = -0.825 K.*

------ W : *isotropic Heisenberg linear chain model for $S=\frac{5}{2}$ as calculated according to Weng's interpolation scheme: J/k ($S=\frac{5}{2}$) = -0.825 K.*

—————— : *isotropic Heisenberg linear chain model with uniaxial single-ion anisotropy, eq. (4.9), as calculated by Blöte for $S=\frac{5}{2}$;*
(B1) extrapolation result using chains of N = 2, 3 and 4 spins, with J/k = -0.82 K and D/k = -0.50 K.
(B2) as B1, but with the N = 3 and N = 4 results only.

than in $MnCl_2.2pz$, we infer that the large value of C_{max} also in this case is due to large single-ion anisotropy of the divalent manganese ions. Therefore, we have fitted the experimental data with the calculations for the isotropic Heisenberg linear chain model with uniaxial single-ion anisotropy. Good agreement between theory and experiment is obtained as can be inferred from fig. 13, where the calculated curves for $J/k = -0.82$ K and $D/k = -0.50$ K are depicted. Since $|D/J|$ is rather large, i.e. approximately 0.6, the extrapolation to $N = \infty$ in the low temperature region is more reliable than in the case of $MnCl_2.2pz$ in which $|D/J|$ is much smaller.

4.2.3 $MnCl_2.2py$. The magnetic susceptibility of $MnCl_2.2py$ has been measured independently by Witteveen [12] and by Richards *et al.* [17]. Both experiments, performed on powders, show that the dominant exchange interactions are antiferromagnetic in this material. From the analysis of the susceptibility results, that extended down to about 2 K, Witteveen [12] concluded that $J/k = -0.69 \pm 0.02$ K, whereas Richards *et al.* [17] found $J/k = -0.59 \pm 0.04$ K from a fit to the high-temperature data. Moreover, Witteveen found increasing deviations between the calculated and experimental results below 20 K, while Richards *et al.* reported that they were able to fit their data adequately down to the lowest temperature, i.e. T = 4 K, using the isotropic Heisenberg linear chain model. The way the experimental results are plotted in ref. 17, however, does not allow a comparison with the experimental results in ref. 12. We shall, therefore, concentrate on the magnetic specific heat data.

As may be seen in fig. 14, the magnetic specific heat data of $MnCl_2.2py$, fitted with the three approximations for the $S=\frac{5}{2}$ isotropic Heisenberg linear chain model display considerable differences with the model calculations at low temperatures. The dashed curves, shown in fig. 14, are calculated for $J/k = -0.59$ K, yielding a good fit to the high-temperature data.

The conclusion that can be drawn from fig. 14 is that also in this case the presence of single-ion anisotropy in the exchange hamiltonian is needed in order to explain the differences between experiment and theory close to $T(C_{max})$. This result is plausible because the distorted octahedral co-ordination geometries of the manganese ions in $MnX_2.2py$ and $MnX_2.2pz$ are very similar. On the other hand, the short-range order

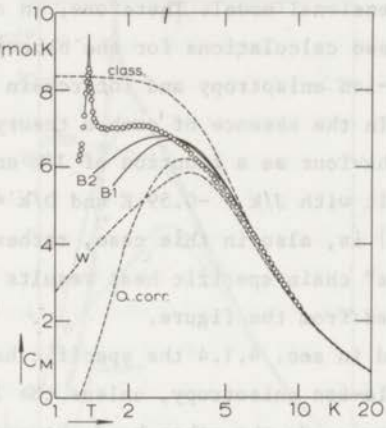

Fig. 14. *The magnetic specific heat of $MnCl_2.2py$ as a function of temperature.*

o o o : *experimental results.*

------ class : *isotropic Heisenberg linear chain model as calculated by Fisher for $S = \infty$, scaled to $S=\frac{5}{2}$: J/k ($S=\frac{5}{2}$) = −0.59 K.*

------ Q. corr.: *second order quantum corrected version of the isotropic classical spin model: J/k ($S=\frac{5}{2}$) = −0.59 K.*

------ W : *isotropic Heisenberg linear chain model for $S=\frac{5}{2}$ as calculated according to Weng's interpolation scheme: J/k ($S=\frac{5}{2}$) = −0.59 K.*

—————— : *isotropic Heisenberg linear chain model with uniaxial single-ion anisotropy, eq. (4.9), as calculated by Blöte for $S=\frac{5}{2}$;*
(B1) extrapolation result using chains of N = 2, 3 and 4 spins, with J/k = −0.59 K and D/k = −0.18 K.
(B2) as B1, but with the N = 3 and N = 4 results only.

accociated with the interchain coupling can also cause an increase of the specific heat in the region just above T_c with respect to the curve of the ideal one-dimensional model. Therefore, in order to explain the C_M data, one would need calculations for the behaviour of C_M for a model that includes single-ion anisotropy and interchain coupling simultaneously in the hamiltonian. In the absence of such a theory we have calculated the specific heat behaviour as a function of J/k and D/k. Fig. 14 illustrates the result with J/k = -0.59 K and D/k = -0.18 K (full curves). Since the ratio $|D/J|$ is, also in this case, rather small the low-temperature "infinite" chain specific heat results are unreliable and are, therefore, omitted from the figure.

As was discussed in sec. 4.1.4 the specific heat maximum is strongly affected by the single-ion anisotropy, unless the latter is sufficiently small or extremely large. On the other hand, however, the high-temperature tails of the magnetic specific heat curves change very little upon introducing single-ion anisotropy, unless the latter is very large in comparison with J/k. Since for $MnCl_2$.2py we are dealing with a relatively quite small single-ion anisotropy, the fitted J/k values only vary little when using different ratios of $|D/J|$. Furthermore, the experimental result for C_{max} allows only a rather small variation of D/k.

As a conclusion from the above mentioned comparison between experiment and theory we can say that also for $MnCl_2$.2py the single-ion anisotropy is not negligible and that D/k takes a value of about -0.2 K. The remaining discrepancy between theory and experiment (see fig. 14) we believe to be mainly due to the interchain coupling. Our final result for J/k is thus in good agreement with that given in ref. 17, whereas the two results are slightly different from the value reported in fig. 12.

4.2.4 $MnBr_2$.2py. By identifying $C_M T^2$ = 220 JK/mol with eq. (4.3) we derive $|J/k|$ = 0.54 K for $MnBr_2$.2py (see table V). Using eq. (4.4) we find from a best fit to the data between T = 6 K and T = 10 K, J/k = -0.55 K. For comparison we show in fig. 15 the quantum corrected classical spin model as well as the classical spin model and the interpolation scheme result for J/k = -0.55 K (dashed curves). Whereas the high-temperature specific heat data are satisfactorily described with J/k = -0.55 K, Witteveen [12] has derived J/k = -0.85 $\pm$ 0.05 K from his

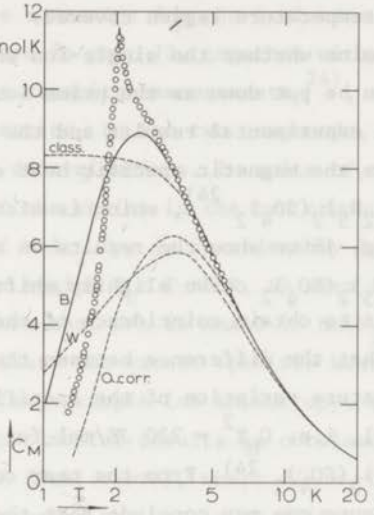

Fig. 15. *The magnetic specific heat of $MnBr_2.2py$ as a function of temperature.*

o o o : *experimental results.*

------ *class* : *isotropic Heisenberg linear chain model as calculated by Fisher for* $S=\infty$, *scaled to* $S=\frac{5}{2}$: $J/k\ (S=\frac{5}{2}) = -0.55$ *K.*

------ *Q. corr.*: *second order quantum corrected version of the isotropic classical spin model:* $J/k\ (S=\frac{5}{2}) = -0.55$ *K.*

------ *W.* : *isotropic Heisenberg linear chain model for* $S=\frac{5}{2}$ *as calculated according to Weng's interpolation scheme:* $J/k\ (S=\frac{5}{2}) = -0.55$ *K.*

——— : *isotropic Heisenberg linear chain model with uniaxial single-ion anisotropy, eq. (4.9), as calculated by Blöte for* $S=\frac{5}{2}$;
(B1) extrapolation result using chains of $N = 2$, *3 and 4 spins, with* $J/k = -0.53$ *K and* $D/k = -0.37$ *K.*
(B2) as B1, but with the $N = 3$ *and* $N = 4$ *results only.*

high-temperature susceptibility results (on a powdered sample). The specific heat, nor the susceptibility results, however, match the theory over the whole temperature region covered.

In order to determine whether the single-ion anisotropy or the interchain coupling can be put down as the prime source of the large difference between the experimental results and the isotropic linear chain model, we compare the magnetic specific heat of $MnBr_2.2py$ with that obtained for $Mn(N_2H_5)_2(SO_4)_2$ [24], which is also a linear chain antiferromagnet. In fig. 16 we show the results on a semilogarithmic scale, with the $Mn(N_2H_5)_2(SO_4)_2$ curve slightly shifted parallel to the temperature axis, so as to obtain coincidence of the high-temperature tails. It is noticed that the difference between the C_MT^2 values of the asymptotic high-temperature variation of the specific heat of the two compounds is very small, i.e. C_MT^2 = 220 JK/mol for $MnBr_2.2py$ and 216 JK/mol for $Mn(N_2H_5)_2(SO_4)_2$ [24]. From the near coincidence of the sharp peaks in this figure one may conclude that the relative interchain

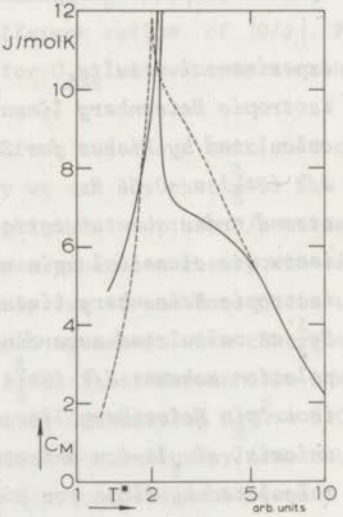

Fig. 16. *The magnetic specific heats of $MnBr_2.2py$ and $Mn(N_2H_5)_2(SO_4)_2$ plotted on a semi logarithmic scale.*

------ *$MnBr_2.2py$.*

——— *$Mn(N_2H_5)_2(SO_4)_2$.*

coupling is about the same for the two compounds, and probably even weaker in $MnBr_2.2py$. We arrive at the same conclusion when the ratio $T(\chi_{max})/T_c$ is taken as a measure for the isolation of the chains. Using the $T(\chi_{max})$ values given in ref. 12, together with the T_c values as obtained from the heat capacity measurements [24], we find approximately equal values for the ratios in the two compounds, within the error limits of the $T(\chi_{max})$ determinations. In spite of the apparently similar degree of isolation of the chains in the two compounds, the short-range order specific heat of $MnBr_2.2py$ is considerably larger than that of $Mn(N_2H_5)_2(SO_4)_2$ in the region $T_c < T < 5$ K, as seen in fig. 16. Since, furthermore, it is known that D/k is small in $Mn(N_2H_5)_2(SO_4)_2$, i.e. $D/k \simeq 0.04$ K, we attribute the excess specific heat above T_c in $MnBr_2.2py$ to the presence of a large single-ion anisotropy. In fact, a good description of the experimental results is obtained with eq. (4.9), as is shown in fig. 15 (full curve), where $J/k = -0.53$ K and $D/k = -0.37$ K. Also in this case we ascribe the remaining difference between experiment and theory mainly to interchain coupling effects.

Although the ratio $|D/J|$ found for $MnBr_2.2py$ is the largest of the present series of compounds, $|D/k|$ is smaller than in $MnBr_2.2pz$. Furthermore, it is seen that for this large value of $|D/J|$ the exchange constants, as determined from best fits to the high-temperature data, according to eq. (4.4) and according to eq. (4.9) yield only slightly different results. In fact, a much larger difference is found when comparing our final results for J/k with those obtained from the analysis of the powder susceptibility measurements. We, however, notice that in the latter single-ion anisotropy was not included.

TABLE VI

	Values for J/k and D/k derived from the specific heat results using eq. (4.12)	
	J/k K	D/k K
$MnCl_2.2pz$	-0.78 ± 0.02	-0.30 ± 0.05
$MnBr_2.2pz$	-0.82 ± 0.02	-0.50 ± 0.05
$MnCl_2.2py$	-0.59 ± 0.03	-0.18 ± 0.05
$MnBr_2.2py$	-0.53 ± 0.02	-0.37 ± 0.10

5. Interchain exchange interactions. The λ-like anomalies observed in the specific heat of $MnBr_2.2pz$, $MnCl_2.2py$ and $MnBr_2.2py$ at T_c = 1.930 K, 1.380 K and 2.055 K, respectively, were attributed to the onset of long-range spin ordering due to a finite coupling between the chains in these materials In order to give an estimate of the interchain exchange constant J'/k, we will use a formula derived by Oguchi [39], that, for a given spin value, relates the ratio $kT_c/|J|$ and the ratio $|J'/J|$. The formula applies to a tetragonal lattice structure of weakly coupled antiferromagnetic linear chains with interactions that are fully isotropic. Since, however, this series of manganese compounds does not obey these conditions only an order of magnitude result can, therefore, be given.

From the experimental T_c-values (table III) and the J/k-values (table VI) obtained from the specific heat data with eq. (4.9) the $|J'/J|$ values, collected in table VII, were calculated. Due to the fact that the specific heat of $MnCl_2.2pz$ does not show evidence of the onset of long-range spin ordering down to T = 1.3 K, we can only estimate a maximum value of $|J'/J|$ for this compound, which result is also given in table VII.

TABLE VII

Values for J'/J derived using Oguchi's formula

	J/k	T_c	J'/J
	K	K	
$MnCl_2.2pz$	-0.78	<1.3	$<0.6 \times 10^{-2}$
$MnBr_2.2pz$	-0.82	1.930	1.5×10^{-2}
$MnCl_2.2py$	-0.59	1.380	1.5×10^{-2}
$MnBr_2.2py$	-0.53	2.055	2×10^{-2}

6. Concluding remarks. The heat capacities of four manganese compounds with general formula MnX_2L_2 where X = Cl, Br and L = pz, py, have been measured in the temperature range between 1.3 K and 80 K. Reliable estimates for the lattice contributions to the specific heats were obtained from the conventional C_pT^2 versus T^5 plots. The remaining low-temperature magnetic specific heats display broad peaks, having maxima with a typical value of 7.2 J/mol K for the Cl-compounds. For

the related Br-compounds the short-range order specific heat maxima are significantly higher. Although we attribute the broad peaks in the specific heats to be due to the presence of dominant linear chain exchange interactions in these materials, it is suggested that the large differences between the C_{max} values for the different compounds are primarily due to the presence of single-ion anisotropy of the divalent manganese ions, rather than interchain coupling. For structural reasons we assume D/k to be negative. Calculations for the isotropic Heisenberg linear chain model, spin $\frac{5}{2}$, with uniaxial single-ion anisotropy have been performed. Within this model the differences between C_{max} values of the various compounds could be satisfactorily explained. The J/k and D/k values, obtained from best fits, are collected in table VI, from which we may conclude that the intrachain exchange constants J/k, that are apparently antiferromagnetic for the present manganese compounds, take values that are comparable with that reported for $MnCl_2.2H_2O$ [15]. The J/k values, however, vary by about 60 per cent through the series.

It is generally accepted that the exchange constant depends strongly on i) the distance between the magnetic ions [41]; ii) the number and nature of the intervening ligands and iii) the bond angles between the bridging atoms [42]. This set of data offers a starting point for such a comparison of the variation of the exchange parameter with the crystallographic parameters, in particular since the crystallographic data of these compounds with dichloride bridged manganese ions are fairly well-known.

In table VIII we have, for comparison, collected the intrachain exchange constants, the Mn-Mn distances within the chains and the bond angles (Mn-Cl-Mn) for $MnCl_2.2pz$, $MnCl_2.2py$, $pyHMnCl_3.2H_2O$ [17] and $MnCl_2.2H_2O$ [14][15]. From table VIII it may be seen that, with the exception of $pyHMnCl_3.2H_2O$, the strength of the intrachain exchange interaction *increases* with increasing distances between the magnetic ions. This is in contrast to what one would naively expect. The exchange parameter is apparently not only determined by the Mn-Mn distance, even when the intervening ligands are the same. In fact, Mc Gregor *et al.* [42] found a similar result for a series of dimeric, di-μ- hydroxo-bridged, copper compounds. The compounds have similar structures but their

TABLE VIII

Comparison between magnetic and crystallographic parameters in dichloride-bridged Mn-chain compounds.

	J/k K	Mn-Mn Å	Mn-Cl-Mn degrees
$MnCl_2.2pz$	-0.78	3.761	92.9
$MnCl_2.2py$	-0.59	3.738	93.54
$MnCl_2.2H_2O$ a)	-0.45	3.691	92.54
$pyHMnCl_3.H_2O$ b)	-0.69	3.664	93.26

a) refs. 14, 15

b) ref. 17

magnetic properties are very different. They, however, found a nearly linear relationship of the bridging angle ϕ and the exchange parameter J/k. Moreover, their results are indicative of an extreme sensitivity of the magnetic properties to minor changes in ϕ. A comparison of the Mn-Cl-Mn angles and the exchange parameters for the present series of Mn linear chain compounds indicates that there is apparently no such simple relation between the two parameters, as may be seen from table VIII. It should, however, be noted that for the Mn compounds, given in table VIII, the bridging angles lie in a rather small range, and their accuracy is limited. Possibly the variations in the exchange parameter that are due to the variations in the Mn-Cl-Mn angle and in the Mn-Mn distance of this series of compounds, are of comparable magnitude. We notice that in order to arrive at the linear relationship of J/k and for the dimeric Cu-compounds, the Cu-Cu distance has not been taken into account [42], which might put some doubt on the relation between J/k and ϕ obtained. In spite of the replacement of the Cl^- ions by the Br^- ions the J/k values remain approximately equal (see table VI). This in contrast to the results on the divalent nickel compounds of the same series, where we found the replacement of the Cl^- ions by the Br^- ions to reduce the, in that case ferromagnetic, intrachain exchange constant by approximately a factor three [23]. In fact both results are in contradiction with the generally accepted rule of thumb that super-

exchange via Br^- ions is stronger than via Cl^- ions. For the present series of manganese compounds the J/k values appear to be most sensitive to the replacement of the ligands pz, py and H_2O.

The zero-field splittings for the divalent manganese ions of this series of compounds are quite large in comparison with the D/k values generally observed for inorganic Mn^{2+} compounds. On the other hand, however, they are of comparable magnitude of those observed for the MnX_2L_4 compounds (see table IV). The large values for D/k are likely to be due to the strong N-donor ligands that occupy the axial positions of the tetragonally distorted octahedral co-ordination geometry about the Mn^{2+} ions. We notice that the dipole-dipole anisotropy has probably the effect to align the spins perpendicular to the chain axis. This has an effect similar to that of the crystalline field. Therefore, the D/k values may have been slightly overestimated, although the dipole-dipole anisotropy in these compounds is quite small in comparison with the single-ion anisotropy.

The degree of magnetic isolation of the linear chains in the compounds MnX_2L_2, as estimated using Oguchi's formula and the values for $kT_c/|J|$, is found to decrease in the sequence of compounds: $MnCl_2.2pz$, $MnBr_2.2pz$, $MnCl_2.2py$ and $MnBr_2.2py$, although the $|J'/J|$ values obtained for $MnBr_2.2pz$ and for $MnCl_2.2py$ are approximately equal (see table VII). However, from the critical entropy values quoted in table III one would conclude that the chains in $MnBr_2.2pz$ are better isolated than those in $MnCl_2.2py$. We notice that for the Ni compounds of the MX_2L_2 series we found the relative magnetic isolation of the chains to vary in the same sequence with respect to the ligands Cl, Br and pz, py. The better isolation of the chains in the pz compounds may have something to do with hydrogen bonding between the pyrazole ligand and the anions in their own chain, whereas the better isolation of the chains in the Cl^- as compared to the Br^- compounds possibly indicates that the halogen ions are also involved in the superexchange mechanism between adjacent chains. We notice that the $|J'/J|$ values for this series of manganese compounds amount to only 2.10^{-2}. For $MnCl_2.2H_2O$ Mc Elearney *et al.* [15] found approximately equal values for J/k and J'/k, thus $|J'/J| \simeq 1$. The transition temperature in $MnCl_2.2H_2O$ is also higher than in the more chain-like MnX_2L_2 compounds. The results on the MnX_2L_2 compounds show

once more the possibility of reducing the magnetic coupling between the chains by means of replacing water molecules by large organic ligands such as pz and py, in the $MX_2.2H_2O$ series.

In summarizing the results we can say that the MnX_2L_2 compounds exhibit predominantly linear chain exchange interactions. Furthermore, it is shown that the presence of single-ion anisotropy greatly affects the thermal properties of the magnetic linear chain system. The J/k as well as the D/k values were determined for this series of Mn^{2+} compounds. The exchange and crystallographic parameters of four compounds with dichloride bridged Mn ions were compared. The results show evidence of a strong dependence of the exchange on the bond angle. However, no firm conclusions can be drawn. In order to elucidate further the relation between exchange and crystallographic parameters, additional crystal structure determinations are required. The variety of ligands available in co-ordination chemistry probably makes the MnX_2L_2 compounds a useful series for the study of possible relations between the intra-chain exchange parameters of dihalide bridged magnetic 3d ions and the crystallographic parameters.

References.

1 For example; Newell, G.F. and Montroll, E.W., Rev. Modern Phys., 25 (1953) 353.

2 Suzuki, M., Tsujiyama, B. and Katsura, S., J. Math. Phys., 8 (1967) 124.

3 Obokata, T. and Oguchi, T., J. Phys. Soc. Japan, 25 (1968) 322.

4 Bonner, J.C. and Fisher, M.E., Phys. Rev., 135 (1964) A 640.

5 Weng, C.Y., Thesis, Carnegie-Mellon University (1968).

6 Fisher, M.E., Am. J. Phys., 32 (1964) 343.

7 Harrigan, M.E. and Jones, G.L., Phys. Rev., B7 (1973) 4897.

8 Kubo, R., Phys. Rev., 87 (1952) 568.

9 Smith, T. and Friedberg, S.A., Phys. Rev., 176 (1968) 660.

10 Dingle, R., Lines, M.E. and Holt, S.L., Phys. Rev., 187 (1969) 643.

11 Reedijk, J., private communication.

12 Witteveen, H.T., Thesis, University at Leyden (1973).

13 Gorter, S., Van Ingen-Schenau, A.D. and Verschoor, G.C., Acta Cryst. (submitted).
14 Morosin, B. and Graeber, E.J., J. Chem. Phys., 42 (1965) 898.
15 Mc Elearney, J.N., Merchant, S. and Carlin, R.L., Inorg. Chem., 12 (1973) 906.
16 Zanetti, R. and Serra, R., Gazz. Chim. It., 90 (1960) 328.
17 Richards, P.M., Quinn, R.K. and Morosin, B., J. Chem. Phys., 59 (1973) 4474
18 Gill, N.S., Nyholm, R.S., Barclay, G.A., Christie, T.I. and Pauling, P.J., J. Inorg. Nucl. Chem., 18 (1961) 88
19 Dunitz, J.D., Acta Cryst., 10 (1957) 307.
20 The samples were kindly prepared by Mr. J.A. Smit.
21 Star, W.M., Van Dam, J.E. and Van Baarle, C., J. Phys., E2 (1969) 257.
22 This thesis, chapter II; Klaaijsen, F.W. *et al.* to be published.
23 Klaaijsen, F.W., Blöte, H.W.J. and Dokoupil, Z., Solid State Commun., 14 (1974) 607; this thesis, chapter IV.
24 This thesis, chapter III; Klaaijsen F.W. *et al.* to be published.
25 Stout, J.W. and Catalano, E., J. Chem. Phys., 23 (1955) 2013.
26 Reedijk, J., Klaaijsen, F.W. and Witteveen, H.T., J. Chem. Soc. Faraday II (1973) 1537.
27 Witteveen, H.T. and Reedijk, J., Solid State Commun., 12 (1973) 557.
28 Anderson, P.W., Phys. Rev., 83 (1951) 1260.
29 Hulthén, L., Ark. Mat. Astron. Fys., 26A (1938) No 11.
30 Davis, H.L., Phys. Rev., 120 (1960) 789.
31 Scales, S.A. and Gersch, H.A., Phys. Rev. Lett., 28 (1972) 917.
32 Reedijk, J., Rec. Trav. Chim., 89 (1970) 605.
33 Reedijk, J., private communication.
34 Klaaijsen, F.W., Reedijk, J. and Witteveen, H.T., Z. Naturforsch, 27a (1972) 1532.
35 Dowsing, R.D., Nieuwenhuyse, B. and Reedijk, J., Inorg. Chim. Acta 5 (1971) 301.
36 Dowsing, R.D., Gibson, J.F., Goodgame, M. and Hayward, P.J., J. Chem. Soc., A (1969) 187.
37 Blöte, H.W.J., to be published in Physica.
38 Blöte, H.W.J. and Huiskamp, W.J., Physica 53 (1971) 445.
39 Oguchi, T., Phys. Rev., 133 (1964) A 1098.

40 Reimann, C.W., Mighell, A.D. and Mauer, F.A., Acta Cryst., 23 (1967) 135.

41 See for example, Rogers, R.N., Finegold, L. and Morosin, B., Phys. Rev., B6 (1972) 1058.

42 See for example, Mc Gregor, K.T., Watkins, N.T., Lewis, D.L., Drake, R.F., Hodgon, D.J. and Hatfield, W.E., Inorg. Nucl. Chem. Lett., 9 (1973) 423.

CHAPTER VI

THE SPECIFIC HEAT OF SOME HEXAMMINE IODINE COMPOUNDS

1. Introduction. The nature of the rotational motion of molecules in ordered phases has been subject of many studies. On the basis of thermodynamic studies Pauling [1] suggested that even in the solid state hydrogen molecules rotate freely. Also in the case of crystalline methane and the ammonium halides it was shown by Pauling that at a discrete temperature a transition may occur from a state in which the molecules are merely vibrating to one in which they are allowed to rotate freely. In more complicated compounds groups of atoms may have also rotational degrees of freedom. In 1941 Ziegler [2] suggested that the large peak in the heat capacity of the complex compound $Co(NH_3)_6I_3$ at T_c = 277 K is due to the motion or reorientation of the ammonia molecules about their Co-N bonds. For the divalent cobalt hexammine iodide, $Co(NH_3)_6I_2$, however, no such transition in the heat capacity was observed down to T = 100 K [2].

Only more recently, low temperature experiments have given evidence for motional processes of the ammonia molecules in the divalent metal hexammine halides. Palma-Vittorelli *et al.* [3] found a sudden broadening of the E.S.R. absorption line of the Ni^{2+} in $Ni(NH_3)_6I_2$ when the sample was cooled through a critical temperature, T_c = 20 K. Similar features were observed with the compounds $Ni(NH_3)_6Br_2$ [4] and $Ni(NH_3)_6Cl_2$ [4] at T_c = 35 K and T_c = 80 K, respectively. It was pointed out that the phase transition of the crystal is closely related to the motion and the geometrical arrangements of the NH_3 groups. An interesting experiment concerning the nature of the transition at T_c was performed by Garofano *et al.* [5]. By means of E.S.R. experiments they determined the transition temperature in the deuterated compound $Ni(ND_3)_6I_2$ which was found to be changed compared to the hydrogenic compound to about 26 K. The ratio between the two T_c's for the nickel iodide compounds is remarkably close to $\sqrt{I_{ND_3}/I_{NH_3}} = \sqrt{2}$, where I_{ND_3} and I_{NH_3} are the moments of inertia about the threefold symmetry axes of the ND_3 and NH_3 molecules. These results suggest that the rotational motion of the ammonia molecules indeed plays a crucial role in the transition.

Motions of the ammonia molecules are also manifest at temperatures

far below T_c, as was found by Kim [6] using N.M.R. techniques, and by Van Kempen *et al.* [7] from heat capacity measurements below 1 K. An explanation of the anomalous, low temperature, heat capacity of the nickel hexammine halides was given in terms of tunneling of the NH_3 groups through a potential barrier. The height of the barrier was found to be relatively low, e.g., as compared to the tunneling barriers for methyl groups in various organic molecules; for instance for $Ni(NH_3)_6I_2$ it is found that V_o/k = 250 K only.

A theoretical explanation of the phenomena mentioned above was given by Bates and Stevens [8], using an electrostatic point-charge model. As a result of their calculations Bates and Stevens arrived at the conclusion that the entropy associated with the non-magnetic transition at T_c (henceforth: 'the transition entropy') amounts to Rln 8. The early experimental results on transition entropies showed considerable deviations from that theoretical value. For instance a value of about Rln 3 was found for the nickel hexammine iodide compound (Miss Voorhoeve, unpublished). The largest problem in arriving to a correct value for the transition entropy was the estimation of the lattice heat capacity. This called for an investigation of the specific heat of a series of isomorphous hexammine salts.

In the first part of this chapter we present heat capacity results on the $M(NH_3)_6I_2$ series, i.e., metal(II)hexammine iodides, in the temperature range between 1.3 and 80 K. A preliminary report for some of these compounds has appeared [9]. As a second part of this research on hexammine iodides we measured the heat capacities of deuterated and partly deuterated samples, which proved to be interesting with respect to the nature of the transition at T_c. The results of these experiments are presented in section 8.

2. Crystal structure. At room temperature the crystal structure of the compounds $M(II)(NH_3)_6I_2$ where M(II) is Ni, Co, Fe, Mn, Zn, Cd and Ca, are all isomorphous [10]. They have the structure of the well-known compound K_2PtCl_6 [11], which has been shown to be face centered cubic with space group F3m3. In addition, for nickel the iodine compound is isomorphous with the chlorine and the bromine compound, which property is found for many of the other metal atoms as well.

The crystal structure is shown in fig. 1. It is visualized most easily as a collection of octahedra $(M(NH_3)_6)^{2+}$ situated at the corners and face centers of the cubes. Following Bates and Stevens [8] we shall hereafter denote a $(M(NH_3)_6)^{2+}$-unit as a separate cluster. The halogen atoms are situated in the positions $(\pm \frac{1}{4}, \pm \frac{1}{4}, \pm \frac{1}{4})$, thus forming cubes around each metal ion. To a first approximation the proton triangles of the NH_3 groups can be considered as lying in the planes of the cubes formed by the halogen atoms.

3. Sample preparation and analysis. Anhydrous metal iodide was allowed to react with dry ammonia gas in a vacuum apparatus. This method is known in the literature as the dry method [12]. Special attention was paid to complete dehydration of the initial halide crystals, whereas in the case of CoI_2, MnI_2 and FeI_2 the crystals were protected against light and air. The reaction of the ammonia gas with the metal iodides

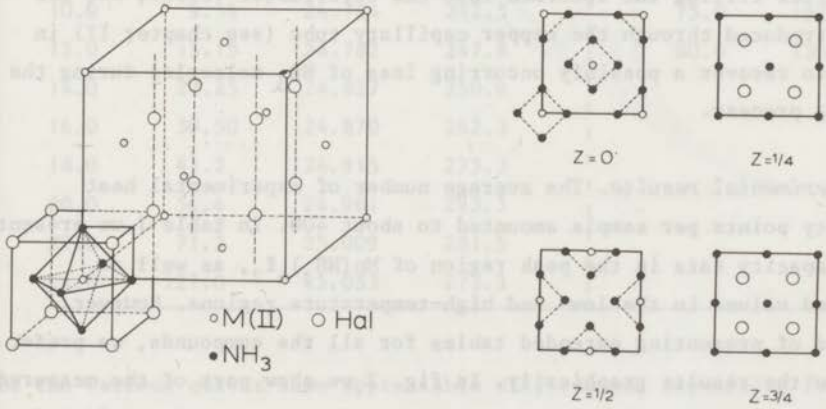

Fig. 1a. *The crystal stucture of the metal hexammine halide, $M(II)(NH_3)_6(Hal)_2$. For one of the metal ions the complete environment is shown. Each of the metal ions is octahedrally co-ordinated by six ammonia molecules; a $(M(II)(NH_3)_6)^{2+}$-unit is defined as a cluster.*

Fig. 1b. *Layer sequence of the unit cell of $M(II)(NH_3)_6(Hal)_2$ at 0, ¼, ½ and ¾ of the height of a cube edge.*

was monitored by weighing the reaction vessel until a constant weight was obtained. The specimens were kept over KOH drying agent in an atmosphere of NH_3 gas, prior to the measurements. It is known that several complex compounds can be formed from MX_2 and NH_3 whose composition differs from the $M(NH_3)_6X_2$-formula. In fact the various number of ammonia ligands co-ordinated to the metal ion can be obtained by pumping off ammonia from $M(NH_3)_6X_2$. Apparently the compounds go through various structures when the ammonia is lost. In samples that contained slightly less than six ammonia ligands per molecule (e.g. with measurements on Fe and Ni compounds with 5.7 NH_3 molecules per metal atom) we found heat capacities which were significantly different from those of the hexammine samples. In fact the common sharp peaks almost totally disappeared. Much attention has, therefore, been paid to the NH_3 content of the samples. Results of our analysis on some samples, directly after preparation, showed that the NH_3 content was better than 6.00 ± 0.05 NH_3 groups per metal atom.

After filling the specimen into the calorimeter vessel, NH_3 gas was introduced through the copper capillary tube (see chapter II) in order to recover a possibly occurring loss of NH_3 molecules during the filling process.

4. Experimental results. The average number of experimental heat capacity points per sample amounted to about 400. In table I we present heat capacity data in the peak region of $Mn(NH_3)_6I_2$, as well as smoothed values in the low- and high-temperature regions. However, instead of presenting extended tables for all the compounds, we prefer to show the results graphically. In fig. 2 we show part of the measured heat capacity points in the temperature range between 1.3 and 80 K for the compounds $M(NH_3)_6I_2$, where M = Ni, Co, Zn, Fe, Mn, Cd and Ca. Large peaks in the heat capacity were observed for all the salts, including the diamagnetic salts. The transition temperatures lie in the range between 19.7 K for $Ni(NH_3)_6I_2$ and 51.8 K for $Ca(NH_3)_6I_2$ (see table II). The height of the sharp λ-like peaks cannot be determined accurately; e.g. the highest C_p value measured for $Zn(NH_3)_6I_2$ in the temperature region of the peak was 1690 J/mol K, which represents certainly only a lower limit. All compounds exhibit very high peaks, but the shapes

TABLE I

Measured and smoothed values of the specific heat of $Mn(NH_3)_6I_2$

T K	C_p J/mol K	T K	C_p J/mol K		T K	C_p J/mol K
1.2	5.54	24.089	134.5		26.0	71.0
1.5	3.82	24.160	140.9		28.0	71.8
2.0	2.40	24.227	150.6		30.0	76.0
2.5	1.71	24.292	155.0		35.0	86.5
3.0	1.40	24.359	167.3		40.0	96.9
4.0	1.33	24.425	182.1		45.0	106.5
5.0	1.75	24.492	190.5		50.0	115.2
6.0	2.58	24.550	199.0		55.0	124.0
7.0	3.77	24.599	211.3		60.0	132
8.0	5.36	24.645	222.2		65.0	139
9.0	7.25	24.691	225.5		70.0	146
10.0	9.54	24.734	242.5		75.0	152
12.0	15.15	24.782	247.8		80.0	158
14.0	22.25	24.827	250.9			
16.0	30.50	24.870	262.3			
18.0	41.2	24.915	275.3			
20.0	54.4	24.961	293.3			
22.0	71.2	25.009	281.5			
24.0	127.0	25.053	273.3			

peak region

of the various curves show appreciable differences, especially for temperatures lower than T_c. We may divide them roughly into two groups; Ni, Co, Zn, Mn salts and Fe, Cd, Ca salts, respectively. Especially for the last group the heat capacity decreases slowly with decreasing temperature when $T < T_c$. At temperatures well above the transition temperatures the specific heat curves exhibit a very similar gradual temperature dependence.

Since the lowest temperature attained in these experiments is 1.3 K we observed only the tails of the anomalous heat capacities of the Ni and Mn salt found below 1 K. Our results fit very nicely to those of

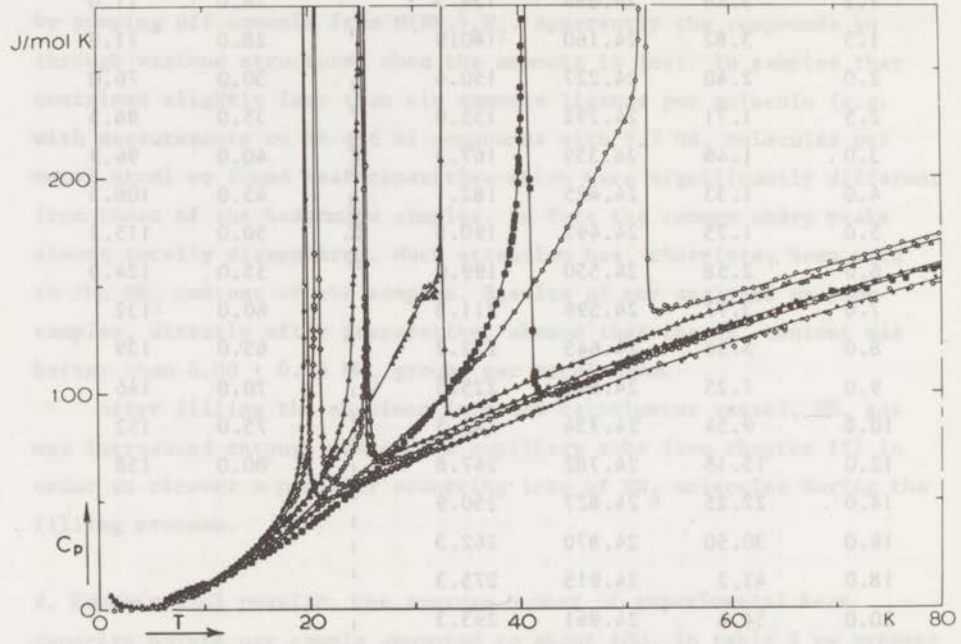

Fig. 2. *The specific heats of* $M(II)(NH_3)_6I_2$ *as a function of temperature.* $M(II)$ = ● *Ni*, ◇ *Co*, ▲ *Mn*, □ *Zn*, △ *Cd*, ■ *Fe and* ○ *Ca. The drawn lines are for visual aid only.*

Van Kempen *et al.* [13] on $Ni(NH_3)_6I_2$ and those of Suga *et al.* [14] on $Mn(NH_3)_6I_2$. In the temperature range between about 4 and 7 K the curves show nearly the same temperature dependence, except that of $Fe(NH_3)_6I_2$, which displays an additional broad maximum.

We notice the large values of C_p for the hexammine iodine compounds, e.g. at T = 20 K, C_p amounts to approximately 50 J/mol K, whereas for the compounds such as $NiCl_2.6H_2O$ and $CoCl_2.6H_2O$, C_p values of only about

10 J/mol K were observed at this temperature [15].

In order to evaluate the entropy content involved in the transition at T_c, we assume that the lattice contribution to the measured heat capacity is obtainable by interpolating the heat capacity smoothly through the transition region. By subtracting this portion from the experimental data we can calculate the entropy contribution which we denote as ΔS_n. The results are given in table II.

TABLE II

Experimental results of the heat capacity measurements on $M(NH_3)_6I_2$

	T_c K	ΔS_n J/mol K
$Ni(NH_3)_6I_2$	19.7	8.2
$Co(NH_3)_6I_2$	20.9	10.5
$Zn(NH_3)_6I_2$	25.44	10.6
$Fe(NH_3)_6I_2$	40.6	23.0
$Mn(NH_3)_6I_2$	25.0	15.6
$Cd(NH_3)_6I_2$	32.6	21.0
$Ca(NH_3)_6I_2$	51.8	29.8

The values found for ΔS_n range from 8.2 J/mol K for $Ni(NH_3)_6I_2$ to 29.8 J/mol K for $Ca(NH_3)_6I_2$. Or written in another way, from approximately Rln 3 to about Rln 32. In fact, the ΔS_n value for $Ni(NH_3)_6I_2$ agrees fairly well with that previously reported (e.g. ref. 16).

In the next section we shall consider some types of phase transitions which may be of interest with respect to the present measurements.

5. Theory. 5.1 Various types of phase transitions.

1) Magnetic phase transitions. The transition entropy is completely determined by the electronic degeneracy of the magnetic ion. It is true that the Co and Ni compounds do show magnetic ordering, but at lower

temperatures than those (i.e. T_c) for the phase transitions discussed. Hence this does not provide an explanation for the transition entropies. Moreover, the diamagnetic compounds, for instance the Zn, Cd and Ca compounds, also display sharp peaks at T_c.

2) Structural phase transitions. These lead to a change in the crystal symmetry. Notable examples are the crystallographic phase transformations in ferroelectrics and antiferroelectrics. In such cases lattice anharmonicity and the occurrence of soft modes are usually invoked to explain the various experimental data. Under conditions of lattice-instability the distinction between the lattice entropy contribution on the basis of the Debye model and the transition entropy becomes artificial. Again, it may be remarked that the transition entropies are usually quite small. Typical examples are the perovskite structure compounds $SrTiO_3$ and $LaAlO_3$, having a jump in the specific heat of about 10^{-1} R (ref. 17). In these cases one finds that distortions arise from rotation of oxygen octahedra accompanied by soft-mode behaviour of the lattice.

3) Collective Jahn-Teller transitions. These can be considered as a special case of the structural phase transitions. Jahn-Teller distortions arise in magnetic ion complexes having orbitally degenerate or nearly degenerate ground states. If the removal of the degeneracy occurs for all ions simultaneously at the same temperature (under the influence of mutual interactions) a phase transition may be observed. This occurs for instance in $DyVO_4$ [18] where the entropy yield is Rln2 since at high temperatures the Dy ion has fourfold degeneracy which is reduced at the transition temperature into two Kramers doublets. The entropy of the spin degeneracy of the lower doublet is separately observable in a magnetic phase transition.

It will be seen that the entropy yield of the Jahn-Teller transition is insufficient to explain the experimental data on the hexammine compounds. Moreover, phase transitions were observed also for non-magnetic hexammine compounds. Jahn-Teller transitions in non-magnetic compounds only occur in the case of alloys, where splitting of the energy bands in conjunction with a lowering of the crystal symmetry may occur.

4) Order-disorder transitions. Apart from alloys (e.g. Cu-Zn), order-disorder transitions are found in cases like NH_4Cl [19] and

ferroelectrics or antiferroelectrics in which two or more equivalent energy minima are encountered. In particular protons in hydrogen-bonded (anti-)ferroelectrics may tunnel between two equivalent minima; long-range electrostatic interactions then lead to a collective phase transition and, simultaneously, to a lowering of the crystal symmetry. In contrast to displacive phase transitions the entropy yield may be substantial and well-defined. In the next section we shall discuss a particular model, proposed by Bates and Stevens [8], which belongs to this category.

5) Molecular orientational ordering. In a few molecular crystals, such as H_2 [20], CH_4 [21] and their isotopic homologues [21][22], experimental results show that apart from the liquid to solid transition, there are additional phase transitions in the solid phase. These are attributed to reorientation of the molecules under the influence of intermolecular interactions. The orientationally dependent part of these interactions may, in the static limit, be replaced by an average effective potential, leading to preferred orientations of the molecular symmetry axes in the solid state. This is comparable to the molecular ordering in liquid crystals. It is to be noted that marked isotope effects are seen in the molecular ordering phase-transition temperature of solid hydrogen and methane, which show a strong influence of dynamic effects relative to static interactions.

5.2 The B-S model. Bates and Stevens [8] considered the various configurations of the six proton triangles, located within one cluster, i.e. a $(M(NH_3)_6)^{2+}$-unit. The electrostatic potential energy, due to the interactions within one cluster only, has minimum values as a function of the angular variation of the six proton triangles. These interactions within one isolated cluster are denoted as *intra*-cluster interactions. Each equilibrium configuration has trigonal symmetry about a body diagonal of the cluster cube and can be characterized by a polar vector along this body diagonal (see fig. 3). Hence, there are eight equivalent configurations yielding a principal minimum energy. In addition Bates and Stevens find eight configurations having, in the Bates and Stevens terminology, an energy subminimum. Similarly sixteen high-energy configurations are found, which are divided into eight having maximum and eight having submaximum energy configurations. The energy differences between the principal minimum and subminimum energy

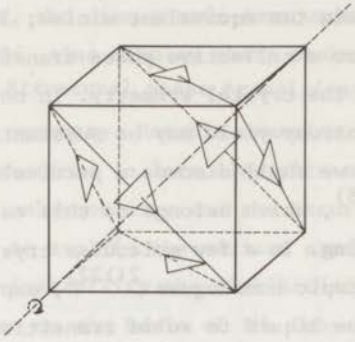

Fig. 3. *An isolated cluster of six proton triangles in a principal minimum energy configuration, according to the B-S model.*

configurations on the one hand and the principal maximum and submaximum energy configurations on the other hand, are found to be small compared to the energy difference between maximum and minimum energy configurations.

The interactions between the proton triangles and the halogen atoms, which lie between the clusters, have also been considered on the basis of classical electrostatic interactions. The influence of the halogen atoms on the angular orientations of the proton triangles is found to be small in comparison with that of the intracluster interactions. The effect of the halogen atoms in the $M(NH_3)_6X_2$ compounds can, therefore, to a first approximation be considered as determining the distance between the clusters.

Each cluster has twelve nearest neighbour clusters in the crystal, because of the f.c.c. symmetry (fig. 1). A relatively important contribution to the electrostatic potential energy of the proton triangle configurations in the $Ni(NH_3)_6X_2$ compounds was found to arise from nearest neighbour cluster interactions (*inter*cluster interactions). Bates and Stevens show that when the intercluster interactions are taken into account the energy minima of a cluster are no longer equivalent. In other words, the intercluster interactions remove the eightfold degeneracy and create preferred configurations of the proton triangles. This may lead to a long-range ordered state in which the clusters have configurations corresponding to ordering of the threefold

TABLE III

Potential energies and barriers (in Kelvin) according to the Bates and Stevens model

	$Ni(NH_3)_6Cl_2$	$Ni(NH_3)_6Br_2$	$Ni(NH_3)_6I_2$
W_1	700	650	520
W_n	715	470	225
$W = W_1 + W_n$	1415	1120	745
$V_1 \simeq \frac{1}{3} W_1$	230	220	170
$V_n \simeq \frac{1}{3} W_n$	240	160	75
$V_o = V_1 + V_n$	470	380	245
V_o (exp.)	555	435	250
$E_1 \simeq \frac{1}{30} W_1$	23	22	17
$E_2 \simeq \frac{1}{6} W_1$	115	110	85
$E_3 \simeq \frac{1}{3} W_1$	230	220	170
E_T	1570	813	267
T_c	80	35	19.7
c (Å)	10.037	10.34	10.875

Caption of table III

W_1 : *the energy difference between the principal maxima and minima due to intracluster interactions only.*

W_n : *the energy difference between the highest and lowest energy due to intercluster interactions only.*

$W = W_1 + W_n$: *similar to W_n, but due to both the inter and intracluster interactions.*

$V_1 \simeq \frac{1}{3} W_1$: *barrier opposing free rotation of the proton triangle (rotation by $2\pi/3$ about the threefold symmetry axis of the NH_3 molecule) for an isolated cluster.*

$V_n \simeq \frac{1}{3} W_n$: *similar to V_1, but due to intercluster interactions only.*

$V_o = V_1 + V_n$: *similar to V_1, but due to both intra and intercluster interactions.*

V_o (exp.) : *experimentally determined potential barrier height at low temperatures, i.e. $T < T_c$ (ref. 13).*

$E_1 \simeq \frac{1}{30} W_1$: potential barrier hindering the flipping between different minimum energy configurations of an isolated cluster. Although the eight low-energy arrangements of an isolated cluster are equivalent, it is found theoretically that the barriers hindering the flipping from a given configuration a to an arrangement b may be different from that to a configuration c. In total three barrier heights are found, namely E_1, E_2 and E_3.

E_T : potential barrier opposing tilting of the proton triangles out of the plane perpendicular to the metal-nitrogen bond. In other words, the barrier which opposes wagging (or rocking) of the NH_3 molecules; this is to be distinguished from V_o, which is the barrier opposing rotations about the metal-nitrogen bond. The values for the barrier heights, which are quoted in the table, are experimentally determined values from dielectric relaxation experiments [16].

In contrast to the barrier heights mentioned thus far, the E_T values for $T < T_c$ were found to be lower than those for $T > T_c$. In the table only the results obtained for $T < T_c$ are given.

The theoretical values were obtained using the following parameters:

a = the distance from the Ni ions to the plane of the hydrogen triangle = 2.5 Å.

r = the distance from a vertex of a proton triangle to its center of gravity = 1 Å.

p = the effective charge of the protons = 0.29e (Cl)
= 0.28e (Br)
= 0.25e (I)

The distance from the centers of neighbouring clusters is taken as half the unit cell dimension: $\frac{1}{2}c$ = 5.02 Å (Cl)
= 5.17 Å (Br)
= 5.44 Å (I)

T_c is the experimentally determined transition temperature.

body diagonal symmetry axes of the various clusters, i.e. parallel alignment. Thus the B-S model predicts a cooperative transition which is due to electrostatic interactions between neighbouring clusters. This seems to be in accord with the experimental findings of Aiello and Palma-Vittorelli [16] on frozen solutions, in which the average distance between two $(Ni(NH_3)_6)^{2+}$ clusters is about 25 Å (compared to about 7.5 Å in e.g. $Ni(NH_3)_6I_2$). Their experiments are characterized by the absence of a transition in the solution down to 15 K. These results suggest the necessity of intercluster interactions for the occurrence of a phase transition.

The transition entropy would, according to the B-S model, be determined by the number of configurations of a cluster above and below T_c. From their calculations Bates and Stevens find that above T_c any cluster can take each of the eight principal minimum configurations, whereas below T_c only one preferred configuration exists for each cluster, thus yielding an entropy change of Rln 8 per mole of $M(NH_3)_6X_2$.

The B-S model calculations predict the occurrence of potential barriers of electrostatic origin, throughout the whole crystal which oppose free rotations of the proton triangles. Some numerical results for the various barrier heights, calculated within the point-charge model are collected in table III, for $Ni(NH_3)_6I_2$, $Ni(NH_3)_6Br_2$ and $Ni(NH_3)_6Cl_2$, along with some experimental results. We use the notation introduced by Aiello and Palma-Vittorelli [16].

5.3 The specific heat of a hindered rotator. We shall consider the specific heat, associated with the rotation of the proton triangles hindered by potential barriers in the hexammine compounds. It may be assumed that the barrier has threefold symmetry. More precisely, among the Fourier components of the barrier potential, having 3n-fold symmetry, the component with threefold symmetry predominates. It is further assumed that the NH_3 molecule executes planar rotations, i.e. about the threefold symmetry axis of the molecule. In a classical model the rotations would be effectively frozen below the top of the barrier, while molecules with enough thermal energy to overcome the barrier would rotate freely. A quantum mechanical approach shows that it is possible for hindered rotations to take place even when the molecule has

insufficient energy to pass over the barrier. Quantum mechanical tunneling permits the molecule to tunnel through the barrier at a rate governed by the effective barrier height. The tunneling process is detectable because it removes the degeneracy of the singlet (A) and the doublet (E) levels. It is the very low temperature Schottky heat capacity, observed for several of the hexammine compounds [13)14)], which provides a measure of the barrier height V_o/k. The thermodynamic functions for a hindered rotator are compiled by Pitzer and Gwinn [23)]. These calculations have proved to be useful in the study of barriers in polyatomic molecules, by means of heat capacity measurements. An interesting property of the hexammine compounds in particular, is that the 'neutral' NH_3 ligands experience a low barrier to rotation. However, the low barrier in conjunction with the small classical moments of inertia of the NH_3 molecules put the hexammine compounds outside the range of applicability of the tables of Pitzer and Gwinn [23)].

The energy spectrum of hindered planar rotation of NH_3 and ND_3 molecules and the proper statistical weights of the energy levels are given in appendix I. From the energy level scheme the specific heat is then easily calculated. In fig. 4 we show the results for the specific heat of six NH_3 molecules as a function of temperature for various values of the barrier height. The low-temperature Schottky anomaly, shown for V_o/k = 100 K only, corresponds to the splitting of the lowest vibrational level which is due to proton tunneling. Calculations for a value V_o/k and a moment of inertia, which are both sufficiently large to provide overlap with the tables of Pitzer and Gwinn [23)], show a good mutual agreement. However, we note that the Pitzer and Gwinn calculations do not cover the tunneling heat capacities at low temperatures.

It is noteworthy that the low-temperature heat capacity results suggest that transitions between the A and E species of the hindered rotational states take place rapidly. This contrasts with, e.g., solid H_2 and CH_4 where ortho, para and in the latter also meta states require a separate treatment.

6. Evaluation of the transition entropy. 6.1 An analysis of the heat capacity. The naive estimate for the lattice heat capacity obtained by

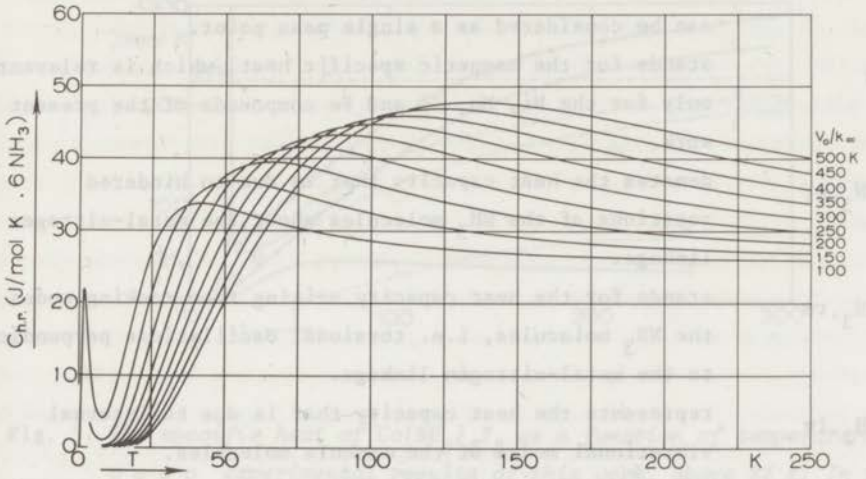

Fig. 4. *Calculated specific heats $C_{NH_3,hr}$ versus temperature for some selected values of the potential barrier height. The ordinate denotes the specific heat corresponding to six moles of NH_3.*

means of an interpolation between the 'normal' heat capacities above and below T_c is inadequate to describe the true behaviour. This follows from intercomparison of the normal heat capacities of the various isomorphous compounds. Consequently the transition entropy values are unreliable. A more careful analysis of the specific heat, taking into account the various contributions, is required. In the present case we assume that the lattice and the molecular rotational excitations may be considered as mutually independent. Under the assumption that the internal vibrations of the ammonia molecules are also independent, the heat capacity of e.g. $Ni(NH_3)_6I_2$, in the extended remperature range can be written as

$$C_p = C_{lv} + C_M + C_{NH_3,hr} + C_{NH_3,rm} + C_{NH_3,im} + C_{tr} , \qquad (1)$$

where

C_{lv} denotes the heat capacity that is due to the lattice vibrations, under the assumption that the NH_3 molecule can be considered as a single mass point.

C_M stands for the magnetic specific heat, which is relevant only for the Ni, Mn, Co and Fe compounds of the present work.

$C_{NH_3,hr}$ denotes the heat capacity that is due to hindered rotations of the NH_3 molecules about the metal-nitrogen linkage.

$C_{NH_3,rm}$ stands for the heat capacity arising from rocking modes of the NH_3 molecules, i.e. torsional oscillations perpendicular to the metal-nitrogen linkage.

$C_{NH_3,im}$ represents the heat capacity that is due to internal vibrational modes of the ammonia molecules.

C_{tr} the specific heat in the region of the transition point which is attributable to collective ordering phenomena.

In this section we shall treat the decomposition of the heat capacity into the various contributions.

For an elaborate analysis of the heat capacities of the metal(II)-hexammine iodides we have chosen $Co(NH_3)_6I_2$ as a representative. The reason for this choice is mainly that for this compound high-temperature ($T > 100$ K) specific heat data are reported in the literature. Fig. 5 illustrates the temperature dependence of the specific heat of $Co(NH_3)_6I_2$ in the 4 to 300 K region. The points below 80 K are from this research, whereas those between 100 and 300 K were reported by Ziegler [2]. The two sets of data fit smoothly as may be seen from the figure. Above the sharp peak at 20.9 K the specific heat increases with increasing temperature to reach the large value of 300 J/mol K at room temperature.

From heat capacity measurements at very low temperatures, $T < 1$ K, Van Kempen *et al.* [13] found no evidence for a magnetic phase transition of the Co(II) spin system. From their results one would conclude magnetic ordering to occur either below 0.1 K or above 1 K. Our results indicate magnetic ordering between 1.3 and 4.2 K, although we could not determine an accurate transition temperature because of the poor quality of the

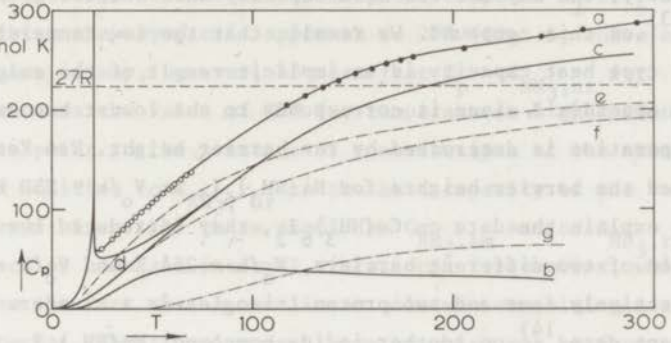

Fig. 5. *The specific heat of $Co(NH_3)_6I_2$ as a function of temperature.*
o o o o experimental results of this work, above 25 K. In the temperature range below 25 K the full line (a) represents the experimental data.
. . . . results reported by Ziegler [2].
——— b calculated specific heat $C_{NH_3,hr}$ (see fig. 4). The hindered-planar rotation with a potential barrier of 250 K.
——— c difference curve of a and b
——— d estimated lattice heat capacity in the temperature region below 70 K.
-.-.- e specific heat of K_2PtCl_6 according to Coulter et al. [27].
-.-.- f specific heat of K_2PtCl_6 scaled by a factor 1.36 according to the corresponding states principle.
-.-.- g difference curve of c, d and f (see text).

low-temperature data. Nevertheless, in the temperature region actually measured, from which the non-magnetic entropy is to be determined, we may assume that C_M is small compared to C_{tr}.

In order to calculate the contribution of the proton triangle hindered rotation to the specific heat, we have to know the height of the barrier against rotation. For $Co(NH_3)_6I_2$ we made use of the

barrier height V_o/k = 250 K which is a mean value of various experimental results.

Firstly, one may use the heat capacity data below 1 K of Van Kempen *et al.* [13] on this compound. We recall that the low temperature Schottky type heat capacity is an implicit result of the calculations given in Appendix I, since it corresponds to the lowest two energy levels whose separation is determined by the barrier height. Van Kempen *et al.* determined the barrier heights for $Ni(NH_3)_6I_2$ as $V_o/k \simeq 250$ K; in order to explain the data on $Co(NH_3)_6I_2$, they introduced the *ad hoc* assumption of two different barriers, V_o/k = 254 K and V_o/k = 167 K for respectively four and two proton triangles in a cluster. However, more recent data [14] on another iodide compound, $Mn(NH_3)_6I_2$, could be fitted again with only a single potential barrier of V_o/k = 250 K.

Secondly, from inelastic incoherent neutron scattering experiments on $Co(NH_3)_6I_2$ Jacob *et al.* [24] determined a value of 266 K for V_o/k, whereas Janik *et al.* [25] found V_o/k = 236 K from similar experiments.

Thirdly, from infrared spectroscopic methods Janik *et al.* [26] deduced that V_o/k = 326 K.

Although the results obtained by the various methods seem in reasonable agreement, they should be treated as estimates because in each of these methods to determine the barrier height somewhat arbitrary assumptions have been made. Therefore, we have assigned equal weights to these various results and take a mean value V_o/k = 250 K for the calculation of $C_{NH_3,\,hr}$.

The specific heat curve for the hexammine compound assuming planar rotations of the NH_3 groups and a hindering potential barrier height of 250 K, is shown in fig. 5 (curve b). The curve c, which remains after subtraction of $C_{NH_3,hr}$ from C_p is also shown in the figure, except for $T < T_c$.

If we assume that the rotational degree of freedom of the ammonia molecules is that for a hindered rotation about the Co-N linkage and if we further neglect contributions from the internal vibrational modes of the ammonia molecule to the specific heat, the above mentioned curve should reach an asymptotic value of 27R at high temperatures (R = gas constant). This prediction relies on the number of vibrational modes of the lattice constituents, each contributing a maximum of R to

the heat capacity. This amounts to 27 for $Co(NH_3)_6I_2$, since a molecule consisting of r atomic groups has 3r vibrational modes. As an example, the specific heat of the isomorphous compound K_2PtCl_6 [27] clearly exhibits the asymptotic approach to 27R (fig. 5, curve e). From the figure it may, however, be seen that $C_p - C_{NH_3,hr}$ for $Co(NH_3)_6I_2$ exceeds the value of 27R for temperatures higher than 160 K. These results point to the presence of contributions of the ammonia molecules in addition to $C_{NH_3,hr}$ to the heat capacity of the Co compound. In terms of eq. (1) these should be $C_{NH_3,im}$ and/or $C_{NH_3,rm}$. The ammonia molecules have six internal vibrational frequencies, which follows from the fact that a non-linear molecule containing n atoms has 3n-6 internal vibrational modes, some of which may be degenerate. For the free ammonia molecule these frequencies are accurately known [28] and are of the order of magnitude 1000 - 3000 cm^{-1}. In the solid, e.g. $Co(NH_3)_6Cl_2$ it was found that these frequencies are approximately the same as for the gaseous molecule, although the NH_3 symmetric deformation mode has a frequency shift of about 200 cm^{-1}. The internal vibrational modes thus will give rise to an appreciable contribution to the heat capacity only at relatively high temperatures. This means that a large portion of the heat capacity indicated by curve g may be due to rocking modes of the ammonia molecule. These modes give rise to a tilting of the protons out of the plane perpendicular to the Co-N linkage.

In view of the approximate character of the results we shall, however, not discuss curve g in detail. The main significance of the analysis of the specific heat of $Co(NH_3)_6I_2$ in terms of the various contributions is a) that the high-temperature (T > 100 K) results can be explained qualitatively and b) that the decomposition of the experimental curve allows one to determine the transition entropy with reasonable accuracy.

At temperatures sufficiently far above T_c, e.g. $T > 3\ T_c$, the transition specific heat is negligible as compared to C_p. A smooth extrapolation to T = 0 K of the high-temperature part of curve c, in line with the usually observed curvature of the lattice heat capacity curve of a solid, is then likely to be represented by curve d. We notice that this estimate for the lattice heat capacity compares favourably with the heat capacity of $Ni(NH_3)_6Cl_2$ [30] (see also section 7.3)

in the 20 to 80 K temperature range, which puts our estimate on a sounder basis. Application of the corresponding states principle [31] to the lattice heat capacities of K_2PtCl_6 and $Co(NH_3)_6I_2$ at temperatures lower than 40 K yields for the ratio $r(K_2PtCl_6)/r(Co(NH_3)_6I_2)$ the value of 1.36, by means of which the lattice heat capacity of the Co compound (curve f) has been determined.

The heat capacity associated with the phase transition of non-magnetic origin is now obtained by subtraction of the curve d from curve c. Numerical integration of the C_{tr}/T data with respect to temperature yields the transition entropy of 42 $\pm$ 5 J/mol K. This value is much larger than the value of 10.5 J/mol K found for ΔS_n (see table II). These values for the transition entropy strongly indicate the dependence of the numerical results on the way of analysing the data. The large spread in the transition entropy values is an unavoidable result of the lack of sufficient information about the numerous parameters which have to be known to derive the lattice heat capacity of the hexammine compounds. The ΔS_n value is certainly a lower limit from the experimental results. On the other hand, the approach as applied in this section will yield the maximum transition entropy obtainable from the experimental results.

6.2 Comparison between theory and experiment. In this section possible mechanisms that lead to a λ-point in the specific heat will be outlined. The observed transition entropy will be compared with that of order-disorder transitions and of molecular orientational transitions. A celebrated example of the order-disorder type transition is found in NH_4Cl [19], where the NH_4-tetrahedra are disordered between two equilibrium orientations above T_c. The observed transition entropy is close to the expected value of Rln 2. As regards the molecular ordering transition we may refer to solid hydrogen and methane.

6.2.1 Order-disorder transition. The symmetry of the proton triangles does not fit the cubic crystal symmetry, which has a fourfold axis as far as the halogen atoms adjacent to the ammonia group are considered. Under the assumption that there are intermolecular potential barriers, arising from the halogen atoms, which oppose the molecular motions of the proton triangles, it is plausible that a low-energy configuration of the proton triangle is obtained when a vertex points to a neighbouring

halogen atom. Presumably, in the disordered state, having higher energy, each proton triangle would rapidly switch between the four orientations in the lattice by rotation through 90^{o} in the plane of the triangle.

In general the disorder entropy will be Rln p, where p is the number of distinguishable arrangements of the molecule in the lattice. If there were complete randomnization with respect to the four orientations, the disorder entropy would be 6R ln4 per mole of $Co(NH_3)_6I_2$. This situation would occur if the proton triangles were independent above T_c and if they exert a barrier to rotation which is small compared to the energy difference between the ordered and the disordered state. The observed transition entropy, however, is found to be only 42 J/mol K. This excludes the possibility of complete randomnization.

The latter statement is consistent with the B-S model in which it is supposed that above T_c the proton triangles of a cluster are correlated. In the B-S model hydrogen bonding effects have been ignored, since the interactions were treated on the basis of classical electrostatic interactions. In this case it is found that for a single cluster eight equivalent low-energy arrangements exist. Further, because of these intracluster interactions, the barrier to rotation for a single triangle of protons has predominantly threefold symmetry. Flipping from one low-energy arrangement to another one can occur through (over) barriers that are essentially lower than the barrier for a single proton triangle to rotate. The transition entropy according to the approach of Bates and Stevens [8] should amount to Rln 8, because each cluster can take up eight low-energy configurations above T_c of which one is preferred below T_c, which is due to the intercluster interactions. Above T_c, it will of course depend on the height of the potential barriers between the low-energy configurations and on the intercluster interaction whether some entropy is already 'frozen in'. This would give rise to the transition entropy being lower than Rln 8. The observed value, however, is not consistent with this model because the experiments give a value much larger than Rln 8. The discrepancy can only be partly removed by including 'sub-minimum' energy configurations, which have been ignored thus far. Hence, each cluster would be allowed to have sixteen low-energy configurations above the lambda point. The transition entropy would then be Rln 16 per mole of $Co(NH_3)_6I_2$; this is also

appreciably lower than the observed value.

As an intermezzo we shall discuss the magnetic entropy in $Co(NH_3)_6I_2$. As concerns the transition entropy in the Co compound we notice an additional complication which arises from the action of the crystal field on the Co^{2+} ions. Thus far we assumed that magnetic ordering takes place at low temperatures, i.e. $T < 4.2$ K, between ions having spin $\frac{3}{2}$, the true spin of the divalent cobalt ion. For the case of cubic symmetry ($T > T_c$) the ground state of the Co ion would be fourfold degenerate. Below T_c the lowering of the symmetry gives rise to a removal of the degeneracy into two Kramers degenerate doublets of which the energy separation may be quite large compared to kT_c. Upon cooling the compound to T_c the magnetic entropy decrease is small because of the cubic field above T_c, whereas if the stationary trigonal field would persist above T_c this decrease would be much larger, to a maximum of kln 2 per Co ion. In the absence of reported data concerning the crystal-field splitting in $Co(NH_3)_6I_2$ these arguments, of course, remain qualitative. Recent Mössbauer experiments on ^{57}Fe in various hexammine compounds, however, show clearly that at T_c the cubic crystal field symmetry vanishes [32)33)].

We conclude from the previous paragraph that the entropy of magnetic origin is not sufficient to explain the difference between the observed and the theoretically predicted transition entropy according to the B-S model. This assertion is based on the analysis of the heat capacity of some diamagnetic hexammine iodides, performed in a manner similar to the one described for the Co compound, and yielding transition entropies which are also larger than Rln 16. We further note that for $Ni(NH_3)_6Cl_2$, a compound studied by various workers [30)34)35)], transition entropies were found that lie in the range between 28.6 and 35.1 J/mol K. The so-called normal heat capacity can be estimated rather reliably in this case, thus making the analysis less arbitrary. Since in the B-S model the number of low-energy configurations for a single cluster does not depend on the particular halogen atom, the transition entropy should be equal for the various compounds. Although the results for the hexammine compounds studied by heat capacity measurements exhibit a considerable scatter, the transition entropies definitely do not fit the theoretical predictions

of this particular model.

Naturally the determination of the normal heat capacity is subject to discussion. For instance, the phase transition from cubic to trigonal symmetry of the crystal field may affect the vibrational spectrum of the crystal, thus making the validity of intercomparison of the lattice heat capacity of the hexammine salts and e.g. that of K_2PtCl_6 somewhat doubtful. Furthermore, the analysis was based on the simplifying assumption that there are no interactions between the vibrational modes of the lattice and the rotational modes of the ammonia molecules. This simplification is untenable in view of recent findings in Mössbauer effect measurements of ^{57}Fe in hexammine halides, which show that the recoilless fraction changes appreciably at T_c [33]. Apparently the lattice is softer above T_c than below, which can hardly be attributed to the protons alone, but more probably reflects the change in the vibrational modes of the crystal near the phase transition temperature. Similarly the heat conductivity [34] of $Ni(NH_3)_6Cl_2$ displays an anomaly at T_c. In the cubic phase the acoustical phonons are scattered by the NH_3 torsional oscillations resulting in a very much lower value of the thermal conductivity as compared to the ordered phase. These considerations would require some adjustments to the analysis of the heat capacity curve. Such readjustments in our opinion, would be insufficient to invalidate the conclusion that the observed entropy considerably exceeds the entropy yield according to the B-S model.

6.2.2 Molecular orientational ordering. In some simple molecular solids weak angular dependent molecular forces in combination with a large rotational constant ($\hbar^2/2I$) of the molecules give rise to transitions which can be explained as due to the ordering of the molecular orientations. Well-known examples are the solid methanes and hydrogen. These systems have been studied extensively theoretically. As to the predictions about the properties of the solid methanes, the classical molecular field approach by James and Keenan [36] has attracted most attention. In order to account for quantum effects this model has been extended by Yamamoto and Kataoka [37].

We shall, ignoring the previous discussions on other models, compare the character of the phase transition in the hexammine halides with

that in the mentioned molecular solids. The basic point is that at high temperatures one assumes that rapid molecular rotations prevent the establishment of a static , orientationally dependent, intermolecular potential. At lower temperatures, molecular reorientations supposedly occur less frequently and the orientational dependence of the intermolecular potential does not average to zero. Hence, in a self-consistent way, a static orientationally dependent contribution is established in passing T_c from above. This would be responsible for a discontinuity in the specific heat. By analogy, considering the hexammine halides the planar rotations of the NH_3 groups and their mutual interactions, one may tentatively assume zero hindering potential above T_c and the establishment of a hindering barrier below T_c. The preferred orientation of proton triangles under the influence of this barrier, selfconsistently, contributes to the potential formation.

In this model the entropy above T_c is that of the free planar rotator, whereas the entropy below T_c corresponds to the hindered rotation. With respect to the change of the height of the barrier in passing through T_c we may distinguish several possibilities. We shall, however, tentatively assume that the change from a low barrier above T_c to a high barrier below T_c is discontinuous at T_c. Since we are mainly interested in the entropy change associated with the phase transition this is a reasonable approximation to which further refinements can be applied at a later stage. We may refer to the theories of Landau [38], Cochran [39] and Devonshire [40] for further considerations on the character of phase transitions in which the crystal symmetry is lowered at T_c.

In this approach to the mechanism of the occurrence of a λ-point some of the earlier made assumptions with respect to the heat capacity have to be revised. For example, the contribution to the heat capacity arising from the proton triangle rotations will be different above and below T_c.

In order to arrive at an estimate of the transition entropies for the various compounds the specific heat of K_2PtCl_6, scaled according to the corresponding states principle [31], was used. The scaling factor of the K_2PtCl_6 lattice heat capacity was obtained under the assumption that the specific heat slightly above T_c can be represented as the sum

of the lattice heat capacity and a contribution due to free planar rotations of the ammonia molecules. For most of the compounds the scaling factor was found to be smaller than 1.1. The transition entropy is then obtained by numerical integration of the excess specific heat, divided by T, with respect to temperature. In table IV the transition entropies ΔS for the various compounds are tabulated. Concerning the low-temperature anomalies in the specific heat we notice that the specific heat curves were extrapolated smoothly from about T = 10 K to T = 0 K, thus ignoring the tunneling splitting contributions to the specific heat observed for some of these compounds. Further, magnetic entropy contributions can be included in the transition entropy determined in this way. However, we expect this to be of importance only in case of $Co(NH_3)_6I_2$ (vide supra) and $Fe(NH_3)_6I_2$ (section 7.1).

TABLE IV

Experimental results from the heat capacity measurements and calculated values for the transition entropy, assuming free planar rotations for $T > T_c$ and hindered rotations when the temperature is lower than T_c.

	T_c K	$-\Delta E$ J/mol	ΔS J/mol K	S(0-250) J/mol K	S(0-∞) J/mol K
$Ni(NH_3)_6I_2$	19.7	360[a]	19.8[a]	14	15
$Co(NH_3)_6I_2$	20.9	320[a]	23.5[a]	15	17
$Mn(NH_3)_6I_2$	25.0	450[a]	21.8[a]	18.5	22
$Zn(NH_3)_6I_2$	25.44	500[a]	22.8[a]	19	22.5
$Cd(NH_3)_6I_2$	32.6	1100[b]	39[b]	22.5	30
$Fe(NH_3)_6I_2$	40.6	1150[b]	53[b]	23	35.5
$Ca(NH_3)_6I_2$	51.8	1750[b]	43[b]	21	42

[a] The low-temperature barrier height V_o/k is assumed to be 250 K.

[b] V_o/k = 500 K.

The torsional oscillation and rotation energy levels for NH_3 molecules, restricted to planar rotations, are shown (on scale) in fig. 6 for various barrier heights. With increasing barrier heights the tunneling

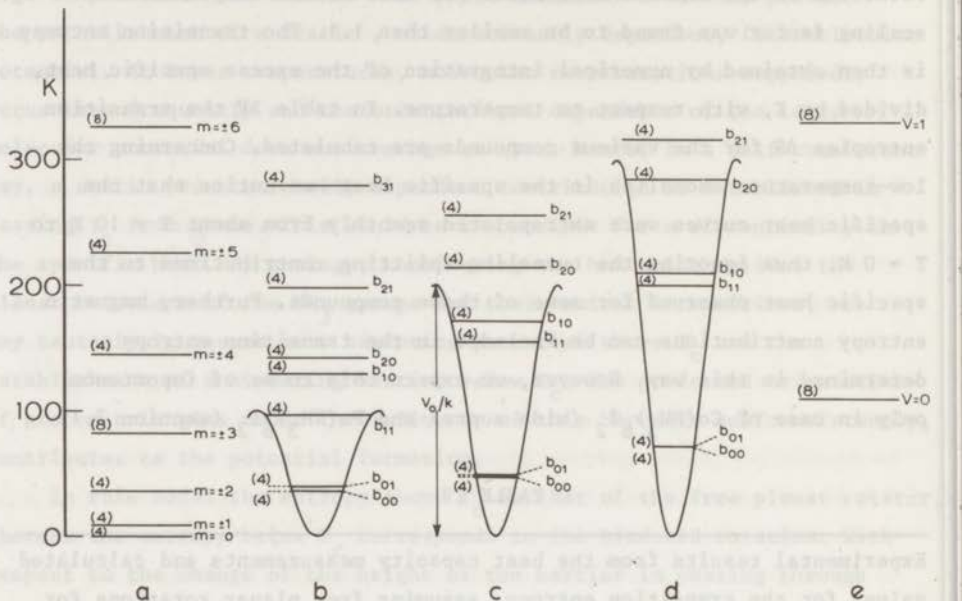

Fig. 6. *Energy level scheme for planar rotational motions of NH_3 molecules in a threefold potential barrier V_o/k. Free planar rotations with $E_m = m^2\hbar/2I$ in which m is the rotational quantum number (a); V_o/k = 100 K (b); V_o/k = 200 K (c); V_o/k = 300 K (d); infinite high barrier (e). The expression for the vibrational energy of a molecule in an infinite high potential well in the harmonic oscillator approximation corresponding to a barrier height V_o/k, is given by $E_\nu = (\nu + \frac{1}{2})\, n\hbar\sqrt{V_o/I}$, in which ν is the vibrational quantum number (ν = 0, 1, 2 ...) n is the symmetry number of the potential barrier ($V = \frac{1}{2} V_o (1 + \cos n\phi)$), h is Planck's constant, I is the classical moment of inertia and V_o/k is the barrier height. For NH_3 $\hbar^2/2Ik$ = 9.1 K, as derived from spectroscopic measurements. Between brackets the statistical weights of the energy levels are given.*

splitting between the two lowest levels decreases and the zero-point energy increases. From this figure it is clear that a change in the barrier height affects not only the position of the energy levels, but also the distance between the subsequent energy levels. Hence, the entropy of the hindered rotator will be strongly dependent on the height of the barrier. The entropy (for six moles of NH_3) as a function of temperature for the planar NH_3 molecular rotations, hindered by threefold potential barriers of various heights is depicted in fig. 7. Above 10 K the largest entropy content is found for the free rotator and S is decreasing when the barrier height increases. Quantum mechanical tunneling through the barriers clearly affects the entropy at low temperatures. The smaller tunneling splitting when the barrier height increases gives rise to a large entropy content (Rln 2 per mole of NH_3) even at very low temperatures. The crossing of the entropy curves at about 10 K results from the small splittings between the two lowest energy levels, whereas the next higher levels are far apart.

The numerical values for the transition entropy (under the conditions mentioned before) derived from, e.g., fig. 7 are given in the

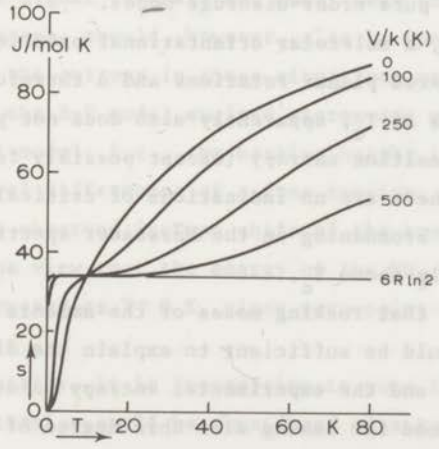

Fig. 7. *The rotational entropy as a function of temperature for a hindered planar rotator (proton triangle) for several values of the threefold potential hindering barrier. The drawn curves represent the entropy for six moles of ammonia.*

fourth column of table IV for barrier changes from 0 to 250 K, while the last column contains the entropy corresponding to a change from 0 to a very high barrier. For all the compounds the observed transition entropy is larger than the calculated values; the discrepancies are of the order of 6 to 10 J/mol K, except for the Co and Fe compounds. However, as we noticed before, in case of these salts the experimental transition entropy contains also (part of) the magnetic entropy. When one subtracts from the observed entropy values the estimated magnetic entropy, i.e. Rln 2 and Rln 5 for the Co and Fe compound respectively, the discrepancies of these two compounds are comparable to that of the others.

6.3 Discussion. For an order-disorder process and for the B-S model one would expect the transition entropy to be independent of the kind of metal and/or halogen atoms (and also of the isotopes). However, according to the present work and that of other experimentalists, it appears that the higher the transition temperature, the larger is the transition entropy. Further, the specific heats of the iodine and the chlorine compounds show marked differences (see section 7.3). This casts some doubt not only on the universality of the B-S model, but also on the applicability of a pure order-disorder model.

On the other hand, a molecular orientational ordering model with the assumption of hindered planar rotations and a threefold barrier whose magnitude changes at T_c, apparently also does not yield the required amount of transition entropy (except possibly for the chlorine compound). Moreover, there are no indications of critical slowing down phenomena such as line broadening in the Mössbauer spectra and the E.S.R. lines immediately above T_c.

It is conceivable that rocking modes of the ammonia molecules, if taken into account, would be sufficient to explain the discrepancy between the calculated and the experimental entropy values. The following arguments may be advanced for taking also this degree of freedom into account. Infrared absorption measurements have revealed low-lying infrared active Raman modes, which are interpreted as NH_3 rocking modes. A coupling between the rotational and rocking modes in the crystal is plausible (mode-mode coupling); such a coupling could result in a static tilting of the NH_3 triangles out of the [100] etc.-planes below

T_c. This might explain: a) the occurrence of a sharp change of the dielectric constant at T_c, b) the strong change of the Mössbauer fraction at T_c, corresponding to a change of the vibrational spectrum of the lattice and the metal ion in particular, c) the change in the heat conductivity at T_c, which is attributed to a static lattice deformation, including tilting of the NH_3 groups. It should be recalled that the light protons by themselves are thought to contribute relatively little to the acoustic phonon scattering. d) Since elastic energy of the lattice is involved, a first order character may be introduced into the phase transition; this is supported by the Mössbauer measurements and to some extent by the specific heat data and could explain the absence of critical slowing-down phenomena.

The above explanation, therefore, is a combination of a rotational molecular ordering (stopping of planar rotations) and a displacive structural phase transition (tilting of the NH_3 molecules). It does not provide, however, quantitative predictions concerning the entropy gain.

Estimates for the transition entropy were given earlier on the basis of either the order-disorder model or the molecular rotational model, which represent two extreme cases of the barrier above T_c, namely a barrier much higher than kT_c and much lower than kT_c, respectively. Intermediate cases, should, however, also be considered. Qualitative estimates for the entropy in these situations may be appreciably more difficult. In the B-S model excited states are not discussed, since it is a classical model, i.e., the barrier height is large compared to the energy level differences of a free rotator. As we shall discuss in section 8, the observed isotope shift of the transition temperature does not support the view that the energy of the NH_3 molecules consists only of potential energy as $T \to 0$ K, since zero-point motions cannot be neglected.

Experimentally, it is interesting to note that the observed transition entropies could be considered as a sum of an order-disorder entropy of Rln 8 per cluster (as in the B-S model) and a rotational entropy decrease at T_c due to a discontinuous change in barrier height. For instance, for $Ni(NH_3)_6I_2$ a barrier of about 100 - 120 K in the disordered state ($T > T_c$) would agree with the experimental transition entropy. In the same fashion we arrive at a barrier height of 100 K for

the manganese compound at $T > T_c$. These values should be compared to the low-temperature barrier height $V_o/k = 250$ K [13)14)]. The larger values for the transition entropy with the Cd and Ca compounds suggest high barrier heights at low temperatures.

On the basis of the model in which the barrier height changes at T_c, one should expect measurable differences for V_o/k determined above and below T_c. As we mentioned before the magnitude of the barrier height in $Co(NH_3)_6I_2$ was determined by means of a number of different methods. However, none of these techniques was applied above as well as below T_c. For instance, the very low temperature thermal measurements of the tunneling splittings apply to $T < T_c$ and, unfortunatèly, the differences between the specific heats of a planar hindered rotator for $T > T_c$ and barriers that lie in the range 0 to 250 K, are quite small in comparison with the lattice contributions. The inelastic incoherent neutron scattering experiments [25)] were performed with the sample at 113 K, while the infrared absorption measurements [26)] were made in the temperature range between 135 and 300 K. The latter two investigations thus apply to $T > T_c$. Nevertheless, the results for the barrier height are of comparable magnitude or even larger than those of the calorimetric experiment. As we noticed before, the assumptions made to determine V_o/k are somewhat arbitrary in these experiments. The resolution of the phonon density plots [24)25)] does not exclude a fit with quite different values for V_o/k. For instance, a frequency distribution corresponding to $V_o/k = 100$ K apparently would also fit the plot for $Co(NH_3)_6I_2$ [25)] and the peak observed at 43 cm^{-1} could be assigned to NH_3 torsional oscillation in this case. With respect to the infrared measurements it was already noted by Janik *et al.* [26)] that the assumption made for the curvature of the wings of the absorption bands can give rise to results that may differ by even a factor of 2 from the true height. Since neutron scattering experiments can yield information about V_o/k at any temperature, such experiments, performed as well above as below T_c, might clarify how the barrier height varies as a function of temperature, while measurements on deuterated samples can yield additional information.

7. Further properties of the hexammine compounds. 7.1 Heat capacity results on $M(NH_3)_6I_2$. In addition to the $Co(NH_3)_6I_2$ compound a number of other salts of the series of metal hexammine iodides was studied by thermal methods. The heights of the barriers hindering the rotation of the proton triangles were reported only for a relatively small number of salts of this series and, when available, are restricted to the low-temperature region, i.e. for $T < T_c$. In fact heat capacity measurements on $Ni(NH_3)_6I_2$ [13] and $Mn(NH_3)_6I_2$ [14] at very low temperatures provide values of 250 K for V_o/k for both compounds. In fig. 8 we show the heat capacity of $Mn(NH_3)_6I_2$, over three decades of temperature,, which exhibits a rich variety of broad and sharp peaks. The data above 1 K are from this research, whereas those below 1 K were obtained by Suga *et al.* [14], also at the Kamerlingh Onnes Laboratory. From the figure it may be seen that the two sets of data fit perfectly. The anomalous heat capacity below 1 K has been interpreted as a superposition of a two level Schottky curve and a magnetic specific heat that is due to three dimensional ordering of the Mn^{2+} spins. From the Schottky curve the level splitting of the two lowest states of the torsional oscillation of the proton triangles has been determined. This splitting yields a measure of the barrier height V_o/k under the assumptions mentioned earlier.

The sharp peak at $T_c = 25.0$ K we attribute to a change of the motional states of the ammonia molecules in the crystal, which was discussed in section 6. Near 3.6 K the specific heat attains a minimum and is found to increase approximately as $T^{2.6}$ between 5 and 20 K. Thus it appears that in $Mn(NH_3)_6I_2$ hindered rotations play an important role in the heat capacity, especially below T_c. In view of the uncertainties unavoidably associated with the lattice specific heat estimates and the lack of reliable values for the barrier heights for $T > T_c$, we shall not report details of the analysis on the $Mn(NH_3)_6I_2$ specific heat. The same arguments hold for the other compounds for which the low-temperature barrier heights are not available in the literature, except for $Ni(NH_3)_6I_2$. But the large values for the specific heat at low temperatures strongly confirm the idea that hindered rotations of the ammonia molecules are present also in these compounds.

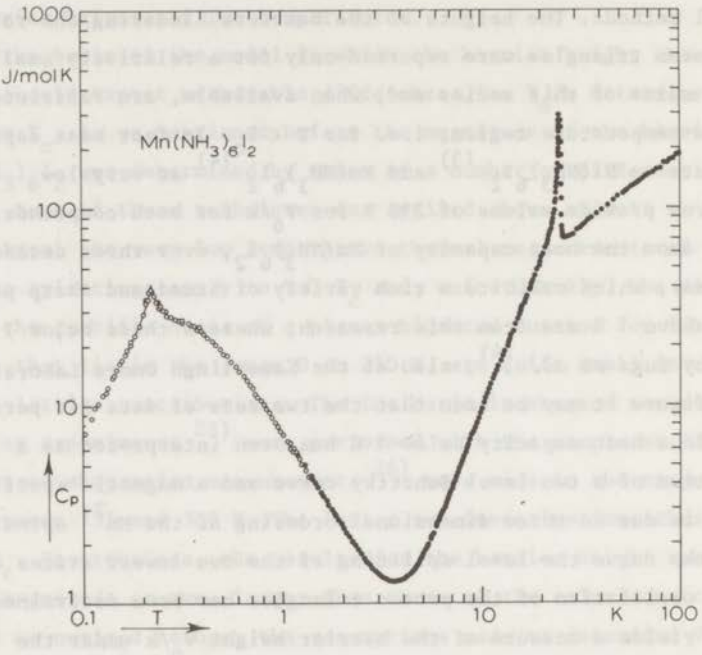

Fig. 8. *The specific heat of $Mn(NH_3)_6I_2$ over three decades of the temperature axis.*

. . . . *experimental results of this work.*

o o o o *results according to ref. 14.*

The heat capacity results on $Cd(NH_3)_6I_2$ and $Ca(NH_3)_6I_2$ can be used to estimate the barrier height for $T < T_c$, although we did not reach temperatures low enough to observe a Schottky type maximum. Since both compounds are diamagnetic the low-temperature contribution that varies proportional to T^{-2}, is likely to be due to the splitting of the lowest vibrational-rotational level of the proton triangle. Analysis of the experimental heat capacity in terms of contributions proportional to T^{-2} and T^3 give evidence for relatively high barriers, i.e. $V_o/k > 400$ K for both compounds, compared to those in the Ni and Mn salts.

Such an argument, concerning the separation of specific heat contributions, is not applicable to $Fe(NH_3)_6I_2$ (see fig. 9). Between T = 6 K and 15 K the measured heat capacity is much larger than that observed for the other hexammine compounds. Probably also the electron spin of the divalent Fe ion is involved in the low-temperature heat capacity. Because of the similarities among the hexammine compounds in structure and in thermal behaviour, we expect a distortion of the crystal field at the Fe ion to be present below T_c (= 40.6 K), in line with the results reported on the nickel hexammine halides (see also ref. 33). If we assume for simplicity spin-only magnetism S=2 for Fe(II), and an axial crystal field the single-ion hamiltonian

$$H = D\{S_z^2 - \frac{1}{3} S (S+1)\} \qquad (2)$$

should describe the zero-field splitting in $Fe(NH_3)_6I_2$. An axial field produces a splitting of the fivefold spin degenerate groundstate into a singlet and two doublets. A good fit to the experimental data is

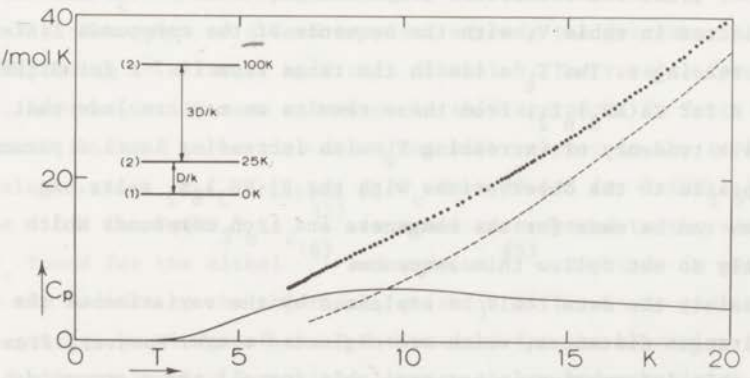

Fig. 9. *The low temperature specific heat of $Fe(NH_3)_6I_2$ as a function of temperature.*

. . . . *experimental results.*

– – – – *estimated non-magnetic specific heat.*

——— *Schottky curve corresponding to the single-ion energy level scheme drawn in the left upper corner of the figure; D/k = 25 K.*

obtained only with D/k positive i.e. a singlet as groundstate. In fig. 9 we show the low-temperature heat capacity results on $Fe(NH_3)_6I_2$ together with a Schottky curve for D/k = 25 K (cf. eq. (2)), which proved to be a best fit value.

Usually the single-ion hamiltonian of eq. (2) is too simple an approximation of the zero-field splitting in divalent iron compounds. However, the limited temperature range in which data were obtained together with the uncertainties in the determination of the non-magnetic specific heat contributions (no values for V_o/k have been reported thus far) prevent a further analysis of the data.

7.2 The transition temperature. The value of the non-magnetic transition temperature of the $Ni(NH_3)_6I_2$ compounds (X = Cl, Br and I) is found to increase with decreasing magnitude of the unit cell dimensions. An eight per cent decrease of c gives an increase of T_c by a factor 4. This is in qualitative agreement with the B-S model which predicts a strong dependence of the value of T_c on the magnitude of the cell parameters and the inter-atomic distances.

For the hexammine iodides the cell parameters, as given by Wyckoff [10], and the transition temperatures, obtained in this work, are collected in table V, with the sequence of the compounds listed with increasing c. The T_c's lie in the range from 19.7 K for $Ni(NH_3)_6I_2$ to 51.8 K for $Ca(NH_3)_6I_2$. From these results we may conclude that there is a tendency of increasing T_c with increasing lattice parameter, thus opposite to the observations with the $Ni(NH_3)_6X_2$ salts. An exception can be made for the manganese and iron compounds which apparently do not follow this sequence.

Possibly the data could be explained by the variation of the metal-nitrogen distances, which are neglected above. However, from X-ray studies this information is not available for all these compounds. On the other hand, from the metal-nitrogen stretching modes $\nu(MN)$, determined by means of far infrared spectra of the metal hexammine complexes [41-43] we expect the metal to nitrogen distance to vary in the sequence Ni(II)-N < Co(II)-N < Fe(II)-N < Mn(II)-N < Zn(II)-N < Cd(II)-N. If we further take into account the ionic radii of the divalent metal ions, the increase of T_c with increasing magnitude of the cell dimensions for the iodide series, would be qualitatively explained.

TABLE V

The unit cell dimensions and transition temperatures of some hexammine iodides

	c	T_c	r(M(II))[a]	M-N str. (ref. 42)
	Å	K	Å	cm^{-1}
$Ni(NH_3)_6I_2$	10.875	19.7	0.70	322
$Co(NH_3)_6I_2$	10.914	20.9	0.74	312
$Zn(NH_3)_6I_2$	10.964	25.44	0.75	282
$Fe(NH_3)_6I_2$	10.965	40.6	0.78	306
$Mn(NH_3)_6I_2$	11.037	25.0	0.82	295
$Cd(NH_3)_6I_2$	11.046	32.6	0.95	277
$Ca(NH_3)_6I_2$	11.24	51.8	1.00	--

a) ref. 44

In fact the sequence of the cell dimensions over the various compounds is about equal to the sequence of the ionic radii. This explanation, however, requires that for instance for the Ni and Zn compound the increase in T_c with the lengthening of the M-N bond in, e.g. passing from a Ni-N complex to a Zn-N complex, exceeds the decrease in T_c corresponding to a larger unit cell dimension. The results for the iron salt, however, still seem anomalous in this approach. In fact, the iron compound is found to be also anomalous with respect to the replacement of halogen atoms. The variation in T_c from 40.6 K for $Fe(NH_3)_6I_2$ to about 110 K for $Fe(NH_3)_6Cl_2$ [32] is small as compared to the variation in T_c found for the nickel [16] and cadmium [45] compounds in passing from the iodides to the chlorides, which is difficult to explain. More precise knowledge of the M-N distances for the hexammine compounds would allow a further comparison between theory and experiment. Furthermore, the electrostatic energy calculations, disregarding dynamical effects and hydrogen bonding, may give misleading results.

7.3 Thermal hysteresis. Heat capacity measurements on $Zn(NH_3)_6I_2$ were performed with increasing as well as decreasing temperature, by means of the usual heat pulse method and the heat leak method, respectively. Within the measuring accuracy the two methods yield the same value for T_c. We found similar results for the other hexammine iodine com-

pounds. In these cases, however, the heat capacity was not measured purposely with decreasing temperature, but only cooling curves were recorded. Since the peaks in the heat capacity of these salts are very large and occur in a narrow temperature range, this method provides an accurate determination of the transition temperature. The general conclusion is that no measurable hysteresis effects were observed for the iodine compounds. These results contrast with those, reported by various workers using different techniques, on $Ni(NH_3)_6Cl_2$ [16)34)] in which thermal hysteresis effects up to 5 degrees were found. Similarly for $Fe(NH_3)_6Cl_2$ [32)] the transition temperature on heating was found to be about 6.5 degrees higher than on cooling the sample, with T_c = 110 K. Hysteresis effects were also reported for $Cd(NH_3)_6Cl_2$ [45)] but it is to be noted that the uncertainty in the temperature measurements was of the same order of magnitude in these experiments. On the other hand, our findings on the iodides are in accordance with those of Aiello *et al.* [16)] on $Ni(NH_3)_6Br_2$ and $Ni(NH_3)_6I_2$. These results point to a behaviour which is different for the Cl^- salts on the one hand and the I^- (and possibly the Br^-) salts on the other hand. In fact, marked differences were observed also in the heat capacities of these nickel salts. In fig. 10 we show the heat capacities of $Ni(NH_3)_6Cl_2$ and $Ni(NH_3)_6Br_2$ as measured by Matsuo *et al.* [30)]. Since the general features of the peak in $Ni(NH_3)_6I_2$ are very similar to those in $Ni(NH_3)_6Br_2$ we did not plot the data for the iodide compound in the figure for reasons of clarity. The sharp peak for the Cl^- sample is characterized by the absence of long- and short-range order specific heat tails; its shape is reminiscent of a delta-function. The sharp peak for the Br^- compound appears to display both long- and short-range order tails. Above approximately 90 K the two curves of fig. 10 are nearly equidistant. The larger C_p values for the Br^- salt are likely to be due to the larger and heavier Br ions with respect to the Cl ions. However, in the intermediate temperature range, i.e. $T_c(Br^-) < T < T_c(Cl^-)$, the differences between the two curves cannot be ascribed to the differences between the molecular weights of the compounds. We notice that the differences between the potential barrier heights, as determined by Van Kempen *et al.* [13)], and consequently the differences between the contributions of the hindered rotation of the proton triangles for the

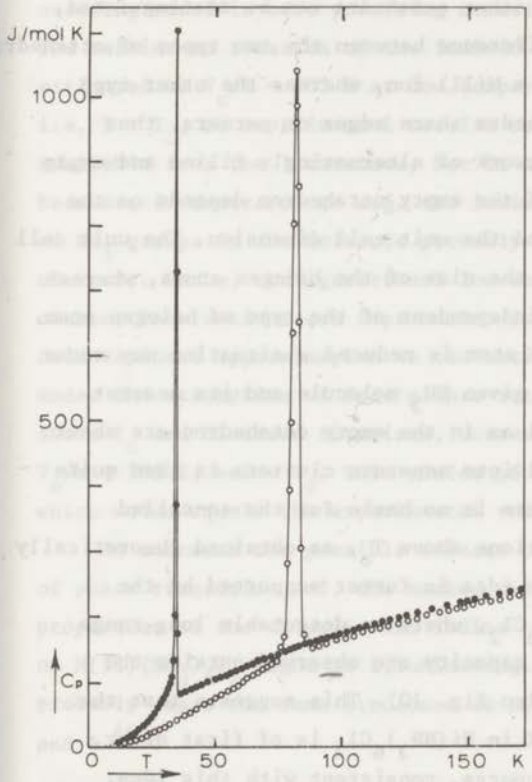

Fig. 10. *The specific heats of* $Ni(NH_3)_6Br_2$*(.) and* $Ni(NH_3)_6Cl_2$*(o) as a function of temperature, according to Matsuo et al.* [30]

two compounds cannot account quantitatively for the observed differences in the specific heats. Without going into details of the analysis we may conclude that the specific heat of $Ni(NH_3)_6Br_2$ as well as that of $Ni(NH_3)_6I_2$ exhibit considerable amounts of long-range order heat capacity whereas this is not observed in $Ni(NH_3)_6Cl_2$. The different thermal behaviour of $Ni(NH_3)_6I_2$ and $Ni(NH_3)_6Cl_2$ does not follow from the B-S model, which treats the intra-cluster and inter-cluster interactions on an unequal basis. The electrostatic point charge model calculations are in fact based on the assumption of the existence of clusters in which the interactions are large compared to the mutual interactions between clusters. A closer analysis of the crystal

structure of the hexammine halides, however, shows that in case NH_3 groups are exactly at the positions $\frac{1}{4}$, 0, 0; 0, $\frac{1}{4}$, 0; 0, 0, $\frac{1}{4}$; $\bar{\frac{1}{4}}$, 0, 0; 0, $\bar{\frac{1}{4}}$, 0; 0, 0, $\bar{\frac{1}{4}}$; also other octahedra can be distinguished, as indicated in fig. 11. The difference between the two types of octahedra is that one type is filled with a M(II) ion, whereas the other type is empty. The two types of octahedra share edges or corners, thus yielding a three-dimensional network of alternatingly filled and empty octahedra. Generally the size of the empty octahedron depends on the size of the filled octahedron and the unit cell dimension. The unit cell dimensions depend critically on the size of the halogen atoms, whereas the Ni-N bond length is rather independent of the type of halogen atom. Thus, if the size of the halogen atom is reduced a situation may occur in which the distance between a given NH_3 molecule and its nearest neighbours in the filled as well as in the empty octahedron are about equal. A division of the crystal into separate clusters is then quite artificial, which means that there is no basis for the so-called equivalent low-energy configurations above T_c, as obtained theoretically for an isolated cluster [8]. This idea is furter supported by the experimental results on $Ni(NH_3)_6Cl_2$, where no detectable long-range order contributions to the heat capacity are observed outside the narrow transition region (see also fig. 10). This suggests that the observed transition at $T_c \simeq 80$ K in $Ni(NH_3)_6Cl_2$ is of first order. The reported hysteresis is, of course, consistent with this idea.

It is interesting to compare the experimental transition entropy for $Ni(NH_3)_6Cl_2$ also with the predictions of the models mentioned in section 6. The B-S model, as a special case of the order-disorder transition yields too low a value as compared to the experimental value

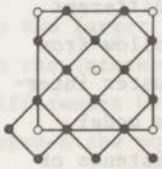

Fig. 11. *The z = 0 layer of the unit cell of $M(II)(NH_3)_6(Hal)_2$. The cross sections of full and empty octahedra formed by proton triangles (see text) are shown. This figure is to be compared with fig. 1b.*

of 32 ± 5 J/mol K, even if the number of equivalent low-energy configurations above T_c is taken as 16. The molecular orientational ordering model is more promising numerically in case of $Ni(NH_3)_6Cl_2$. The barrier to rotation of the individual proton triangles is estimated as V_o/k = 555 K at low temperatures [13]. At high temperatures, i.e. $T > T_c$, no experimental results concerning the barrier height are available from the literature, but it may be assumed that it is low because, in contrast to e.g. the iodine compounds, the arrangements of NH_3 groups in the molecule probably do not allow a separation into clusters. Hence, configurational low-energy arrangements due to intra-cluster interactions are improbable. In terms of the molecular orientational approximation we can estimate the transition entropy, e.g. under the assumption of free planar rotations of the proton triangles above T_c and hindered rotations, corresponding to a barrier height V_o/k = 555 K, below T_c. This yields ΔS = 32 J/mol K (see e.g. fig. 7), which value equals the experimental value within the uncertainty limits.

As concerns the possible effects of the halogen atoms on the type of phase transition, cf. the marked differences between the thermal properties of the chlorine and iodine hexammine compounds, experiments on $M(II)(NH_3)_6F_2$ might be illuminating. Some of these compounds probably have the same structure as $M(II)(NH_3)_6X_2$ where X = Cl, Br and I [46].

8. Deuterated and partly deuterated hexammine iodides. 8.1 Introduction. The result that the NH_3 groups play a predominant role in the phase transition of the hexammine halides leads to the question as to the influence of deuteration. We recall strong isotope effects on phase transitions in various other systems:

a) Order-disorder transitions. Taking the familiar example of potassium dihydrogen phosphate (KH_2PO_4), one finds an upward shift of T_c by a factor 1.9 upon deuteration [43]. It is usually assumed that the proton in KH_2PO_4 has two equivalent positions and that a preferential ordering in one position is favoured by the electric dipole energy. Proton tunneling would prevent the formation of the ordered state above T_c if the tunneling frequency (times $\hbar$) exceeds the dipole energy. Hence the smaller tunneling rate for the deuterium would be responsible for a

higher T_c, other factors being equal. Considered from a somewhat different viewpoint, the large isotope shift has been construed as evidence for a considerable proton-phonon coupling, since otherwise the ordering energy would remain the same upon deuteration and a shift in the ordering temperature would be difficult to explain. This is corroborated by the order-disorder transition in NH_4Cl. A phase transition in NH_4Cl occurs at 242 K (in ND_4Cl at 250 K) from a disordered, randomly distributed orientation of the ammonia molecules, to an ordered state. Neutron scattering and infrared studies have revealed that characteristic frequencies of vibrational and torsional modes of the NH_4 groups are considerably decreased upon deuteration. It is plausible that this frequency decrease with deuteration will also be found in most other compounds. This will result in a correspondingly higher entropy of the deuterated compound and, hence a steeper free energy versus temperature curve. Since presumably the ordered state is more strongly affected than the disordered state, an upward shift of T_c is to be expected.

b) Molecular solids, e.g. H_2 and CH_4. The transition points of D_2 and CD_4 are higher than those of the light isotopes [44]. Molecular interactions leading to an ordered state may not be the same for the light and heavy isotopes, but in addition the ground states of the molecules are considerably influenced by the statistics, which are different for the two isotopes. This makes a comparison less meaningful.

We performed heat capacity measurements on the paramagnetic $Ni(ND_3)_6I_2$ and on the diamagnetic $Zn(ND_3)_6I_2$ salts. In order to investigate the effect of hydrogen on the specific heat and on the phase transition of deuterated samples, we measured the heat capacity of a sample that contained about 50% deuterium and 50% hydrogen.

Powdered samples of $Ni(ND_3)_6I_2$ and $Ni(NH_3/ND_3)_6I_2$ were prepared according to the wet method [12]. The notation $Ni(NH_3/ND_3)_6I_2$ means that this compound contains equal amounts of deuterium and hydrogen. Infrared spectroscopic methods and standard chemical analysis were used to check the composition of the samples [49]. Anhydrous reagent-grade ZnI_2 was allowed to react with gaseous ND_3 in a specially constructed apparatus to obtain a white powdered sample of $Zn(ND_3)_6I_2$. The heat capacity measurements on both nickel compounds were performed using the method

of compression of the sample to obtain better internal thermal contact. This method could not be employed in case of $Zn(ND_3)_6I_2$ because of the relatively high dissociation pressure of the salt. Therefore, a small amount of helium gas was introduced in the capsule, which contained the loosely packed powdered sample, to improve the internal thermal contact.

8.2 Experimental results and discussion. In fig. 12 we show the results of the heat capacity measurements on $Ni(ND_3)_6I_2$ and $Ni(NH_3/ND_3)_6I_2$ in the temperature range between 1.3 and 80 K. For comparison we plotted the data obtained with $Ni(NH_3)_6I_2$ in the same figure. From the figure it may be seen that for each of the compounds a sharp peak is observed. The transition temperature is found to increase from 19.7 K for $Ni(NH_3)_6I_2$ to 26.5 K for $Ni(ND_3)_6I_2$. For the mixed sample $Ni(NH_3/ND_3)_6I_2$, T_c was found to lie between $T_c(H)$ and $T_c(D)$. The experimental results show that the increase of the moment of inertia upon deuteration is qualitatively observed. It may be remarked that the ratio of the transition temperatures $T_c(D)/T_c(H)$ amounts to 1.34, which value is close to $\sqrt{I_{ND_3}/I_{NH_3}} = \sqrt{2} = 1.41$.

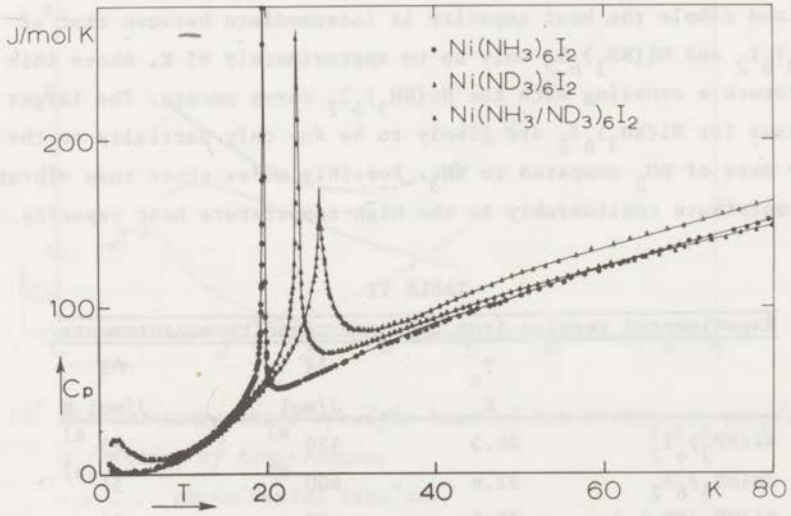

Fig. 12. *The specific heats of $Ni(NH_3)_6I_2$ (·), $Ni(NH_3/ND_3)_6I_2$ (▲) (see text for the notation) and $Ni(ND_3)_6I_2$ (Δ) as a function of temperature.*

The transition temperature T_c = 23.6 K observed for the mixed sample is slightly higher than the mean value of T_c(H) and T_c(D). The fact that the heat capacity of $Ni(NH_3/ND_3)_6I_2$ displays a sharp (single) peak is a strong indication of a cooperative character of the proton triangle motions in the mixed crystal, and hence in the hydrogenic and deuterated salt. As concerns the deuteration and the part deuteration of the iodide samples with respect to the transition temperature, the thermal results are very similar to those of E.S.R. experiments on $Ni(NH_3)_6Cl_2$, on the deuterated sample and on a sample containing equal amounts of hydrogen and deuterium [50].

From fig. 12 it may be seen that all three peaks are sharp with large C_p values. Although the low-temperature side of the anomalies have similar shapes, the high-temperature tails show marked differences with respect to the short-range order heat capacity that apparently increases with the amount of deuterium. Outside the transition region there is also a noticeable difference between the curvature of the high-temperature heat capacity curves. For the pure H and pure D samples these are found to be nearly equidistant, which result is comparable with that observed by replacing the metal ions. But for the mixed sample the heat capacity is intermediate between that of $Ni(NH_3)_6I_2$ and $Ni(ND_3)_6I_2$ only up to approximately 65 K. Above this temperature a crossing with the $Ni(NH_3)_6I_2$ curve occurs. The larger C_p values for $Ni(ND_3)_6I_2$ are likely to be due only partially to the larger mass of ND_3 compared to NH_3. Possibly modes other than vibrational ones contribute considerably to the high-temperature heat capacity.

TABLE VI

Experimental results from the heat capacity measurements

	T_c K	ΔE J/mol	ΔS J/mol K
$Ni(ND_3)_6I_2$	26.5	450 [a]	23 [a]
$Zn(ND_3)_6I_2$	32.6	600 [a]	31 [a]
$Ni(NH_3/ND_3)_6I_2$	23.6	~ 400	~ 21

a) The low-temperature barrier height V_o/k is assumed to be 250 K.

The most striking differences between the thermal results on these three nickel compounds are, however, observed in the low temperature region, i.e. $T < 5$ K. In fig. 13 we show the heat capacity of the $Ni(ND_3)_6I_2$ sample as a function of temperature for $1.3 < T < 8$ K. The heat capacity attains a distinct minimum at $T = 3.6$ K. Below 1.3 K a peak in the heat capacity appears, which has been observed in detail by Van Kempen *et al.* [13]. The origin of this peak lies in the antiferromagnetic ordering of the Ni^{2+} spins. Attempts to fit our data in the temperature range between 1.3 and 3 K assuming a T^3 term for the lattice and a T^{-2} term for the magnetic contribution to the heat capacity were, however, unsuccessful. We notice that our data do not extrapolate smoothly to the results of ref. 13, which were obtained below 1 K. These results point to an additional contribution to the heat capacity, which is probably to be related to the purity of the samples. Evidence for a qualitative explanation of the anomalously large

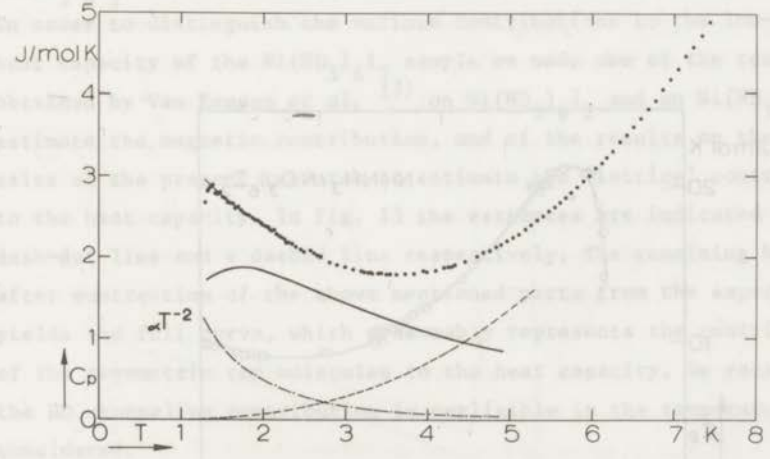

Fig. 13. *The low-temperature specific heat of the $Ni(ND_3)_6I_2$ sample as a function of temperature.*

. . . . *experimental results.*

– – – – *estimated 'lattice' heat capacity.*

–.–.–.– *estimated magnetic specific heat.*

——— *heat capacity which is ascribed to hindered rotation of asymmetric top molecules NHD_2 (see text).*

heat capacities observed on the $Ni(ND_3)_6I_2$ samples is obtained from the investigations on $Ni(NH_3/ND_3)_6I_2$, which will be discussed below.

In fig. 14 the low-temperature heat capacity of $Ni(NH_3/ND_3)_6I_2$ is shown as a function of temperature. The data for T < 5 K need some comment. The time required for attaining thermal equilibrium in the sample increased drastically when the temperature of the sample was decreased until below about 5 K. Since, however, an unexpected increase of the heat capacity was observed below this temperature it was measured in more detail, although between 1.3 and 3 K more than one hour was required to attain internal thermal equilibrium of the sample after the heat was supplied. Above 5 K this time was usually only of the order of one minute or less. The accuracy of the results is estimated to be fairly well represented by the scatter of the data points. Returning to fig. 14 we notice the large values of the specific heat of the broad peak, about 21 J/mol K at T = 2.2 K. Whether this anomaly is a superposition of two broad peaks or a single one cannot be decided because of the scatter in the data.

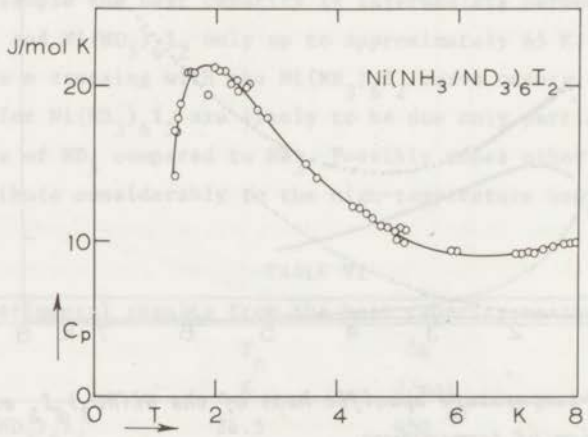

Fig. 14. *The low-temperature specific heat of* $Ni(NH_3/ND_3)_6I_2$ *as a function of temperature.*
o o o o experimental results.
The drawn line is for visual aid only.

From the large amount of entropy under this anomaly ($\Delta S = \int_{T=1.2}^{3K} C_p/T \, dT$ = 17.6 J/mol K), we conclude that the ammonia molecules are involved. We notice that there are four types of molecules, i.e. NH_3, NH_2D, NHD_2 and ND_3 in the statistical ratio 1:3:3:1, respectively. The greater part (6/8) of the molecules are, therefore, asymmetric top molecules [51], whereas NH_3 and ND_3 are symmetric tops. It is apparently the fact that NH_2D and NHD_2 are asymmetric tops that gives rise to the drastically different low-temperature behaviour of the specific heat of the mixed sample as compared to that of the pure H and D samples.

Rigorous calculations for hindered rotations of *asymmetric* top molecules are required to describe the observed phenomena in the heat capacity of $Ni(NH_3/ND_3)_6I_2$ in a quantitative way and to decide whether the broad peak is to be attributed to NH_2D or to NHD_2 or to both. One may be able to determine which molecules are involved by means of heat capacity measurements on deuterated samples that contain a known, small amount of hydrogen impurities and the reversed case. As regards the $Ni(ND_3)_6I_2$ sample, we are in fact dealing with the first mentioned case. In order to distinguish the various contributions to the low-temperature heat capacity of the $Ni(ND_3)_6I_2$ sample we made use of the results obtained by Van Kempen *et al.* [13] on $Ni(ND_3)_6I_2$ and on $Ni(NH_3)_6Br_2$ to estimate the magnetic contribution, and of the results on the iodide salts of the present research to estimate the 'lattice' contribution to the heat capacity. In fig. 13 the estimates are indicated by a dash-dot line and a dashed line respectively. The remaining heat capacity after subtraction of the above mentioned parts from the experimental data yields the full curve, which presumably represents the contribution of the asymmetric top molecules to the heat capacity. We recall that the ND_3-tunneling contribution is negligible in the temperature region considered.

An estimate of the amount of hydrogen impurities in the measured deuterated sample can be obtained if we assume that the broad peak of $Ni(NH_3/ND_3)_6I_2$ is due to NHD_2 molecules alone. From a comparison of the maxima of the heat capacity curves for $Ni(NH_3/ND_3)_6I_2$ and for this $Ni(ND_3)_6I_2$ sample we would arrive at the conclusion that the measured $Ni(ND_3)_6I_2$ sample contained 99 per cent D and 1 per cent H, which is plausible in view of the limited purity of the preparation components.

The heat capacity of $Zn(ND_3)_6I_2$ is found to show rather similar features as $Ni(ND_3)_6I_2$ when compared to the pure hydrogen compounds. In fig. 15 we show the results obtained on $Zn(ND_3)_6I_2$ and, for comparison, those on $Zn(NH_3)_6I_2$. The two peaks appear to be sharp and the shapes show close similarities both above and below T_c. The transition temperatures are found to be 25.44 K and 32.6 K for the hydrogenic and the deuterated compound, respectively. The ratio $T_c(D)/T_c(H)$ thus amounts to 1.28, which is close to the value found for the nickel iodide compounds. The isotope shift of the transition temperatures was also observed in other hexammine compounds, e.g. $Ni(NH_3)_6Cl_2$ [16] and $Ni(NH_3)_6Br_2$ [16]. The ratio $T_c(D)/T_c(H)$ decreases in the sequence I, Br, Cl, which is also the sequence of increasing transition temperatures. For $Zn(NH_3)_6I_2$ the ratio $T_c(D)/T_c(H)$ as well as the value of T_c lie inbetween those for $Ni(NH_3)_6Br_2$ and $Ni(NH_3)_6I_2$. Aiello and Palma-Vittorelli [16] suggest that a motional proton-lattice coupling is responsible for the decreasing ratio when T_c increases.

The high-temperature specific heat of $Zn(ND_3)_6I_2$ is found to be larger than that of $Zn(NH_3)_6I_2$ and is thus consistent with the results obtained for the nickel compounds.

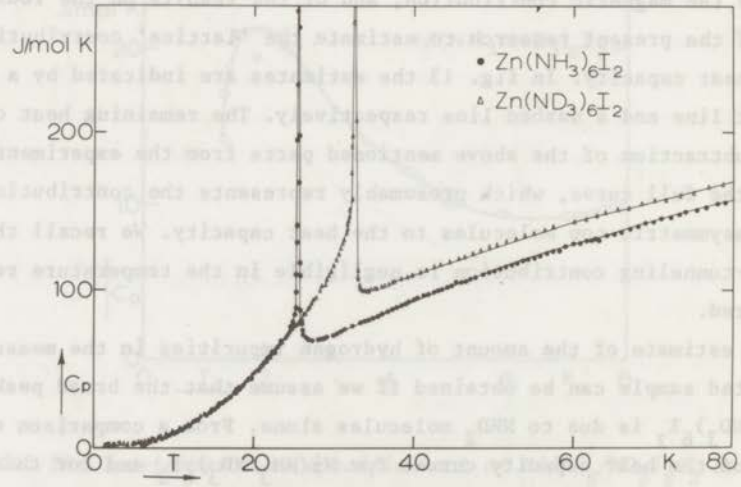

Fig. 15. *The specific heats of $Zn(NH_3)_6I_2$ (.) and $Zn(ND_3)_6I_2$ (Δ) as a function of temperature.*

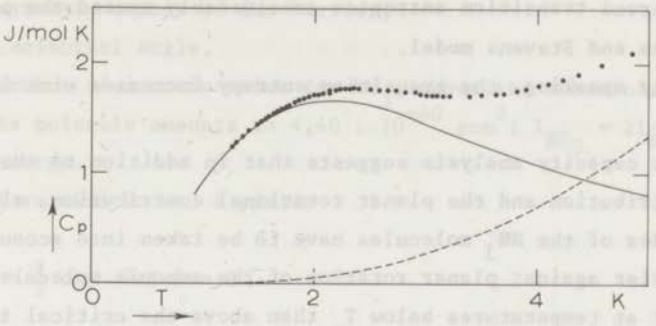

Fig. 16. *The low-temperature specific heat of the* $Zn(ND_3)_6I_2$ *sample as a function of temperature.*

. . . . *experimental results.*

– – – – *estimated 'lattice' heat capacity.*

——— *difference curve after subtraction of the 'lattice' heat capacity from the measured specific heat (see text).*

The low-temperature heat capacity results on $Zn(ND_3)_6I_2$ are shown in fig. 16. Since the Zn^{2+} ions are diamagnetic, a magnetic specific heat contribution does not occur. This is reflected in the specific heat near 1.3 K where C_p tends to decrease whereas with the paramagnet $Ni(ND_3)_6I_2$, C_p was found to increase. We attribute again the broad peak of fig. 16 to the presence of hydrogen impurities. Under the same assumptions as with $Ni(ND_3)_6I_2$ we calculate from the maximum C_p-value that in the measured $Zn(ND_3)_6I_2$ sample approximately one per cent of the deuterium atoms is replaced by hydrogen atoms.

9. Conclusions. The heat capacities of metal hexammine iodides, $M(II)(NH_3)_6I_2$, where M(II) may be a paramagnetic or a diamagnetic ion, were determined in the temperature range between 1.3 and 80 K. These compounds, which are isomorphous at room temperature, exhibit interesting features upon cooling to low temperatures, in particular since the motion of the ammonia molecules is involved. From the heat capacity results the following conclusions can be drawn:

1) All hexammine compounds studied show sharp phase transitions, which are associated with the cooperative freezing of the motions of the NH_3 molecules.

2) The observed transition entropies considerably exceed the prediction of the Bates and Stevens model.

3) Generally speaking, the transition entropy increases with increasing T_c.

4) The heat capacity analysis suggests that in addition to the lattice phonon contribution and the planar rotational contribution, also rocking modes of the NH_3 molecules have to be taken into account.

5) The barrier against planar rotation of the ammonia molecules is much larger at temperatures below T_c than above the critical temperature.

6) The partly deuterated compounds show heat capacity contributions from the rotations of the asymmetric top molecules NHD_2 and NH_2D.

7) Comparison with results of other experiments suggest:

a) the compounds behave quite differently at low temperatures, although they are isomorphous at room temperature.

b) first-order character of the phase transition is observed for the chlorides (and several other anions), but much less for the bromides and iodides.

c) the crystalline field at the metal(II) ions changes from cubic to a lower symmetry when the sample is cooled through T_c.

d) the transition temperature is considerably increased upon deuteration of the sample; also partly deuterated samples have a higher transition temperature than the pure hydrogenic samples, but lower than the deuterated one.

Appendix I. The energy levels and the heat capacity of hindered planar rotations of NH_3 and ND_3 molecules in a threefold potential barrier.

For the potential

$$V(\phi) = \frac{V_o}{2} (1 + \cos 3\phi)$$

the Schrödinger equation of a planar rotator takes the form

$$\frac{\partial^2\psi}{\partial\phi^2} + \frac{2I}{\hbar^2} \{E - \frac{V_o}{2} (1 + \cos 3\phi)\} \psi = 0 \qquad (A\text{-}1)$$

where V_o stands for the height of the potential barrier,

3 is the symmetry number of the barrier,

ϕ is the azimuthal angle,

I is the moment of inertia which for NH_3, about the threefold symmetry axis of the molecule amounts to $4{,}40 \cdot 10^{-40}$ gcm^2; $I_{ND_3} = 2I_{NH_3}$ and

E is the energy.

The transformation $2x = 3\phi$ yields

$$\frac{\partial^2\psi}{\partial x^2} + (a - \frac{s}{2}\cos 2x)\,\psi = 0 \qquad \text{(A-2)}$$

$$\text{or } \frac{\partial^2\psi}{\partial x^2} + (b - s\cos^2 x)\,\psi = 0 \qquad \text{(A-3)}$$

i.e. the ordinary Mathieu differential equation in the canonical form. The characteristic value, denoted by b, depends on the single parameter s. Both quantities are related to the parameters of eq. (A-2) by the relations

$$b = a + \tfrac{1}{2}s;\ a = \frac{4}{9}(E - V_o/2)(2I/\hbar^2);\ s = \frac{4}{9}V_o\,(2I/\hbar^2). \qquad \text{(A-4)}$$

We are interested in the solutions of eq. (A-3) which have the periodicity 2π. The application of the Fourier expansion $\psi = \sum_{m=-\infty}^{\infty} A_m e^{imx}$ on eq. (A-4) yields, after some manipulation, an infinite set of homogeneous linear equations for the coefficients A_m. The complete determinant factors into three infinite subdeterminants, each of which must be zero. The expansion of each subdeterminant yields an implicit equation for a separate set of eigenvalues b, in the form of the sum of two infinite continuous fractions. The iterative machine calculations give finally the eigenvalues b for each value of the parameter s. The characteristic values are collected in standard tables of Mathieu functions [52)53)].

The eigenvalues b, for summetry number 3, are presented graphically in fig. 17 as a function of the parameter s, for $0 < s < 60$. The sequence of the monotonically increasing first 21 energy levels is: b_{00}; b_{01}; b_{11}; b_{10}; b_{20}; b_{21}; . . . . . ; $b_{10,1}$. Here we have used the notation $b_{\nu,\sigma}$, where ν stands for the vibrational quantum number and σ is equal to 0 or 1 for a singlet level (A-species) or a doublet level (E-species), respectively. The eigenvalues b thus can be read from fig. 17 or, more

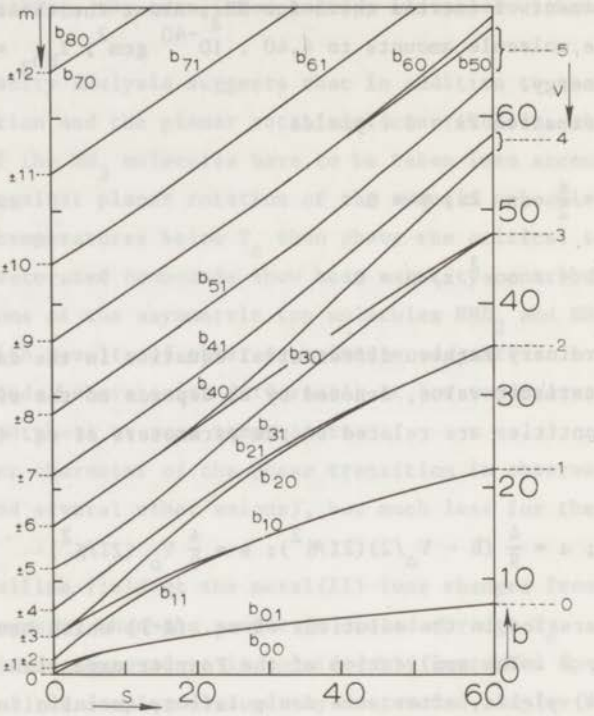

Fig. 17. *Energy level diagram of a hindered planar rotator. The rotations are opposed by a threefold potential barrier.*

$s = \frac{4}{9}(2I/\hbar^2)V_o$;

$b = \frac{4}{9}(2I/\hbar^2)E$;

m is the rotational quantum number in the limit of free rotation (s = 0).

ν is the vibrational quantum number in the limit of infinite barrier height (s = ∞).

accurately, from the tables [52)53)], using numerical interpolation techniques.

For small values of s, i.e. a low barrier, the energy levels go over into the quadratic set of levels for a *free planar* rotator, viz. $E_m = \frac{\hbar^2}{2I} m^2$; these doublet levels (except the ground state m = 0 which

is a singlet) are labeled with the rotational quantum number m in fig. 17. For large values of s, i.e. a high barrier, the eigenvalues converge towards the triply degenerate set of levels for a harmonic oscillator, labeled with the vibrational quantum number ν. For intermediate values of s the eigenvalue curves at comparable magnitude of the hindering barrier height, i.e. $b \simeq s$ or $E \simeq V_o$, display the characteristics of the transition between the two types of limiting level schemes; for $E < V_o$ the vibrational behaviour prevails and for $E > V_o$, the rotational one. In table A-I the energy of the first 21 levels is given for a set of nine values of the barrier height V_o/k; i.e. V_o/k = 100, 150, . . . , 500 K for NH_3. In the second column of the table the total statistical weight (g) of the energy levels, including the nuclear spin degeneracy of the protons, are given. For ND_3 similar results are collected in table A-II. The rotational specific heat of the planar rotators is calculated in the temperature range between 0 and 250 K. In order to fulfill the preset convergence limit put on the numerical accuracy of the heat capacity results (figs. 4 and 18), the computer program performed the calculation of additional higher rotational levels.

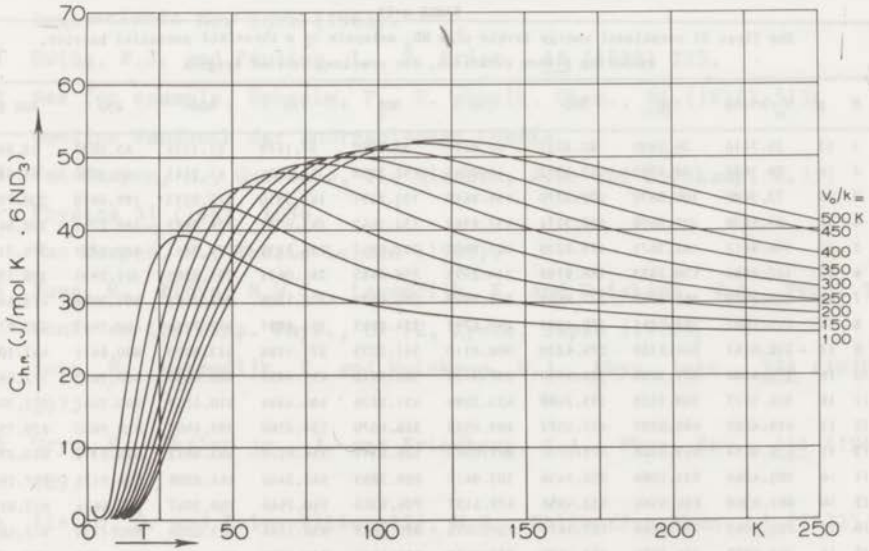

Fig. 18. *Calculated specific heats $C_{ND_3,hr}$ versus temperature for some selected values of the potential barrier height. The ordinate denotes specific heat values corresponding to six moles of ND_3.*

TABLE A-I

The first 21 rotational energy levels of a NH_3 molecule in a threefold potential barrier, executing planar rotations, for various barrier heights

N	g	V_o/k=100	150	200	250	300	350	400	450	500 K
1	4	36.6194	48.1510	57.4832	65.4616	72.5378	78.9689	85.0505	90.4658	95.7032
2	4	40.8051	50.3048	58.6974	66.1668	72.9564	79.2302	85.0704	90.5727	95.7690
3	4	96.9946	127.1416	154.6978	179.4799	201.7614	222.0118	240.5554	257.8057	273.9280
4	4	129.3678	151.2516	171.9678	191.5854	210.1817	227.8378	244.6348	260.6489	273.9524
5	4	142.7127	177.9094	213.8824	249.6809	284.7342	318.6722	351.2478	382.3110	411.7983
6	4	198.1763	226.4785	255.9732	286.2280	316.5746	346.3567	373.9578	402.5072	428.5986
7	4	279.0295	305.9856	333.8058	362.6165	392.5484	423.6535	455.9382	489.1492	523.0296
8	4	378.6027	404.8094	431.4194	458.3631	485.5622	512.9349	540.3998	567.8796	595.3024
9	4	378.6423	405.0061	432.0282	459.8118	488.4718	518.1193	548.8406	580.6796	613.6220
10	4	496.6387	522.5649	548.8608	575.5385	602.6076	630.0703	657.9578	686.2666	715.0338
11	4	632.9589	658.6585	684.6354	710.8964	737.4456	764.2801	791.4176	818.8469	846.5972
12	4	787.5370	813.0832	838.8488	864.8352	891.0448	917.4803	944.1464	971.0491	998.0650
13	4	787.5381	813.0861	838.8502	864.8349	891.0414	917.4648	944.1144	970.9786	998.1964
14	4	960.2523	985.5543	1010.9736	1036.5191	1062.2128	1087.9824	1113.8912	1139.9188	1166.0826
15	4	1151.3523	1176.6543	1202.0736	1227.6191	1253.3128	1279.0824	1304.9913	1331.0188	1359.2302
16	4	1360.6433	1385.9474	1411.3712	1436.9169	1462.5850	1488.2692	1514.2866	1540.3187	1566.4784
17	4	1360.6523	1385.9543	1411.3736	1436.9191	1462.6128	1488.3824	1514.2912	1540.3188	1566.4826
18	4	1588.1523	1613.4543	1638.8736	1664.4191	1690.1128	1715.8824	1741.7912	1767.8188	1793.9826
19	4	1833.7605	1858.9567	1884.2194	1909.5662	1935.0146	1960.4960	1986.0730	2011.7251	2037.4630
20	4	2097.6605	2122.8567	2148.1194	2173.4662	2198.9146	2224.3960	2249.9730	2275.6251	2301.3630
21	4	2097.6605	2122.8567	2148.1194	2173.4662	2198.9146	2224.3960	2249.9730	2275.6251	2301.3630

TABLE A-II

The first 21 rotational energy levels of a ND_3 molecule in a threefold potential barrier, executing planar rotations, for various barrier heights

N	g	V_o/k=100	150	200	250	300	350	400	450	500 K
1	11	28.7416	36.2689	42.5251	47.8516	52.7092	57.1678	61.3124	65.2033	68.8815
2	16	29.3487	36.4782	42.5352	47.8845	52.7238	57.1731	61.3143	65.2050	68.8820
3	16	77.3489	100.8870	120.2770	136.9640	151.8291	165.3810	177.9253	189.6970	200.7857
4	11	85.9839	105.0908	122.3174	137.9762	152.3467	165.6571	178.0877	189.7791	200.8423
5	11	106.9412	142.3671	175.6239	205.8991	233.0807	257.5235	279.7441	300.2201	319.3196
6	16	127.9866	158.2873	186.9789	214.2993	238.6485	261.0651	281.9362	301.5952	320.1582
7	16	166.9029	196.2742	227.9691	261.5148	295.6539	329.1508	361.1691	391.3968	419.6407
8	11	215.7097	242.7811	270.1999	297.6512	324.8645	351.6297	377.7963	403.2647	427.9786
9	11	216.0141	244.2359	274.4230	306.8110	341.2275	377.1194	413.8033	450.6411	487.1004
10	16	274.4304	301.3038	328.9789	357.5169	386.9910	417.4452	448.8037	480.7643	512.8851
11	16	342.3177	368.7228	395.7088	423.2986	451.5276	480.4546	510.1719	540.7547	572.3964
12	11	419.4251	445.5207	472.0572	499.0325	526.4370	554.2506	582.4407	610.9620	629.7558
13	11	419.4254	445.5224	472.0732	499.0983	526.6319	554.7276	583.4612	612.9312	643.2522
14	16	505.4868	531.1064	556.9456	583.0413	609.3855	645.2446	662.8208	689.9124	717.2691
15	16	601.0368	626.6564	652.4956	679.6151	704.9355	740.7946	758.3707	785.4624	812.8191
16	11	705.6868	731.3064	757.1456	783.2413	809.5855	836.1744	863.0208	890.1134	917.4691
17	11	705.6872	731.3074	757.1476	783.2425	809.5823	836.1747	863.0197	890.1218	917.4867
18	16	819.4368	845.0564	870.8956	896.9913	923.3355	959.1946	976.7708	1008.8624	1031.2191
19	16	942.1097	967.5073	993.0365	1018.7315	1044.5829	1070.5874	1096.7524	1128.0658	1149.5506
20	11	1094.0597	1099.4573	1124.9865	1150.6815	1176.5329	1202.5374	1228.7024	1255.0195	1281.5006
21	11	1094.0597	1099.4573	1124.9865	1150.6815	1176.5329	1202.5374	1228.7024	1255.0195	1281.5007

References

1 Pauling, L., Phys. Rev., 36 (1930) 430.

2 Ziegler, W.T., J. Am. Chem. Soc., 63 (1941) 2700.

3 Palma-Vittorelli, M.B., Palma, M.U., Drewes, G.W.J. and Koerts, W., Physica 26 (1960) 922.

4 Palma-Vittorelli, M.B., Palma, M.U. and Persico, F., J. Phys. Soc. Japan 17 (1962) suppl. B1, 475.

5 Garofano, T., Palma-Vittorelli, M.B., Palma, M.U. and Persico, F., Paramagnetic Resonance, ed. W. Low (1963) Vol II, p. 582.

6 Kim, P.H., J. Phys. Soc. Japan 15 (1960) 445.

7 Van Kempen, H., Duffy jr, W.T., Miedema, A.R. and Huiskamp, W.J., Physica 30 (1964) 1131.

8 Bates, A.R. and Stevens, K.W.H., J. Phys., C2 (1969) 1573.
Bates, A.R., Thesis University Nottingham (1965).
Bates, A.R., J. Phys., C3 (1970) 1825.

9 Klaaijsen, F.W., Suga, H. and Dokoupil, Z., Physica 51 (1971) 630.

10 For example, Wyckoff, R.W.G., J. Am. Chem. Soc., 44 (1922) 1239, Wyckoff, R.W.G., Crystal Structures, 2nd. Edn. Vol. 3, p. 783, Interscience New York (1965).

11 Ewing, F.J. and Pauling, L., Z. Krist., 68 (1928) 223.

12 See for example, Ephraim, F., Z. physik. Chem., 81 (1913) 513; Gmelins Handbuch der Anorganischen Chemie.

13 Van Kempen, H., Garofano, T., Miedema, A.R. and Huiskamp, W.J., Physica 31 (1965) 1096,
Van Kempen, H., Thesis Leiden (1965).

14 Suga, H., Blöte, H.W.J., Lagendijk, E. and Huiskamp, W.J., Proc. Int. Conf. on Low Temp. Phys., LT 12, Kyoto, Japan (1970);
Suga, H., Lagendijk, E. and Huiskamp, W.J., Phys. Lett., 32A (1970) 297.

15 Uryu, N., Skalyo jr., J. and Friedberg, S.A., Phys. Rev., 144 (1966) 689.

16 Aiello, G. and Palma-Vittorelli, M.B., Collective Phen., 1 (1973) 87.

17 Garnier, P.R., Phys. Lett., 35A (1971) 413.

18 Cooke, A.H., Martin, D.M. and Wells, M.R., Solid State Commun., 9 (1971) 519.

19 Simon, F., Ann. Physik, 68 (1922) 241,
Simon, F. and Ruhemann, M., Z. phys. Chem., 129 (1927) 339.
20 Hill, R.W. and Ricketson, B.W.A., Phil. Mag., 45 (1954) 277.
21 Clusius, K., Z. phys. Chem., B3 (1929) 41.
see also Colwell, J.H., Gill, E.K. and Morosin, J.A., J. Chem. Phys., 39 (1963) 635; 42 (1965)3144.
22 Grenier, G. and White, D., J. Chem. Phys., 40 (1964) 3015.
23 Pitzer, K.S. and Gwinn, D.W., J. Chem. Phys., 10 (1942) 428.
24 Jacób, W., Janik, J.M., Bajorek, A., Parlinski, K. and Sudnik-Hrynkiewicz, M., Physica 35 (1967) 441.
25 Janik, J.A., Jacób, W. and Janik, J.M., Acta Phys. Pol., A38 (1970) 467.
26. Janik, J.M., Janik, J.A., Migdal, A. and Pytasz, G., Acta Phys. Pol., A40 (1971) 741.
27. Coulter, L.V., Pitzer, K.S. and Latimer, W.M., J. Am. Chem. Soc., 62 (1940) 2845;
Bailey, C.A. and Smith, P.L., Phys. Rev., 144 (1959) 1010.
28 Herzberg, G., Infrared and Raman Spectra ; D. Van Nostrand Company, Inc., N.Y., 1945.
29 Shimanouchi, T. and Nagakawa, I., Inorg. Chem., 3 (1964) 1805.
30 Matsuo, T., Suga, H. and Seki, S., Bull. Chem. Soc. Japan, 44 (1971) 1171.
31 Stout, J.W. and Catalano, E., J. Chem. Phys., 23 (1955) 2013.
32 Asch, L., Adloff, J.P., Friedt, J.M. and Danon, J., Chem. Phys. Lett., 5 (1970) 105.
33 Asch, L., Thesis University of Strassbourg (1974).
34 Elgsater, A. and Svare, I., J. Phys. Chem. Solids, 31 (1970) 1405.
35 Smith, S.J., Bunting, J.G. and Steeple, H., J. Phys. Chem. Solids, 35 (1974) 893.
36 James, H.M. and Keenan, T.A., J. Chem. Phys., 31 (1959) 12.
37 See for example, Yamamoto, T. and Kataoka, Y., J. Chem. Phys., 48 (1968) 3199.
38 Landau, L.D., Phys. Z. Sowjet Union, 11 (1937) 26.
39 Cochran, W., Adv. Phys., 10 (1961) 401.
40 Devonshire, A.F., Phil. Mag., 40 (1949) 1040.
41 Nagakawa, I. and Shimanouchi, T., Spectrochim. Acta, 22 (1966) 759.
42 Sacconi, L., Sabatini, A. and Gans, P., Inorg. Chem., 3 (1964) 1772.
43 Nakamoto, K., 'Infrared spectra of inorganic and co-ordination

compounds', 2nd Edn., Wiley Interscience, p. 154.

44 Huheey, J.E., 'Inorganic Chemistry: principles of structure and reactivity', Harper & Row (1972) p. 74.

45 Trapp, C. and Shyr, C-I., J. Chem. Phys., 54 (1971) 196.

46 Patil, K.C. and Secco, E.A., Can. J. Chem., 50 (1972) 567.

47 See for example, Blinc, R., J. Phys. Chem. Solids, 13 (1960) 204.

48 See for example, Gopal, E.S.R., 'Specific Heats at Low Temperatures', Heywood Books London (1966).

49 The samples of $Ni(ND_3)_6I_2$ and $Ni(NH_3/ND_3)_6I_2$ were kindly prepared and analysed by G.A. Brokaar of the Chemistry Department of the Leyden University.

50 Aiello, G., Palma, M.U. and Persico, F., Phys. Lett., 11 (1964) 117.

51 Weiss, M.T. and Strandberg, M.W.P., Phys. Rev., 83 (1951) 567.

52 Tables Relating to Mathieu Functions, Columbia Univ. Press, New York (1967).

53 Kilb, R.W., Tables for Mathieu Eigenvalues and Eigenfunctions for Special Boundary Conditions, Dept. of Chem., Harvard Univ., (1956).

SAMENVATTING

In dit proefschrift worden soortelijke-warmtemetingen in het temperatuurgebied van 1.3 tot 80 K besproken met het doel informatie te verkrijgen over ordeningsverschijnselen in vaste stoffen. In polykristallijne verbindingen zijn in het bijzonder de volgende ordeningsverschijnselen onderzocht: 1) magnetische ordening in verschillende series coördinatieverbindingen van 3d-overgangsmetalen en 2) moleculaire ordening van roterende ammoniak groepen in complexe verbindingen.

In hoofdstuk I wordt een algemene inleiding tot de soortelijke warmtemetingen gegeven. De meetopstelling en meetmethode, alsmede ijkresultaten van metingen aan zuiver koper en benzoëzuur (C_6H_5COOH) worden besproken in hoofdstuk II.

In hoofdstuk III - V zijn de metingen die betrekking hebben op magnetische ordening, behandeld. Onderzocht zijn verbindingen, waarvan op grond van de kristalstructuur verwacht kan worden dat ze zich als magnetische lineaire ketensystemen zullen gedragen. Dat wil zeggen, de magnetische wisselwerking vindt voornamelijk plaats tussen naaste-buur spins die gerangschikt zijn in goed geïsoleerde lineaire ketens. Aangezien de lineaire ketensystemen een relatief eenvoudig veel-deeltjes probleem vormen, zijn theoretisch voor een aantal modellen de thermodynamische grootheden als functie van de temperatuur bekend.

Omdat voor één-dimensionale systemen met grote spinwaarde weinig experimentele gegevens beschikbaar zijn, hebben wij de soortelijke warmtemetingen speciaal aangevat aan verbindingen waarvan de reële spinwaarde van het 3d-metaalion groter is dan $\frac{1}{2}$. Parallel hiermee hebben Reedijk en Witteveen onderzoek verricht naar de spectroscopische en magnetische eigenschappen van deze verbindingen. In hoofdstuk III worden soortelijke warmte resultaten getoond voor de serie verbindingen $M(II)(N_2H_5)_2(SO_4)_2$ waarbij M(II) een twee-waardig metaalion voorstelt: M(II) = Cu, Ni, Co, Fe en Mn ($S = \frac{1}{2}$ t/m $\frac{5}{2}$). Door deze resultaten te combineren met die van susceptibiliteitsmetingen, was het mogelijk te concluderen dat de magnetische wisselwerking tussen de ionen in de keten dominant is en van een antiferromagnetisch karakter. In de gevallen M = Cu, Mn blijken de experimentele gegevens in redelijke benadering geïnterpreteerd te kunnen worden met het Heisenberg model voor magnetische lineaire ketens

met resp. $S=\frac{1}{2}$ en $S=\frac{5}{2}$. De aan de Co verbinding uitgevoerde experimenten tonen aan dat dit een goed voorbeeld is van het één-dimensionale XY-model, waarin twee ruimtelijke componenten van de naaste-buur spins (met effectieve spin $S'=\frac{1}{2}$) gelijk participeren in de interactie. Dit wordt toegeschreven aan de eigenschappen van het kristalveld ter plaatse van het Co-ion in deze verbinding. Het optreden van kristalveld anisotropie van de paramagnetische ionen wordt eveneens aangetoond in de Ni- en Fe-verbinding. Terwijl deze anisotropie voor $Fe(N_2H_5)_2(SO_4)_2$ tot een gecompliceerde situatie aanleiding geeft, blijkt dat voor de nikkel-verbinding de soortelijke warmte resultaten goed beschreven kunnen worden met het aannemen van een axiaal anisotrope bijdrage tot het kristalveld die groot is t.o.v. de intra-keten interactie. Bij lage temperaturen blijken de nikkel spins zich als een antiferromagnetische Ising keten te gedragen. Naast de intra-keten interactie is er ook een inter-keten interactie, die, als de temperatuur laag genoeg is, lange-drachts ordening tot gevolg heeft. Dit is waargenomen in het geval dat M = Co, Fe en Mn.

In de hoofdstukken IV en V worden verschillende aspecten behandeld van de magnetische interacties in de chemische ketenverbindingen met de algemene formule $M(II)X_2L_2$ waarbij M(II) = een twee-waardig 3d-metaalion, X = Cl of Br en L = pyrazool of pyridine. In het bijzonder wordt aandacht geschonken aan de nikkelverbindingen (hoofdstuk IV) en aan de mangaanverbindingen (hoofdstuk V) van deze serie. De gemeten soortelijke warmte kan beschreven worden met een intra-keten interactie welke groot is t.o.v. de interketen wisselwerking. De resultaten tonen verder aan dat zowel voor de nikkel (S=1) als voor de mangaan ($S=\frac{5}{2}$) zouten het maximum van de magnetische soortelijke warmte niet voor alle verbindingen gelijk is, zoals op grond van bijvoorbeeld het Heisenberg lineaire ketenmodel verwacht zou worden. Met behulp van recente berekeningen voor het Heisenberg lineaire ketenmodel met een additionele uniaxiale kristalveld anisotropie kan aannemelijk gemaakt worden dat kristalveld-splitsingen hiervan de oorzaak zijn. De intra-keten interactie en kristalveld anisotropie parameters J/k en D/k zijn voor alle acht hierboven genoemde verbindingen bepaald. Het blijkt dat vooral in de nikkelverbindingen buitengewoon grote kristalveld-splitsingen optreden waarvoor nog geen verklaring gegeven kan worden. De inter-keten interactie parameter voor elk van de zouten is berekend met gebruikmaking van een door Oguchi

gegeven relatie tussen de intra-keten interactie parameter J/k, de overgangstemperatuur naar een drie-dimensionaal geordende toestand T_N en de spinwaarde S. Het blijkt dat de pyrazool liganden de ketens beter isoleren dan de pyridine liganden.

In hoofdstuk VI worden onderzoekingen naar de ordening van moleculen in metaal(II)hexamine jodiumverbindingen beschreven. Een tiental zouten met algemene formule $M(II)(NH_3)_6I_2$ waarbij M(II) = Ni, Co, Fe, Mn, Zn, Cd en Ca zijn met behulp van soortelijke warmte metingen onderzocht. Alle onderzochte hexamines vertonen een scherpe fase-overgang bij een nauwkeurig bepaalde temperatuur T_c. Dit blijkt gepaard te gaan met een verlaging van de kristalsymmetrie. Bovengenoemde verschijnselen hangen nauw samen met de rotatietoestand van de NH_3 moleculen. De NH_3-groep kan beschouwd worden als een vlakke rotator, gehinderd door electrostatische potentiaal barrières. Aangenomen moet worden dat voor al deze moleculen de rotatietoestand bij T_c collectief verandert. Deze verandering correspondeert met een aanzienlijke entropieverlaging. De entropie behorende bij de fase-overgang is experimenteel bepaald en vergeleken met theoretische resultaten verkregen met modellen voor de orde-wanorde en moleculaire reoriëntatie -overgangen. In het bijzonder is aandacht geschonken aan een door Bates en Stevens voor de hexamineverbindingen voorgesteld model dat gebaseerd is op klassieke electrostatische wisselwerking tussen de ammoniakmoleculen. Hoewel men zou verwachten dat al deze isomorfe verbindingen dezelfde entropieverandering hebben, blijkt dit niet het geval te zijn. Dit hangt mogelijk samen met het karakter van de fase-overgang. Voor de chloorverbindingen (en enkele andere anionen) is een eerste orde karakter gevonden, terwijl dit niet het geval is voor de broom- en jodiumverbindingen. Het vervangen van waterstof door het zwaardere deuterium heeft markante gevolgen voor de overgangstemperatuur. Grote veranderingen van de overgangstemperatuur zijn eveneens waargenomen voor de gedeeltelijk gedeutereerde verbinding. Uit de gevonden resultaten blijkt duidelijk dat men hier te maken heeft met een coöperatief proces. Dit wordt ondersteund door de resultaten van de metingen aan de gedeeltelijk gedeutereerde verbindingen, waarvoor bij lage temperaturen soortelijke warmte bijdragen van de asymmetrische top-moleculen NH_2D en NHD_2 zijn waargenomen. Geconcludeerd moet worden dat ook in vaste stoffen bij lage temperaturen gehinderde rotaties en quantum mechanisch tunnelen een belangrijke rol kunnen spelen.

Op verzoek van de faculteit der Wiskunde en Natuurwetenschappen volgt hier een overzicht van mijn studie.

Na het behalen van het eindexamen H.B.S.-B aan de Rijkshogereburgerschool te Vlissingen begon ik in september 1960 mijn studie aan de Rijksuniversiteit te Leiden, waar ik in 1964 het kandidaatsexamen Natuurkunde en Wiskunde met bijvak Sterrenkunde aflegde. Sindsdien was ik werkzaam op het Kamerlingh Onnes Laboratorium in de werkgroep soortelijke warmte vaste stof, welke onder leiding stond van Prof.Dr. C.J. Gorter, terwijl de dagelijkse leiding bij Dr. Z. Dokoupil berustte. Als candidaat assisteerde ik aanvankelijk Prof.Dr. J. Ferreira da Silva bij het onderzoek aan supergeleidend niobium, en Drs. J. Scheffer bij de metingen aan magnetische isolatoren. In 1968 werd een begin gemaakt met de automatisering van de opstelling, terwijl tevens het temperatuurbereik werd uitgebreid tot dat van vloeibare zuurstof. Nadat ik het doctoraalexamen experimentele natuurkunde, met bijvak klassieke mechanica had afgelegd, begon ik aan het in dit proefschrift beschreven onderzoek van ordeningsverschijnselen in vaste stoffen. In juni 1969 werd ik benoemd tot wetenschappelijk medewerker.

Vanaf 1965 was ik in verschillende functies werkzaam als assistent bij het natuurkunde practicum. Voorts ben ik sinds 1969 als leraar verbonden aan het Instituut voor Middelbare Akten in de Exacte Vakken te Den Haag.

Op 1 augustus 1974 werd ik benoemd tot docent natuurkunde aan de Leraren Opleiding van de Gelderse Leergangen te Nijmegen.

NASCHRIFT

Tijdens mijn onderzoek zijn vele medewerkers van het Kamerlingh Onnes Laboratorium mij tot grote steun geweest. De waardevolle discussies met Dr. Z. Dokoupil en mijn promotor zijn bepalend geweest voor het tot stand komen van dit proefschrift. Prof.Dr. C.J. Gorter heeft voortdurend belangstelling getoond voor het onderzoek en was altijd bereid tot het voeren van discussies en het geven van suggesties. De prettige contacten met Prof.Dr. R.L. Carlin, die ook het manuscript kritisch gelezen heeft, heb ik bijzonder gewaardeerd. Dr. H.W.J. Blöte berekende de lineaire keten soortelijke warmtes vermeld in de hoofdstukken IV en V. De stimulerende discussies met Dr. H.F.P. Knaap en de waardevolle suggesties van Dr. H.W. Capel hebben zeer tot het tot stand komen van dit proefschrift bijgedragen.

Met veel genoegen denk ik terug aan de prettige samenwerking met de medewerkers van de Gorleaus Laboratoria van de Rijksuniversiteit te Leiden en van de afdeling Chemie van de Technische Hogeschool Delft. Hierbij wil ik in het bijzonder noemen Dr. J. Reedijk en Dr. H.T. Witteveen, die vooral bijgedragen hebben aan het tot stand komen van de hoofdstukken III - V. Voor de experimenten beschreven in hoofdstuk VI mag de stimulerende bijdrage en de prettige samenwerking met Dr. H. Suga niet onvermeld blijven.

Bij de metingen en de uitwerking daarvan werd ik op bekwame wijze geassisteerd door Drs. H.B.S. Hemmers, Drs. R.O. Knaap en de heer H. den Adel.

De technische hulp van de heer T. Nieboer, die onder meer de akelig dunne caloriemeters in grote aantallen vervaardigde, was zeer belangrijk voor het welslagen van het onderzoek. De automatisering van de meetopstelling werd voor een belangrijk deel gerealiseerd door de heer J. v.d. Zeeuw. Voor de programmatuur van de computer programma's werd de deskundige hulp van de heer J.A. van Bentveld gewaardeerd. De medewerkers van de cryogene afdeling hebben voor een niet aflatende stroom vloeibare helium en waterstof naar kamer 00.08 gezorgd. De tekeningen werden in vlot tempo vervaardigd door de heer W.J. Brokaar en de foto's werden afgedrukt door de heer W.F. Tegelaar. Het manuscript werd op vaardige wijze getypt door Henny Klaaijsen-Streefkerk.